Electronic transport in spin-glasses and mesoscopic wires : correlations of universal conductance fluctuations in disordered conductors

Mathias Solana

Communauté
UNIVERSITÉ Grenoble Alpes

THÈSE

Pour obtenir le grade de

DOCTEUR DE la Communauté UNIVERSITÉ GRENOBLE ALPES

Spécialité : **Physique de la matière condensée et du rayonnement**

Arrêté ministériel : 7 août 2006

Présentée par

Mathias SOLANA

Thèse dirigée par **Laurent Saminadayar**
et codirigée par **François Lefloch**

préparée au sein **de l'Institut Néel - CNRS**
et de **l'École doctorale de Physique**

Electronic transport in spin-glasses and mesoscopic wires: correlations of universal conductance fluctuations in disordered conductors

Thèse soutenue publiquement le **29 Juin 2018**,
devant le jury composé de :

M. David Carpentier
Directeur de recherche, ENS Lyon, Président
M. François Ladieu
Docteur, CEA/IRAMIS/SPEC, Rapporteur
M. Rodolfo Jalabert
Professeur, Université de Strasbourg, Rapporteur
M. Clemens Winkelmann
Maitre de conférence, INP Grenoble, Examinateur
Mme. Anne Anthore
Maitre de conférence, Université Paris Diderot, Invitée
Laurent Saminadayar
Professeur, Université Grenoble Alpes, Directeur de thèse
François Lefloch
Docteur, CEA/INAC, Co-Directeur de thèse

Abstract

The experimental work developed during this PhD is situated at the interface of two fields of condensed matter physics, namely spin glasses and mesoscopic physics.
Spin glasses have been widely studied and are one of the problem that has been the most discussed over the years, both on a theoretical and experimental point of view. It is characterized by very peculiar properties that come to light as it exhibits a magnetic phase transition at low temperatures that is already unusual. Indeed, this transition is due to a mix of frustration and disorder in the magnetic structure of the system, making it an exceptional model system for glasses and frustrated systems in general.
After many efforts, theoreticians managed to describe the fundamental state of the system by the mean of two different and apparently incompatible approaches. The first one, called RSB theory, is based on a mean-field approximation and predicts a complex phase space with an unconventional hierarchical organization. The second is based on more phenomenological approach and is named Droplet theory. It points towards a unique ground state and explain all the observation by slow relaxation processes.
However, the question of the true nature of the spin glass phase is still heavily debated.
Mesoscopic physics, for its part, addresses the question of electronic transport for samples in which the electrons keep their phase coherence.
If the electrons remains coherent, it is possible to see interference effects that are quantum signs of what happens at the atomic level. In this work, it is used to probe the magnetic and static disorder in spin glasses. Indeed, it is possible to interpret the change in those interferences as changes in the microscopic disorder configuration and to know exactly how the spin glass state evolves.
Some work have already tried to use coherent transport in spin glasses but this remains an open field.
This work has then be dedicated to the implementation of transport measurement in spin glasses and mesocopic conductors.
The first part will be focused on a the experimental setup that was used to perform very precise transport measurements and on the processing of the data taken out of them.
In a second part, we will present some general physical characteristics of our samples such as their resistance dependence to the temperature or magnetic field, before extracting the quantum signature in magnetoresistance measurements.
Finally, we will discuss the results obtained. We show that strong changes in the microscopic disorder happen even at low temperatures, in opposition to what is believed. We argue that those observed changes are purely structural and come from systems that are widely distributed in energy.

Contents

Acknowledgement

Le moins que je puisse dire c'est que ces quatre années de thèse auront été un périple parfois digne de l'Odyssée. Le point de départ est connu, l'arrivée également. Mais le chemin est périlleux, semé d'embûches, de détours et de rencontres. Et tout comme Ulysse qui n'aurait pas pu rejoindre Ithaque sans ses compagnons d'infortune, je n'aurais probablement pas accompli tout ce chemin sans les gens qui m'ont entouré et que je souhaiterais remercier ici.
Je remercie donc mon jury de thèse, avec en premier lieu mes rapporteurs François Ladieu et Rodolfo Jalabert dont les commentaires à mon endroit, corrections et questions furent des plus intéressantes pour approfondir mon sujet de thèse. Merci à vous. De même je tiens à remercier David Carpentier, mon Président de jury, pour les discussions de travail que nous avons pu avoir ainsi que pour sa bonne humeur. Pour terminer je voulais remercier les deux autres membres de mon jury Anne Anthore et Clemens Winkelmann. Merci Anne pour m'avoir introduit au monde la physique mésoscopique il y a déjà sept ans de cela et de m'avoir aidé à découvrir la Finlande.
Mais avant d'en arriver à la soutenance, il y a un longue traversée à la rame. Et il n'est pas possible de voguer sur les flots sans quelqu'un pour nous apprendre à naviguer. Je tiens donc à remercier Laurent Saminadayar, mon directeur de thèse, pour m'avoir donné l'envie de plonger dans les profondeurs insondables de la physique des verres de spins, m'avoir initier aux mystères (non moins insondables) de la cryogénie, ainsi que pour les nombreuses discussions historiques ou philosophiques qui auront émaillées ces quatre années. Merci Laurent.
Même en sachant mener sa barque, il y a parfois besoin d'un sextant (ou d'une boussole, soyons progressistes !) pour nous rappeler le cap à suivre. Ce sextant aura été mon second directeur de thèse François Lefloch. Alors que le navire tanguait sérieusement, tu nous as permis de garder le cap. Et quand bien même Charybde nous a aspirés, tu nous a permis de ne pas nous faire dévorer par Scylla. Merci François.
Dans la même optique, j'aimerais remercier la direction de l'Institut Néel ainsi que celle du département QUEST en la personne d'Étienne Bustaret et Laurence Magaud. Merci pour votre assistance et votre écoute dans certains moments difficiles. Votre aide m'aura été précieuse.
Il ne faudrait pas non plus oublier que lors de telles épopées il faut des provisions. Un mot donc à toutes ces personnes au sein de l'Institut Néel qui m'ont fourni aide et soutien tout au long. Je pense notamment au personnel du liquéfacteur Johan, Raphaël et Kévin qui m'auront fourni approximativement 50000 litres d'hélium liquide au total, sans lesquels ma thèse aurait coulé tel le Bismarck.
Mais bien sûr il y a besoin d'un équipage, de compagnons à nos côtés. A cet égard, je ne puis me plaindre tant leur concours aura été bien au-delà du simple aspect scientifique.

Merci à toutes les personnes que j'ai pu croiser dans cette grotte qui me servait de port d'attache, le bâtiment M, en particulier à PAM, Greg, BB, Baptistouille, Klaus et Bambi. Tous, jeunes, vieux, stagiaires, permanents, thésards, vous m'avez apporté quelque chose et je vous en remercie.
Mais simplement en rester là ne saurait rendre hommage à ceux qui, au plus proche, ont eu à supporter mes doutes, mes espoirs, mes désillusions et mes victoires, mes plus fidèles lieutenants. Merci à Guillaume Forestier pour m'avoir guidé à mes débuts, m'avoir épaulé et bu moult boissons houblonnées avec moi ! Merci également à Candice "Miss Toto" Thomas pour ces longues soirées d'hiver au coin d'un cryostat à chanter avec moi sur des rythmes endiablés. Je serai là, toujours pour toi. Cela étant dit, comment ne pas finir par celui qui aura le plus partagé avec moi cette expérience unique qu'est la thèse. Merci Vivien "VV" Thiney. Tu as été un précieux compagnon de voyage et j'espère que nos destinations divergentes n'entacheront pas ce lien.
Cependant, tel la partie émergée de l'iceberg, je n'ai ici mentionné que les gens rencontré au gré des courants insensés de l'océan de la recherche. Et, bien que ce périple ait occupé une grande partie de ma vie ces quatre dernières années, il serait criminel d'oublier ceux qui m'auront accompagné sur la terre ferme. Tout d'abord les Parisiens (ou pour le moins connus en région parisienne): Noëlle, Nathan, Ana, Audric, Mathexis, Fred, Wilhelm et j'en passe... qui sont là depuis longtemps et que je remercie pour leur soutien sans faille tout au long des années. Et merci Camille d'avoir eu la force (et l'honneur) de me supporter depuis déjà 15 ans (à une vache près !). Ensuite évidemment les Grenoblois: Virginie, Annina, Eduardo, Laureen, Yves, Ketty, Olivier, Laure,... qui m'auront supporté au jour le jour hors des murs de la physique. Il y a également ceux qui se retrouvent entre deux tels Alice, Mélinda et Thibaut, que j'aurai vu autant à Paris qu'à Grenoble.
Enfin j'aimerais remercier Soan. J'ai probablement passé le meilleur Noël de ces 10 dernières années avec toi ! Le lien que l'on a pu tisser est rare et malgré les turpitudes de nos vies respectives, il a et aura toujours de la valeur à mes yeux.
Je n'oublierai pas non plus les "Finlandais" sans qui je n'y serais certainement jamais retourné: Rémi, Guillaume, Benoit et surtout Céleste. Merci d'être restée à mes côtés petite nouille! Tu sais ce que ça signifie pour moi.
Une pensée aussi pour ces entités qui, pour des raisons différentes, m'auront beaucoup apporté: les arbitres de rugby alpins pour ces nombreux matchs à arbitrer, le Shakesbeer, le Synesthète et le Jardin du thé pour m'avoir fait découvrir et initié respectivement aux différentes bières, vins et thé d'exceptions. Et enfin la Fédération Galloise de Rugby pour avoir éliminé l'Angleterre de sa propre Coupe du monde dès les phases de poules pour ce qui restera certainement l'une de mes meilleures soirées grenobloises.
Merci également à ma famille qui a su me soutenir tout au long de cette aventure.

Pour terminer, je souhaiterais remercier une nouvelle fois tous mes amis qui ont partagé avec moi ces quatre dernières années et qui sauront se reconnaitre. Je ne vous oublierai pas et j'espère que vous serez encore là de nombreuses années.

Introduction

The fascinating glassy state

What is the common point between a stained glass window, honey, chocolate or even shaving cream?
In this simple question, that could be the beginning of a joke, lies a very deep question in condensed matter physics: what is a glass?
Surprisingly, each of those examples are indeed glasses. At first sight it seems really strange to gather under the same name so different kind of items. However one can see the link between them through their atomic structure.
What we call a glass in our daily life is in fact more precisely a “structural glass", meaning that they look like a solid. That statement would naturally lead us to the common believe that they are crystals. But it is totally wrong.
Indeed, crystals are perfectly organized structure with a long range order and a translation invariance. Basically it is the same arrangement of atoms (an atomic "brick") repeated over and over in every direction as if a child was playing with the same lego brick. If you know this elementary brick, you’re able to find every property of this material. This approach led to most of the major discoveries in condensed matter physics such as the description of electronic conduction bands. But in the case of a glass, this picture falls apart!
Just imagine this crystalline perfection but in which each atoms is moved by a mad scientist in a totally chaotic way... Now you have the perfect picture of a glass! The most common way to get a glass is to take a liquid and cool down so fast that it doesn’t have the time to crystallize (it is "quenched"). Indeed, in a liquid, atoms are free but, when frozen, they get stuck at their position in a disordered way. One can then see a glass as a snapshot of a liquid at a certain time. Then, on the contrary of a crystal, we end up with a totally disordered system. Thus, from a microscopic point of view, no part of a glass seems like the other and then no elementary brick nor long range order can be set! In that case it is obviously much harder to describe the physical properties of such a system but some of them can be guessed.
Intuitively one can deduce from the quench process that the system has no time to reach the crystalline phase which is the ground state of the system. It is trapped in a metastable state. The glassy state is then not static but dynamic and will evolve towards the crystalline phase on huge time scales ranging from few seconds to centuries...

To summarize, glassy systems have several peculiar properties: they are disordered despite being solid (with no long range order or symmetry), they exhibit a phase transition between the liquid and glassy phases at a given temperature and their dynamic is very slow.

From this discussion we determined the features of structural glasses. But they can be extended to other systems that are thus also glasses. For example the disorder can be not only structural but also magnetic. It is the case in the well known spin glasses, that will be at the centre of this thesis.

Spin glasses, a model system

Actually, a spin glass is not really what one would immediately call a glass. Indeed, it is usually a piece of a certain non-magnetic material with magnetic moments (or ions) inside. Moreover, its structure does not evolve over time. The spins remain at the same place as well as the atoms of the material.
However, if we look into more details, it is definitely a glass.
As previously explained, calling something a glass is equivalent to say that there is disorder, phase transition and slow dynamics.
In the case of spin glasses, this disorder is set with the magnetic moments. Indeed, those moments are like tiny little interacting magnets randomly spread in the material lattice. If one considers only those magnets, we will see that it forms a glass-like pattern in space since they are randomly distributed. From that, we have the disorder. But we also need a phase transition.
Since those magnets do not move, we cannot expect a structural phase transition. Here, we face a magnetic one.
We can make a parallel with ferromagnetic compounds[67]. Above the Curie Temperature T_c, the magnetic atoms are totally free to flip as they want. But, as the thermal energy drops, they will get ordered and will all align in the very same direction.
The same process happens in spin glasses when the temperature gets lower than the average interacting energy between spins. Above this temperature T_g, we are in a paramagnetic phase, whereas, below it, the magnetic spins will “freeze" in a certain configuration but in a very unconventional way, because of the disorder!
So what about slow dynamics?
Many experiments displayed several peculiar features in those systems: ageing, memory, frequency dependence (that will be detailed later) and slow dynamic in particular[69].

Those unusual behaviours led to many theoretical works over the years, starting from a “simple" first-neighbours interaction model[68], to very complex mean-field theory[60] or scaling ones[26, 27].
Actually, those theories can be extended to many other fields out of physics! Indeed, to model such system, one needs to take into account many-body random interactions that can be found in a wide range of applications such as finance, computer science (travelling salesman problem) or even biology. Spin glasses are thus a model system for many more applicable systems and finding the good model for it has many implications.
However, the two major theories, namely RSB and Droplet ones, are incompatible and, yet, the question of knowing which one is relevant (if any) is still heavily debated.
A way to address this question would be to probe the internal structure of the spin glass

and, to do so, we can use coherent electronic transport.

The electronic coherent transport as a probe

When one talks about electronic coherent transport, the underlying subject is often mesoscpic physics.
Indeed, mesoscopic physics sits right between nanophysics (below the nanometre) and macroscopic physics (above millimetre length)[65], where the lengths are of the order of the phase coherence length of electrons L_ϕ.
This particularity places mesophysics at the interface between two worlds: the “classical" and the quantum one.
Through transport measurement at this scale, one can measure classical values that are governed by the sample on a macroscopic level (such as resistance) BUT with quantum corrections (such as Universal Conductance Fluctuations) due to coherence effect at the atomic level.
If one can interpret those corrections, it is possible to probe the sample on an atomic level and, more specifically, the disorder inside the samples.
We will see that measuring the resistance of the samples as a function of the magnetic field gives us a unique fingerprint of the disorder, giving us the opportunity to compare them by calculating their correlation.
In our case, we rely on the interaction between electrons and magnetic spins to observe changes on those resistance measurements and thus in the magnetic configuration.
Moreover, observing and analysing those changes as a function of the temperature would be a strong indication to determine which of the competing theories is the good one.

Outline of the manuscript

First, I will start by giving a theoretical and experimental overview of the two main physical domains used during my PhD, namely spin glasses and coherent electronic transport.
Once those tools will have been developed, I will present the setup and techniques used to measure with a high accuracy the resistances of our samples as well as to treat those data to recover disorder measurements.
In the following, the general transport characteristics of our samples will be detailed and interpreted.
In particular we will focus on resistance measurements as a function of the temperature and then as a function of an applied magnetic field.
The quantum corrections to the resistivity will be extracted and compared to qualitatively and quantitatively probe the changes in the microscopic disorder configuration.
We will show that changes are observed for temperatures much higher than T_g. However, those changes are also shown on non-spin glasses samples. We then argue that those changes are structural and have to be interpreted in terms of widely energetically distributed moving systems in our samples.

CHAPTER 1

Spin glasses: A theoretical and experimental overview

Since our main focus is to probe the disorder inside a spin glass, we need to present its main features to understand the physics involved.
In this first chapter, we will try to summarize the long history of spin glasses.

1.1 How to make a spin glass: disorder and frustration

From a general point of view, a system is said frustrated when it cannot minimize all the energetic constraints at the same time. This concept is at the hearth of the spin glass state[50].
This frustration can be induced either by the structure of the system itself i.e. its topology or via the disorder.

1.1.1 Geometrical frustration

In the case the frustration is induced by the geometry, it is said geometrical.
The most striking example of geometrical frustration is the triangular lattice of Ising spins[1] with anti-ferromagnetic coupling as shown in Fig.1.1.

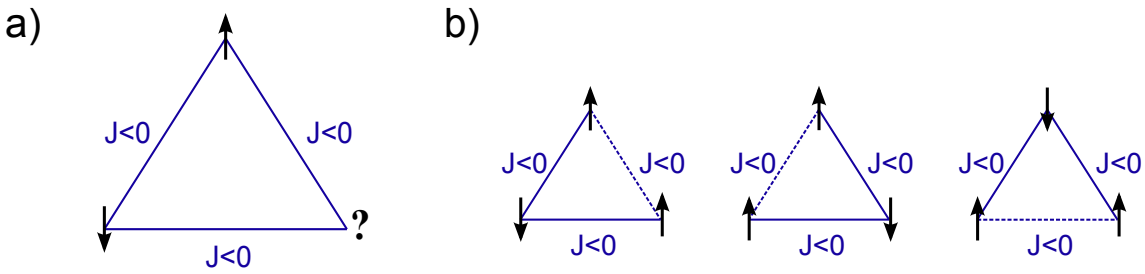

Figure 1.1: Example for the frustration concept with the Ising anti-ferromagnetic triangle. a): One can see that whatever direction the spin "?" takes on the last vortex, one of the bond will not be satisfied. b): Three examples of possible configurations minimizing the energy. We see that for any configuration the total energy is the same (one bond unsatisfied): the system ground state is degenerate in energy.

In that case each vertex of the triangle is occupied by an Ising spin and cannot move. If two of those spins are fixed (here in vertexes 1 and 2), whatever will be the orientation of the third one, the energy of one of the bond will not be minimized because of the

1 Ising spins can only take two values (-1 or +1), in opposition with Heisenberg spins that can take any values between -1 and +1. In our case it means that Ising spins can only be "up" or "down".

anti-ferromagnetic coupling: the system is frustrated. Another important feature of this example is that, whatever is the spin configuration, the system energy doesn't change. The unsatisfied bond changes but not the total energy: all the configurations are energetically equivalent i.e. the system has a three-fold degenerate ground state.
This kind of frustration can be found in so called spin ice systems. But to create a spin glass, an ingredient is missing: disorder.

1.1.2 Disorder and frustration

In the previous example the frustration was induced in a perfectly defined structure. As we saw earlier, this cannot happen in the case of a glass. Let's assume three Ising spins randomly distributed in a 2D space with a distance dependent coupling (in sign and amplitude). Then this random distribution leads to disorder and one can end up with a situation as in Fig.1.2

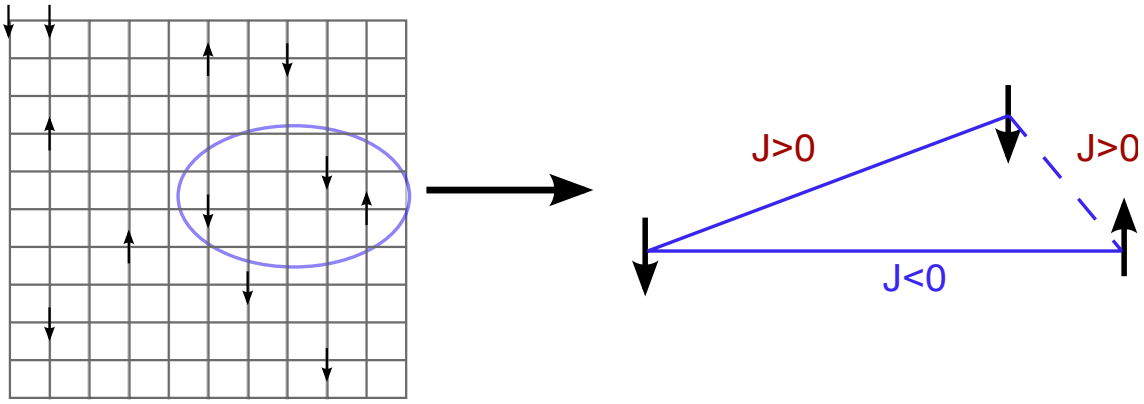

Figure 1.2: Example of frustration induced by the disorder. The spins are here placed on a lattice and are coupled with a distance-dependent interaction (sign and amplitude). If we take only the spins inside the blue elipse, we see that frustration is induced.

Now imagine billions of spins like that. On can intuitively see that, scaling up the previous example, many bonds can be unsatisfied.
It is important to stress that this kind of frustration is different from the geometrical one seen before. There is no simple way to go from one metastable configuration to another. However they can be very close in energy (if the number of unsatisfied bounds is approximately the same) and close to the lowest possible energy.
This is exactly what happens in a spin glass.

1.1.3 Canonical spin glasses

A spin glass is exactly what we defined in the previous paragraph but in 3D.
It is simply magnetic impurities (rare earth elements) *randomly* diluted in a non magnetic metallic host (noble metal) e.g. Mn diluted in Ag, or Fe diluted in Au. The magnetic moments of those atoms are coupled via the so called RKKY (Ruderman-Kittel-Kasuya-

Yosida) interaction[40, 63, 79]:

$$J_{RKKY}(r) \propto \frac{\cos(2k_F r)}{(k_F r)^3} \tag{1.1}$$

It is a long-range, indirect-exchange interaction that alternates between ferromagnetic or anti-ferromagnetic according to the distance (see Fig.1.3). The mix between the randomness in space and this RKKY interaction thus induces a magnetic frustration due to disorder!

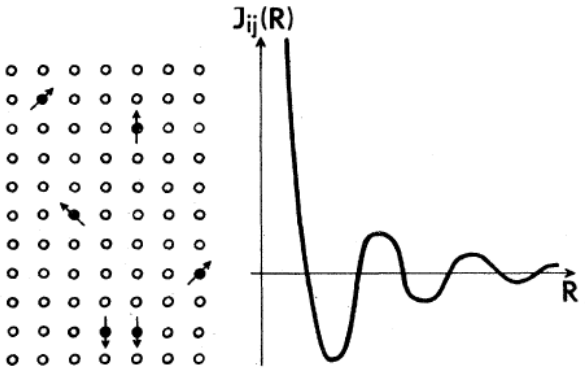

Figure 1.3: Representation of the RKKY interaction potential as a function of the distance. We see that the J_{ij} amplitude is reduced with the distance and alternates in sign.

Let's now consider the energy in such a system.
It is possible to define the mean distance $\bar{r}$ between two interacting spins and thus the mean interaction energy $< J >= J_0/\bar{r}^3$[15]. It is then possible to define a temperature $T_g =< J > /k_B$ such that, below T_g, the interaction energy becomes prominent.
At high temperature ($T > T_g$), the thermal energy $E_{th} = k_B T$ is larger than $< J >$. The spins are thus thermally activated and can flip freely. The system is in a paramagnetic phase. However, when the temperature is lowered such that $T < T_g$, they cannot flip anymore and start to organize depending on the orientation of the other spins via their interactions. They are *frozen*.
This temperature T_g is called *glass temperature* and is the equivalent, in the structural glasses, of the transition temperature between the liquid and glassy states.
Intuitively one could think that a transition should appear at $T = T_g$ as in structural glasses. But, on the other hand, the fact that we need to use a mean interaction energy could lead us to think that there is rather a smooth slow down of the dynamics, the most interacting spins freezing first followed by the less ones.
The solution is to look for the usual signature of a transition i.e. the divergence of a thermodynamic quantity at $T = T_g$. In 1972, Cannella & Mydosh were the first to find a sharp peak in the susceptibility (but surprisingly not in the specific heat!) (Fig.1.4 (a)) around the predicted glass temperature, proving the existence of a real transition between the paramagnetic phase and the glass one[19].

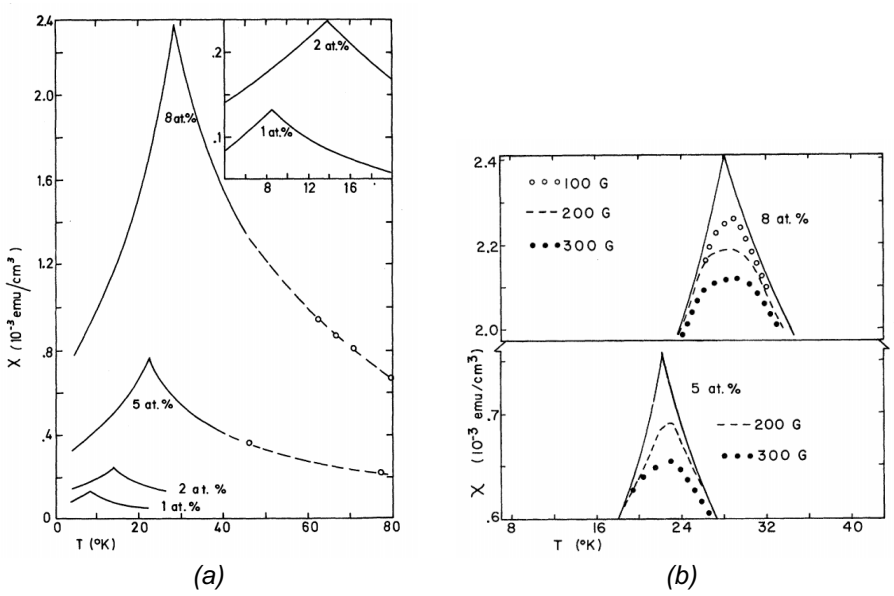

Figure 1.4: (a) Magnetic susceptibility as a function of the temperature $\chi(T)$ in AuFe for several concentration ranging from 1% to 8%. A non-diverging peak is observed and shifts towards lower temperatures as the concentration is lowered. (b) Magnetic susceptibility as a function of the temperature $\chi(T)$ in AuFe for concentrations of 8% (higher panel) or 5% (lower panel) and for different constant magnetic field applied. The peak is smoothed as the field increases but is not shifted. It has to be noted that this effect happens even for really small magnetic fields compared to any other caracteristic energy of the system. From [19].

This was the start of an intense theoretical as well as experimental work for about 30 years and that's what will be described in the next section.

1.2 Theoretical models and related experiments

1.2.1 A first approach: the Edwards-Anderson model

As seen previously, the disorder needed to create a spin-glass comes from the randomness in the spins positions. From a thermodynamic point of view, this picture leaves us with two random variables: the distance between spins r and the corresponding interaction energy $J(r)$. The first step to the understanding of this spin glass phase is to determine an order parameter. Unlike ferromagnet, there is no long-range order, and so, usual *spatial* correlations cannot be used as order parameter. In 1975, instead of that, Edwards ans Anderson (EA) had the idea to rather use an order parameter based on *time* correlations[66]. They thus define this parameter as:

$$q_{EA} = \lim_{t\to\infty} [\langle \mathbf{S}_i(0) \mathring{\mathrm{u}} \mathbf{S}_i(t) \rangle_T]_{dis} \tag{1.2}$$

with $\langle\ \rangle$ being the thermal averaging and $[\ ]_{dis}$ the averaging over the disorder. Basically it consists in observing if a spin still has the same orientation at $t = 0$ and at $t \to \infty$. For

$T > T_g$, the spin orientation is not fixed and then $q_{EA} = 0$. On the opposite, if the system is totally frozen at $T \ll T_g$, the spin configuration will be the same over the time and $q_{EA} = 1$.

Their second important idea was to transfer the randomness that lies in the position (random positionning) to the interaction parameter (random interactions) while positioning spins on a regular square lattice. This model allows then to cleverly simplify the problem by, on the one hand, taking a simple lattice but, on the other hand, introducing a non-trivial interaction parameter distribution. The interaction parameter J is thus taken with Gaussian distribution probability centred on 0 and defined by:

$$P(J) = \frac{1}{\sqrt{2\pi\Delta'^2}} \exp\left(-\frac{J^2}{2\Delta'^2}\right) \tag{1.3}$$

with Δ being the variance of the distribution.
We thus obtain the following Hamiltonian:

$$\mathcal{H} = -\frac{1}{2}\sum_{\langle i,j\rangle}^{N} J_{ij} S_i \cdot S_j + h\sum_{i}^{N} S_i \tag{1.4}$$

in which the first term corresponds to the spin-spin coupling and the second one to the effect of an external magnetic field. We stress that, in this model, only first neighbours interact.
Once one gets the Hamiltonian, it seems natural to calculate the free energy of the system via the partition function $\mathcal{Z}$ defined as

$$\mathcal{Z} = Tr(\exp\left(\frac{-\mathcal{H}}{k_b T}\right)) \tag{1.5}$$

In a usual system, the free energy is defined by

$$\mathcal{F} = -k_B T \ln(\mathcal{Z}) \tag{1.6}$$

But in the case of a spin glass, the system has a *quenched disorder* i.e. the structural disorder is fixed (the spins don't move in the sample), only the spin direction changes. Then , to average over the disorder, one has to average ln Z over the Gaussian distribution $P(J)$ of the interactions. Thus the formula for the free energy becomes:

$$[\mathcal{F}[J]]_{dis} = -k_B T[\ln(\mathcal{Z})[J]]_{dis} \tag{1.7}$$

and we end up with this calculation:

$$[\mathcal{F}[J]]_{dis} = -k_B T \int [\ln(\mathcal{Z})[J]] dP(J) = -k_B T \int [\ln(\mathcal{Z})[J]] P(J) dJ \tag{1.8}$$

which usually cannot be easily carried out due to the non-Gaussianity induced by the

logarithm.
At this point one has to use the so-called replica trick:

$$\ln \mathcal{Z} = \lim_{n \to 0} \left[\frac{1}{n} (\mathcal{Z}^n - 1) \right] \tag{1.9}$$

thus

$$[\ln \mathcal{Z}[J]]_{dis} = \lim_{n \to 0} \left[\frac{1}{n} ([\mathcal{Z}^n[J]]_{dis} - 1) \right] \tag{1.10}$$

and then for n positive, we can express $Z^n[J]$ in terms of n identical replicas of the system with the same disorder distribution:

$$\mathcal{Z}^n[J] = \prod_{\alpha=1}^{n} Z_\alpha[J] \tag{1.11}$$

where $\mathcal{Z}_\alpha$ is the partition function of the αth replica.

The integral is then easy to calculate since we replaced the logarithm by

$$[\mathcal{Z}^n[J]]_{dis} = \int P[J] \mathcal{Z}^n[J] d[J] \tag{1.12}$$

At the end of the calculation we have to take the number of spins $N \to \infty$ and $n \to 0$.

This mathematical trick, even if very common in statistical physics, was the first key to explore the glass phase and was really the beginning of the intense theoretical interest in this field.
Unfortunately, this theory led to poor results concerning the matching with experiments. Indeed, the equations are solvable only for $T \to T_g$ and $T \to 0$. It predicts well (at least qualitatively) the peak in the magnetization discussed earlier but fails, for example, to explain the effect of a small static field as seen by Cannella and Mydosh in the same experiment (see Fig.1.4(b)).
We are now facing an impasse. This theory, despite being simple and yet elegant (replacing site disorder by a Gaussian distribution of the interactions), fails to predict most of the experimental results and even predicts non-oserved effects (a peak in the specific heat). However, EA considered only first neighbour interactions while RKKY leads to a long range correlation. The solution to this impasse resides thus in establishing a true mean-field theory (i.e. consider not only first-neighbours interactions) while keeping this simple model.

1.2.2 A mean field theory: the Sherrington-Kirkpatrick model

Following this attempt, still in 1975, Sherrington and Kirkpatrick (SK) proposed the first mean-field model, based on the EA model but with infinite-range interactions[68].
Basically, the mean field approximation allows to consider only the action of an effective mean field on a spin i instead of the individual action of each other spins on it. The retroaction from the spin i to the field is not considered such that fluctuations are not taken

into account. It simplifies a N-body problem to a much easier 1-body solvable problem. Using this approximation leads to assume (unphysically) the probability distribution $P(J)$ to be the same for every spin pair no matter how far they are in reality.
In addition, SK changes slightly the form of $P(J)$ to include the possibility of ferromagnetism by introducing a mean value $J_0^{'}$ for J. Moreover, since the interactions are now assumed infinite ranged, one has to make $J_0^{'}$ and $\Delta^{'}$ intensive values. Thus we define $\Delta = \Delta^{'} \times \sqrt{N}$ and $J_0 = J_0^{'} \times N$ (with N the number of spins), leading to the new $P(J)$:

$$P(J) = \sqrt{\frac{N}{2\pi\Delta^2}} \exp\left(-N\frac{(J - J_0/N)^2}{2\Delta^2}\right) \tag{1.13}$$

If one repeats the replica trick, we end up with the following formula for the free energy (assuming no external magnetic field):

$$\begin{aligned} -\mathcal{F}/k_BT &= \lim_{n\to 0}\frac{1}{n}\left\{\exp\left[\frac{\Delta^2 Nn}{4(k_BT)^2}\right]\iint_{-\infty}^{+\infty}\prod_{(\alpha\beta)}\left(\frac{N}{2\pi}\right)^{1/2}\frac{\Delta}{k_BT}dy^{(\alpha\beta)}\right. \\ &\left.\prod_{(\alpha)}\left(\frac{NJ_0}{2\pi k_BT}\right)^{1/2}dx^{(\alpha)} \times G - 1\right\} \end{aligned} \tag{1.14}$$

with

$$\begin{aligned} G &= \exp\left[-\frac{N\Delta^2}{(k_bT)^2}\sum_{(\alpha\beta)}\frac{1}{2}(y^{(\alpha\beta)})^2 - \frac{NJ_0}{k_BT}\sum_{(\alpha)}\frac{1}{2}(x^{(\alpha)})^2\right] \times \\ &\exp\left[N\ln \mathrm{Tr}\,\exp\left[\left(\frac{\Delta}{k_BT}\right)^2\sum_{(\alpha\beta)}y^{(\alpha\beta)}S^{(\alpha)}S^{(\beta)} + \frac{J_0}{k_BT}\sum_{(\alpha)}x^{(\alpha)}S^{(\alpha)}\right]\right] \end{aligned} \tag{1.15}$$

where x and y are integration dummy variables, α and β are replica indices ranging from 1 to n, $(\alpha\beta)$ represents a couple of replicas.

From that equation SK calculated the integral using the steepest descent method to find the saddle points $y_0^{\alpha\beta}$ (with $G'(y_0^{\alpha\beta}) = 0$) . By taking $\partial G/\partial y^{(\alpha\beta)} = 0$ and $\partial G/\partial x^{(\alpha)} = 0$ we obtain:

$$y_0^{(\alpha\beta)} = \langle S^{(\alpha)}S^{(\beta)}\rangle \tag{1.16}$$

that can be identified as the order parameter previously defined q_{EA}, but with something more subtle! Indeed, it is not a comparison between the same replica at different times anymore, but a comparison between two replicas at equilibrium, that we will call ***overlap***! For $T > T_g$, the spins are continuously flipping in the two replicas and thus $y_0^{(\alpha\beta)} = \langle S^{(\alpha)}S^{(\beta)}\rangle = 0$. But for $T < T_g$, the spins in both of the replicas are frozen and $y_0^{(\alpha\beta)} \neq 0$.

Since we identified $y_0^{(\alpha\beta)}$ as the order parameter, we will rename it $q^{(\alpha\beta)}$.
Following the same reasoning, we can also find the equivalent point for $x^{(\alpha)}$:

$$x_0^{(\alpha)} = \langle S^{(\alpha)} \rangle \tag{1.17}$$

that represents the local magnetisation $m^{(\alpha)}$ and so, the order parameter between the paramagnetic and the ferromagnetic transition.

The main assumption SK made is to consider each replica as indistinguishable such that the parameters are independent of their replica indices: $q = q^{(\alpha\beta)} = y_0^{(\alpha\beta)}$ and $m = m^{(\alpha)} = x_0^{(\alpha)}$. Then taking the replica limit $n \to 0$, we obtain the so called ***replica-symmetric*** model!

Replacing those values in (1.15), one can now express the free energy in a much simpler way around this saddle point:

$$\begin{aligned} \frac{[F]_{dis}}{N k_B T} &= -\frac{\Delta^2(1-q^2)}{(2k_BT)^2} \\ &\quad + \frac{J_0 m}{(2k_BT)^2} - \frac{1}{\sqrt{2\pi}} \int \mathrm{dz}\, \exp\left(-\frac{z^2}{2}\right) \ln\left[2\cosh\left(\frac{\Delta q^{1/2}}{k_BT} z + \frac{J_0 m}{k_BT}\right)\right] \end{aligned} \tag{1.18}$$

Since $\frac{\partial [F]_{dis}}{\partial q} = 0$ and $\frac{\partial [F]_{dis}}{\partial m} = 0$, we have two auto-coherent relations:

$$q = \frac{1}{\sqrt{2\pi}} \int \mathrm{dz} \exp\left(-\frac{z^2}{2}\right) \tanh^2\left[\frac{\Delta q^{1/2}}{k_BT} z + \frac{J_0 m}{k_BT} + \frac{h}{k_BT}\right] \tag{1.19}$$

and:

$$m = \frac{1}{\sqrt{2\pi}} \int \mathrm{dz} \exp\left(-\frac{z^2}{2}\right) \tanh\left[\frac{\Delta q^{1/2}}{k_BT} z + \frac{J_0 m}{k_BT} + \frac{h}{k_BT}\right] \tag{1.20}$$

Once those equations are set, it is possible to calculate $q(T)$ and $m(T)$ and a phase diagram can thereby be established.

Moreover, since $\chi(T) = \partial m(T)/\partial h$ and we have the evolution of $m(T)$, we can obtain the susceptibility:

$$\chi(T) = \frac{[1 - q(T)]}{k_BT - J_0[1 - q(T)]} \tag{1.21}$$

We stress that in the SK model $\chi(T)$ depends on $q(T)$ and thereby on the possibly applied magnetic field!
When computed, this dependence qualitatively fits with the experimental data obtained by Cannella and Mydosch. But that's not the main success of the SK model!
In the ternary system $Pd_{1-y-x}Fe_yMn_x$, one can control the J_0/Δ parameter (J_0 and Δ being defined in eq.(1.13)), via the x and y concentration, and experimentally retrieve a phase diagram as a function of the temperature and J_0/Δ. And, impressively, it turns out to be the exact same image than the one predicted by SK (show in Fig.1.5) with even the para $\to$ ferro $\to$ spin glass transition!

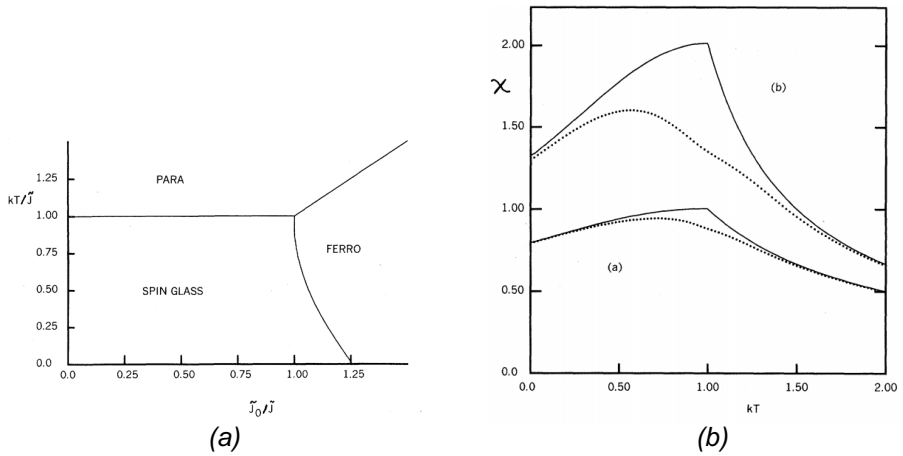

Figure 1.5: (a) Phase diagram obtained by SK with their model as a function of the temperature and J_0/Δ parameter. This phase diagram is exactly the same than the one obtained experimentally. (b) Magnetic susceptibility curves obtained theoretically as a function of the temperature $\chi(T)$ for $J_0/\Delta = 0$ and $J_0/\Delta = 0.5$ (up curve and low curve respectively). The dashed lines are the one obtained for a constant magnetic field of $h = 0.1\Delta$ applied. The smooth of the curve observed experimentally when a magnetic field is applied is qualitatively retrieved. From [68].

However, once again, SK predicts a cusp in the specific heat which is not observed experimentally and, more problematically, a negative entropy is predicted at zero temperature. This leads, of course, to question the limits of the SK solution validity.

1.2.3 The instability of the SK solution: a step towards (even more) complexity

In 1978, de Almeida and Thouless (AT) studied in detail the SK solution and showed that it is stable above T_g no matter the conditions, but is deeply unstable in the ferromagnetic and spin glass phases[5]. Indeed, in the SK solution, the susceptibility becomes negative at low temperature, being completely at odds not only with experiments but also with correlation-function susceptibility, defined positive. AT thus defined a line called AT line, in the B-T plane, separating the region in which SK is stable from the one where it is unstable (see Fig.1.6).

AT showed that this instability comes from the the last choice of SK in their model viz. the symmetric solution $q = q^{(\alpha\beta)} = y_0^{(\alpha\beta)}$ and $m = m^{(\alpha)} = x_0^{(\alpha)}$. Taking this assumption leads to an invalid solution to the mean-field model even if above the AT line the SK solution seems valid.
From that statement, the only choice left to describe the low-temperature phase is to find a solution in which the replica symmetry is broken.
This new solution was developed in 1979 by Giorgio Parisi and is called the ***Replica Symmetry Breaking*** (RSB) solution!

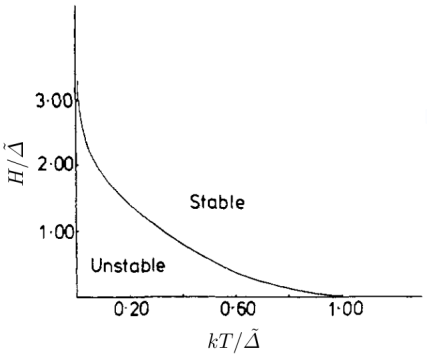

Figure 1.6: Diagram showing the AT line separating the stable zone from the unstable one for the SK solution. This diagram is taken for $J_0 = 0$ and inthe case of an applied magnetic field H. From [5].

The Parisi solution: Breaking the replica symmetry

After multiple attempts in finding a good solution that would break the replica symmetry, Parisi finally proposed the breakthrough[60] which has been eventually found as the good solution to this problem (at least in the mean field limit[32, 70]).
Since he does not take the assumption that every $q^{(\alpha\beta)}$ are equivalent, the order parameter now becomes a matrix M whose dimension is $(n \times n)$ with n the number of replica.
The idea of Parisi is to perform several operations on that matrix according to the so called *Replica Symmetry Breaking* protocol. Let's have a look at it, step by step:

$$M = \begin{bmatrix} \overbrace{\begin{bmatrix} 0 & q_1 & q_1 & q_1 \\ q_1 & 0 & q_1 & q_1 \\ q_1 & q_1 & 0 & q_1 \\ q_1 & q_1 & q_1 & 0 \end{bmatrix}}^{m_1} & \begin{matrix} \\ \\ q_0 \\ \\ \end{matrix} \\ \begin{matrix} \\ \\ q_0 \\ \\ \end{matrix} & \begin{bmatrix} 0 & q_1 & q_1 & q_1 \\ q_1 & 0 & q_1 & q_1 \\ q_1 & q_1 & 0 & q_1 \\ q_1 & q_1 & q_1 & 0 \end{bmatrix} \end{bmatrix} \Bigg\} n$$

Figure 1.7: The matrix M after a one-step RSB procedure. The matrix is cut into blocks of size $(m_1 \times m_1)$ (one-step RSB). The diagonal blocks are then filled with a new value q_1 (except for diagonal values set at 0) replacing the previous value q_0. The values in the off-diagonal blocks remain unchanged with the value q_0. Here, n=8 and m_1=4

One-step RSB First, one has to consider the previously defined $n \times n$ matrix M filled with q_0 (i.e $q^{(\alpha\beta)} = q_0 \; \forall(\alpha,\beta)$, the SK solution). Now we will start breaking it. In the RSB procedure, Parisi take that matrix and divide it into blocks of size $(m_1 \times m_1)$ with , of course, $1 \leq m_1 \leq n$. In the blocks along the diagonals, q_0 is replaced with a new value q_1 while the off-diagonal blocks remain unchanged with value q_0. In this configuration one

can define a distribution $P(q)$ that is the fraction of elements with value q over the total number of elements.
An example is showed in Fig.1.7 with $n = 8$ (i.e. a 8×8 matrix). After one step with the RSB procedure (taking $m_1 = 4$), we end up with a new matrix and $P(q) = \frac{n-m_1}{n-1}\delta(q - q_0) + \frac{m_1-1}{n-1}\delta(q - q_1) = P(q_0) + P(q_1)$ with $P(q_0) = \frac{32}{64} = \frac{1}{2}$ and $P(q_1) = \frac{32}{64} = \frac{1}{2}$.
At this point, it has to be noticed that n is still a positive integer and that we have now to take the replica limit $n \to 0$. The previous relation $1 \leq m_1 \leq n$ is then 'turned around' in this limit and becomes $1 \geq m_1 \geq 0$.
We end up with three parameters for the matrix, namely q_0, q_1 and m_1, that all have to fulfil the auto-coherence relations of equilibrium (exactly as in the steepest descent method) i.e $\frac{\partial[F]_{dis}}{\partial q_0} = 0$, $\frac{\partial[F]_{dis}}{\partial q_1} = 0$ and $\frac{\partial[F]_{dis}}{\partial m_1} = 0$.
One can now calculate the new entropy at T=0 and, unfortunately, still find a negative entropy BUT a bit less than in the SK solution! This encouraged Parisi to repeat this procedure several times[57]!

full-step RSB Let's call K the number of RSB-steps performed on the matrix. For K=2, we divide again the m_1-sized blocs in smaller blocs of size $1 \leq m_2 \leq m_1 \leq n$. Again the non-diagonal blocs remain unchanged while, in the diagonal ones, a new value q_2 is introduced. In fact, for any K, $1 \leq m_K \leq m_{K-1} \leq ... \leq m_1 \leq n$ (with $m_0 = n$ and $m_{K+1} = 1$) and we have $(K+1)q_i$ ranging from q_0 to q_K.
From the previous definition, one can extend the formula for $P(q)$ to larger matrices:

$$P(q) = \frac{1}{n-1}\sum_{i=0}^{K}(m_i - m_{i+1})\delta(q - q_i) \tag{1.22}$$

So when one takes the replica limit $n \to 0$, we end up with:

$$P(q) = \sum_{i=0}^{K}(m_{i+1} - m_i)\delta(q - q_i) \tag{1.23}$$

And since $P(q)$ is defined positive, we have to, as previously, 'turn around' the relation on the m's to $1 \geq m_K \geq m_{K-1} \geq ... \geq m_1 > 0$.

When K becomes very large, one can see that the value q_i becomes *continuous* (since we have many values q_i between 0 and 1), and one can rewrite it in a most convenient way as a function:

$$q_i = q(x) \qquad if \qquad m_i \leq x \leq m_{i+1} \tag{1.24}$$

Studying numerically the previously described equation used to find the saddle points $q^{(\alpha\beta)}$ and $m^{(\alpha)}$, one can assume that q_i form an increasing function such that $q_{i+1} > q_i$.
Eventually we have to get to the limit $K \to \infty$.
Now $q(x)$ is an increasing continuous function and , extending the equation 1.23 to

$$M = \left[\begin{array}{cc} \overbrace{\begin{bmatrix} \begin{bmatrix} 0 & q_2 \\ q_2 & 0 \end{bmatrix} & q_1 & q_1 \\ q_1 & q_1 & \begin{bmatrix} 0 & q_2 \\ q_2 & 0 \end{bmatrix} \\ q_1 & q_1 & \end{bmatrix}}^{m_1} & q_0 \\ q_0 & \begin{bmatrix} \overbrace{\begin{bmatrix} 0 & q_2 \\ q_2 & 0 \end{bmatrix}}^{m_2} & q_1 & q_1 \\ & q_1 & q_1 & \\ & q_1 & q_1 & \begin{bmatrix} 0 & q_2 \\ q_2 & 0 \end{bmatrix} \end{bmatrix} \end{array}\right] \Bigg\} n$$

Figure 1.8: The matrix M after two steps with the RSB procedure. Compared to Fig.1.7, the diagonal blocks are cut again into blocks of size $(m_2 \times m_2)$ and the ones on the diagonal are filled with a new value q_2 replacing q_1. The rest of the matrix remains unchanged with values q_0 or q_1 . Here, n=8, m_1=4 and m_2=2

continuous q_i's, one can show that:

$$P(q) = \frac{\mathrm{d}x(q)}{\mathrm{d}q} \qquad with \qquad q(x(q)) = q \tag{1.25}$$

This approach with $K \to \infty$ is called ***the full-step RSB*** and solves many problems in the SK solution: it suppresses the low temperature negative entropy (we recover $S(T = 0) \to 0$) and it captures well the susceptibility behaviour without peak in the specific heat[58]!
But beside those nice achievements, one has to note that we end up with a continuous order parameter q ranging from 0 to 1[59]. It is totally at odd with usual phase transitions where the order parameter is either 0 or 1!

1.2.4 Physical interpretation of the RSB solution

For now we've been talking only in terms of matrices, calculus and formula. But what about the physical meaning of all this?
When we defined the order parameter $q^{(\alpha\beta)}$ we didn't really give it a physical signification. We named it overlap, but what does it mean? If we look at the formula, it basically represents how different the spin configuration of a given replica is from another. In the SK solution, all the replicas are taken **equivalent** and this assumption is crucial in understanding the physical implications of this solution. First of all, we used the work 'replicas' for quite a while without giving to this term any physical meaning other than just a mathematical artefact.
In 1983, Parisi had the idea to start from a physical point of view to find a new order parameter for a spin glass revealing that q_{EA} is not a good one since it can be non-zero also for ferromagnet and not only for spin glasses. The spin glass order parameter $q_{\alpha\beta}$

proposed by Parisi [1] is then

$$q_{\alpha\beta} = \frac{1}{N}\sum_{i=1}^{N} m_i^{\alpha} m_i^{\beta} \tag{1.26}$$

which is the overlap of the magnetization between two states.
Using arguments about the magnetic susceptibility, Parisi proved that this physical order parameter is **exactly** equal to the one in the RSB model in the replica limit!
This calculation proves that the so called ***replicas are in reality the different ground states*** of the system.
In fact, on a more physical way, one can see a replica as being the same system but heated up over T_g and then cooled down again such that both replicas are in the same conditions[48]. For SK, it means that every replica taken in the spin glass phase is equivalent to any other, meaning any spin configurations taken below T_g is energetically equivalent at equilibrium[2] **without any particular relations** between them. One can then see that behind this assumption, just taken to easily calculate the free energy, stands a really deep assumption on the nature of spin glasses themselves:
In the SK solution, there are several equivalent degenerated ground states in which the system eventually falls!
This is the classical picture of a phase space in which potential wells are more or less deep and one of them is the ground state. But we've already discussed that this solution doesn't match with experiments or even with simple physical intuition (cf. the negative entropy). Parisi then proposed to break this replica equivalence, and this leads to reconsider the previously defined structure of the phase space.
By breaking the replica symmetry, Parisi indirectly destroyed the idea of equivalent ground states in the low temperature phase. But with what kind of phase space did he replace this picture? As done previously, just wonder about the meaning of the Parisi order parameter. In the RSB, $q^{(\alpha\beta)}$ is given with a probability distribution. If we stick to the previous picture of replicas, it means that, in the same conditions (same sample, same temperature) two cool-downs can lead to many different equilibrium states **with particular relations between them**. Indeed, since $q^{(\alpha\beta)}$ is taken between 0 and 1, it means that some states are 'closer' (their spin configuration is not so different) while some other are 'further'. For example if $q^{(1,2)} > q^{(1,3)}$, the states 1 and 2 are closer than the states 1 and 3.
Even if the words 'closer' or 'further' are used here in a figurative way, it is in fact possible to define a value $d_{\alpha\beta}$ representing a true (from a mathematical point of view) distance between two states:

$$d_{\alpha\beta} = 1 - q_{\alpha\beta} \tag{1.27}$$

So, if two configurations are the same, $q_{\alpha\beta} = \langle S^{(\alpha)} S^{(\beta)} \rangle = 1$ (the overlap is maximal) and $d_{\alpha\beta} = 0$. The distance is then null and the states are identical!

1 Be careful, this is a priori different from $q^{(\alpha\beta)}$
2 In reality they are the same for $T = 0$. For $0 < T < T_g$, the thermal energy activates some spins and prevent the two states to be exactly the same, even if they are really close! That's the reason why $q \neq 1$ at $T \neq 0$.

Surprisingly, one can also show that the probability $P'(q)$ of having the overlap $q_{\alpha\beta} = q$ given by:

$$P'(q) = \sum_{\alpha\beta} P_\alpha P_\beta \delta(q_{\alpha\beta} - q) \tag{1.28}$$

(where we sum over all the equilibrium states and P_α and P_β are the probability to fall in the α and β states respectively) is exactly the same than the previously defined $P(q)$ if averaged over the disorder!

It is now clear that here lies the deep and non-trivial interpretation of the RSB. We've showed that the totally mathematical definition of the replicas is not only an identification for some equilibrium states characteristics, but it represents **fully** those physical states (or 'energy valleys' in phase space, or even 'spin configuration' according to your preferential denomination)!

One could say that the answer to how the system looks like is not yet given. It is true. Even if we now know exactly where to look for. We said before that the main difference between the SK and the Parisi solution is in the way of considering the replicas: symmetric or not. For $T > T_g$, the SK solution is stable and both solution are identical: $P(q)$ is just a delta function centred on zero (paramagnetic phase). Below T_g things are different. In the RSB, $P(q)$ is now a symmetric function with maximum values on $-q_m$ and q_m (it is even possible to show that $q_m = q_{EA}$ the order parameter for Edwards and Anderson) but can take any value between them as pictures in Fig.1.9

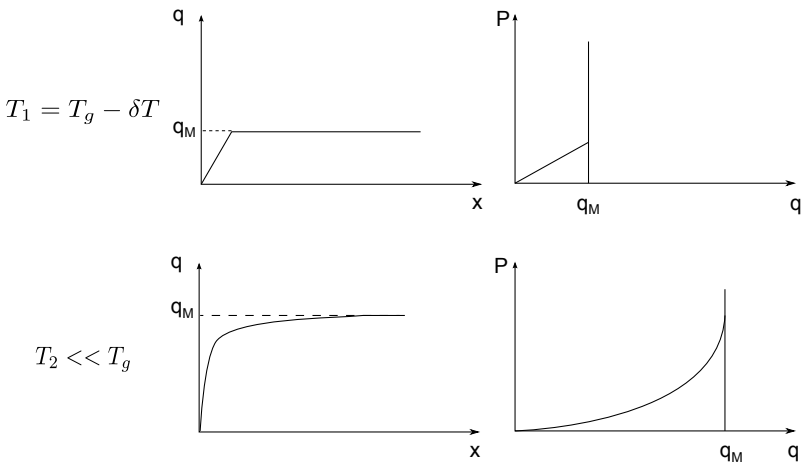

Figure 1.9: Representation of the $P(q)$ for two temperatures at zero magnetic field. From [50].

This $P(q)$ also depends strongly on the temperature. Indeed, when the temperature is decreased, q_m increases and

$$\lim_{T \to 0} q_m = 1$$

meaning that the new created states at low temperature are closer to each other.

This peculiar dependence on temperature is really at the heart of the understanding of

the spin glass phase as described by the RSB scheme. When the temperature goes from $T_1 > T_g$ to $T_2 < T_g$, the picture of the phase space changes. We move from a paramagnetic phase where there is just one energy valley to a more complicated phase space in which the replicas are broken: the phase space is fragmented in multiple valleys with overlap q_0 . If the temperature is again lowered, it corresponds to break even more the replicas (more steps in the RSB procedure), meaning that the valleys break into sub-valleys whose overlap between them is q_1 (we remind here that $q_1 > q_0$). As long as the temperature decreases the valleys continue to subdivide into sub-valleys with higher overlap. One of the most striking consequence of this behaviour is that, despite the total absence of order in the system, the phase space is ordered in a ***ultrametric*** way i.e. the fragmentation of the valleys is hierarchical[51]!
This particularity can (almost) easily be explained with the above-defined distance $d_{\alpha\beta}$. let's take three states α, β and γ. Then for $T < T_g$,

$$d_{\alpha\beta} \leq \max(d_{\alpha\gamma}, d_{\gamma\beta}) \tag{1.29}$$

which leads, for the overlap, to

$$q_{\alpha\beta} \geq \min(q_{\alpha\gamma}, q_{\gamma\beta}) \tag{1.30}$$

Even though the mathematical formalism is important, another way of visualizing it is to represent the ultrametric hierarchy of states as a 'reverse family tree' as pictured in Fig.1.10.

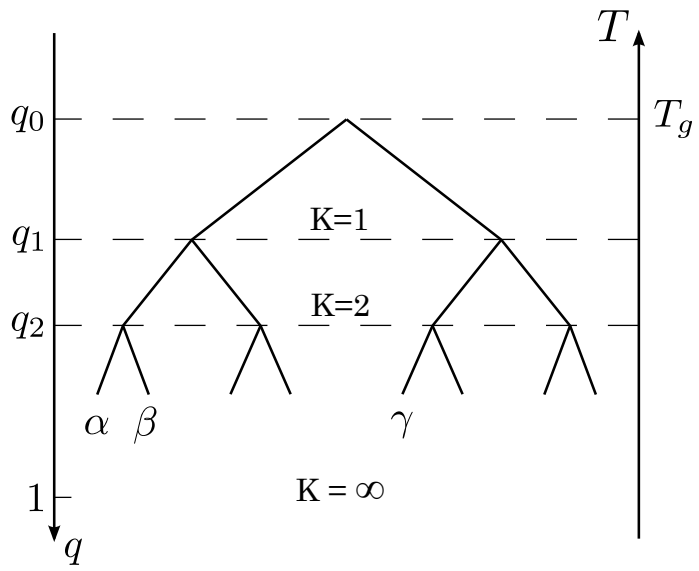

Figure 1.10: Representation as a tree of the hierarchical structure of the spin-glass phase space.

The replica breakings are represented by branches splitting into several new branches.

To determine the overlap between states, one needs to find their 'closer common ancestor'. Let's note that, if T stays stable, two branches cannot cross and then, even if the states are degenerated in energy, the system cannot pass from one state to another.

This mean-field theory, wich has be proven to be the right one in infinite dimensions (true mean-field), exhibits astonishing properties. Among them, the ability to define a distance between states, a hierarchical (here ultrametric) structure of the energy landscape or even a continuous order parameter. Moreover, it describes quite well the magnetic properties of the system.
However, we can see two major weaknesses in this solution. The first one is that it is proved to be right ***only*** in infinite dimensions! So what is the upper critical dimension? And, more important, is it superior to 3? If it is the case, this theory and experiment can be totally decorrelated...
The second one lies in the fact that we have no clues about the dynamics of the system. Indeed this formalism is made for states ***at equilibrium*** and nothing is said about the vitrification itself despite the numerous experiments revealing strong dynamical behaviours in spin glasses.
This lack of informations about dynamics led some other theoreticians to imagine another angle of attack. They tried to give a phenomenological picture of the spin glass phase instead of a microscopically based theory.

1.2.5 Scaling theories

Alternative theories rose from those weaknesses. For example, in the middle of the 80's, Fisher and Huse proposed a new theory to explain the spin glasses behaviour: the droplet model[26, 27]. In their theory, they take the same formalism than Edwards and Anderson, i.e. a regular lattice with random bonds between first neighbours but consider that all the behaviours in the spin glass phase comes from the excitations of a **unique** ground state at zero temperature. This ground state is defined as a unique spin configuration Γ and its energetically equivalent symmetric $\overline{\Gamma}$ in which every spins are flipped on the other direction.
Let's take a ferromagnetic case for simplicity.
For Fisher and Huse those excitations correspond to thermally activated flipping of *compact* groups of spins of size L(later called 'domains' or 'droplet'), containing L^d spins (d being the dimension). One can see that those excitations will create tensions on the interface with the rest of the sample, then requiring some energy ΔE to be created. Since the dimension of the interface is $d-1$ one can express the energy needed by

$$\Delta E \sim \gamma(T) L^{d-1} \tag{1.31}$$

where $\gamma(T)$ represents the interfacial tension coefficient.
If $d-1>0$, the system will need more energy for large domains and thus this flipping is not favoured. The ordered phase is then preserved for a finite temperature. In the opposite, if $d-1<0$, even the smallest energy fluctuation will allow to create a flipped domain.

The ordered ferromagnetic phase is then destroyed except at zero temperature.
In this system, the lower critical dimension is then 1: for $d < 1$, no transition can exist for $T \neq 0$.

Now, come back to the spin glasses case.
It is pretty similar to the ferromagnetic case. However, in our case, we have frustration and disorder that can make the droplet shape really complicated as seen in Fig.1.11 [1].

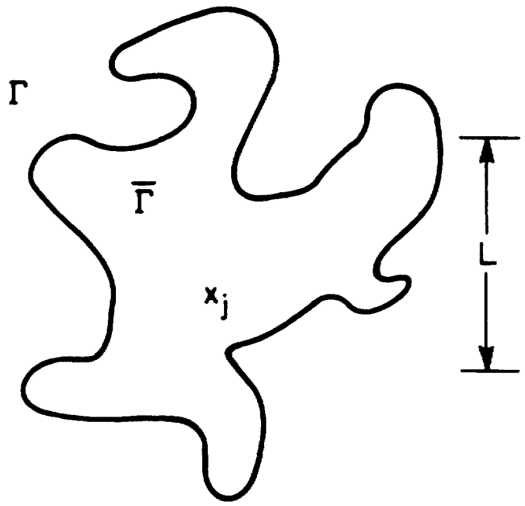

Figure 1.11: Representation of a droplet as in the Droplet theory, taken as fractal.

The number of spins at the border is then not L^{d-1} and, instead, the energy grows with L^θ with $\theta \leq (d-1)/2$. The equation 1.31 becomes:

$$\Delta E_{sg} \sim \gamma(T) L^\theta \tag{1.32}$$

One can thus see that if $\theta < 0$, no transition can exist and if $\theta > 0$, a finite temperature transition is possible. Numerical calculations gave $\theta \approx -0.29$ for $d = 2$ and $\theta \approx 0.19$ for $d = 3$, showing that a spin glass transition is possible only for $d = 3$[33].
We stress that this model is set for one specific assumption: short-range interactions for Ising spins.

One can see that the strength of this model is to propose a dynamical behaviour in the spin glass phase with this flipping process, i.e. the creation and destruction of those droplets. As said before, one assume the droplets to be created by thermal fluctuations, and so the dynamics are governed by droplets whose creating energy ΔE_{sg} is below $k_B T$.

1 Fisher and Huse even infer that it is fractal

Droplets of size L are then given a relaxation time

$$\tau_r = \tau_0 \exp\left(\frac{B_L(T)}{k_B T}\right) \tag{1.33}$$

with $B_L(T) = B_0(T)L^{\psi}$ representing the height of the energy barriers the droplet has to pass to relax, $\theta < \psi < d-1$ an independent exponent, and τ_0 a relaxation time constant. Equivalently, a creation or relaxation process on a time scale t involves a droplet of size

$$L_r = \left(\frac{T}{B_0}\ln\left(\frac{t}{\tau_0}\right)\right)^{\frac{1}{\psi}} \tag{1.34}$$

It is even possible to qualitatively account for famous experiments as the one made by E.Vincent et al. in 1997 about ageing[69]. In this experiment, a AgMn spin glass sample is studied through magnetization measurement. The protocol consists in three steps as explained in Fig.1.12

The first one is to cool down the sample from $T_1 > T_g$ to a temperature $T_2 < T_g$ with a small magnetic field h being applied. Then, h is maintained during a waiting time t_w while the system is at T_2: this is step 2. And, finally, after t_w, the magnetic field h is cut and magnetization M is measured over time. Results are displayed in Fig.1.13.

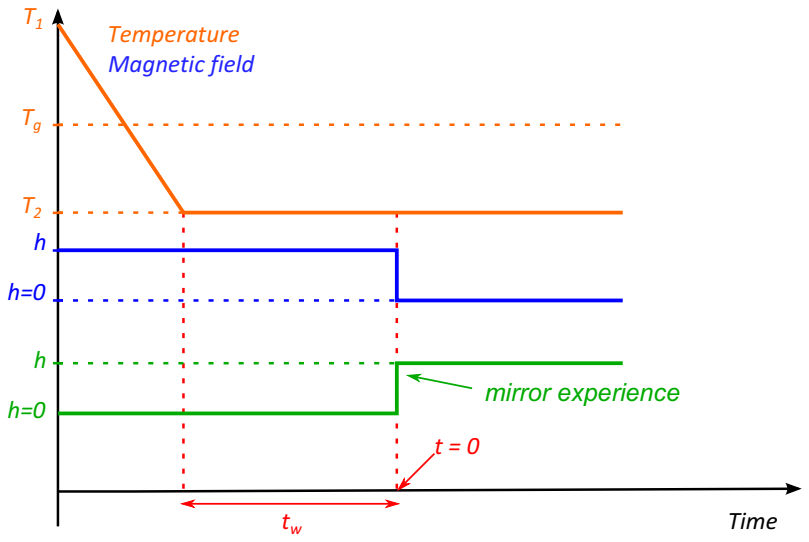

Figure 1.12: Experimental protocol for ageing experiment. The temperature is first lowered from $T = T_1 > T_g$ to $T = T_2 < T_g <$ under a magnetic field and we wait during a time t_w. The field is then shut down and the magnetization is recorded.

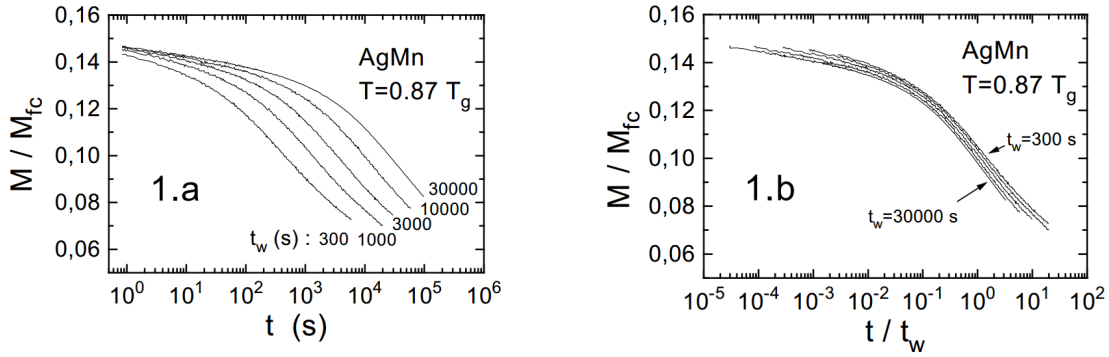

Figure 1.13: 1.a Recorded measurement of the magnetization as a function of time after the ageing experiment protocol. 1.b Same data but with the time being normalized by t_w. We see that data almost superimpose and have the same inflexion in their slope for $t \approx t_w$. From [69].

The magnetization is normalized with the magnetization M_{FC} measured when h is applied. We clearly see that the relaxation of M is strongly dependant on the waiting time t_w. As t_w is increased, the relaxation gets slower: this behaviour is called *ageing*!
This phenomenon can be seen as the glass becoming 'stiffer' over time i.e. it reaches a more stable energy state. Thus, if the external conditions change, the system will have more difficulties to get out of this stable state, inducing an evolution on longer time scales. Moreover, the scaling on t_w,pictured on the right panel of Fig.1.13, shows a sudden change in the slop around $t \approx t_w$. An explanation was given by Lundgren[46] observing that this relaxation is unusual in the sense that it is slower than a simple exponential. This consideration led him to conclude that it could be the result of several relaxations with different time scales.
And here comes the droplet interpretation. When we wait for a time t_w, the size of the droplets involved in the dynamics is $L_{t_w} \propto \ln(t_w)$ as seen in eq.(1.34) . So when the field is stopped the system will relax to another equilibrium state. However, at time $t < t_w$, only small sized droplets can flip, resulting in small changes since the larger droplets governing the magnetization are still making the system 'stiff'. But, as time increases and finally reaches the limit $t \geq t_w$, the domains involved in relaxation become greater than the one created previously while waiting, and replace them: the previous spin configuration is then 'erased'. The relaxation is then no more affected by the 'rigidity' created during t_w. This behaviour cannot be explained by the Parisi mean-field theory whereas the droplet model is powerful in explaining such experiments.

So if this model can explain features that the mean field theory cannot, why isn't it the only one in the community?
Actually, it has several important defaults. The first (and probably main) comes from a simple argument from Imry[35]: the magnetization M scales as $N^{1/2}$ in a disordered magnetic sample, meaning that, since N evolves as L^d, we get $M \propto L^{d/2}$. If a field is applied, the spins may align to the field and the free energy is then reduced by a factor

$L^{d/2}$. The stability condition for a spin glass is, since the interface energy still goes as L^{θ}: $(d/2) < \theta$. However, we've seen earlier that $\theta \leq (d-1)/2 \leq d/2$ leading to the conclusion that the stability condition can never be satisfied. In other words, the spin glass state *cannot subsist under any magnetic field* in the droplet model.
This limitation can be overcome by another simple argument. Close to the transition, it is possible to determine $\tau_L(h)$, the relaxation time of a droplet of size L under field through scaling arguments. If the observation time t_{obs} is small compared to $\tau_L(h)$, the system *appears* to be frozen even if not! Equivalently, one can say that there exist a field $h(t_{obs})$ below which the system seems to be frozen for the observer. But we should stress that this kind of glassy 'transition' is a dynamical effect and not at all a thermodynamic one.

1.2.6 Spin glasses: an experimental overview

For now we spoke about theory but also about some related experiments that fitted with it.
But unfortunately, there exists many famous experiments that are not explained by any theory but provides us with many peculiar properties of the spin glasses. Those one might not be explained but are much than worth to present!

Frequency dependence In 1981, Mulder[49] made a similar experiment than the one made by Cannella and Mydosh in 1972, namely he measured the susceptibility in a CuMn spin glass. In his case, he determined the susceptibility with different measure frequency. It is most of the time unnecessary since there is no dependence in usual magnetic transitions. However in spin glasses it is!
Surprisingly, the position of the maximum is clearly dependent on the measure frequency as can be seen on Fig.1.14.

Of course this moving peak is in contradiction with the idea of a real phase transition. However we can see that this dependence remains small and ,finally, it is smaller and smaller as frequency is decreased. Then, T_g is usually defined as $T_g = \lim_{\omega \to 0} \max \chi'(\omega)$. This behaviour is explained by the fact that several relaxation times are present in a spin glass and thus a time dependence in measurements are expected.

Irreversibility induced by small magnetic fields We presented earlier that the susceptibility peak is smoother with even small magnetic fields. But we are not done yet!
We have first to define two experimental protocols: -Field cooled (FC) protocol: a magnetic field h is applied all long during the measurement starting from above T_g. The susceptibility is measured when cooling down the sample
-Zero field cooled (ZFC) protocol: the sample is cooled down below T_g and only then is applied the magnetic field h. The susceptibility is measured by heating up the sample.

The results obtained by Nagata in 1979 for both protocols[52] are displayed on Fig.1.15. For $T > T_g$ both susceptibility curves are perfectly superimposed. However, for $T < T_g$, in a FC protocol χ reaches a plateau while in the ZFC protocol, we recover the previously observed peak around T_g as T is lowered!

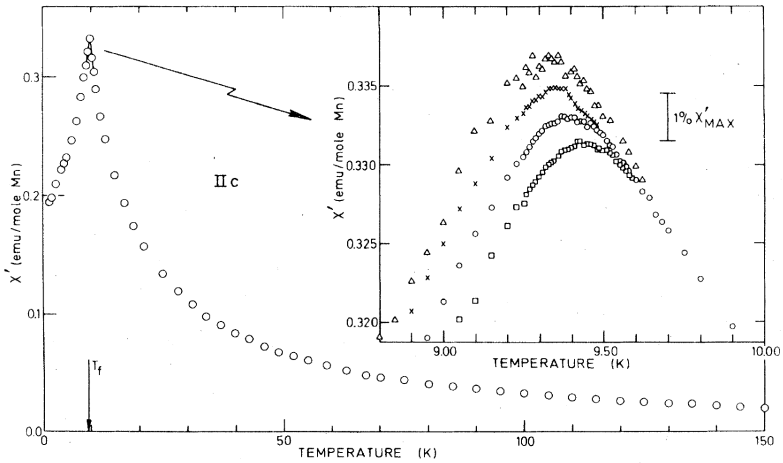

Figure 1.14: Real part of the magnetization in CuMn as a function of the temperature $\chi^{'}(T)$ with 1% of Mn. The panel shows the same measurement for different AC frequency: as the frequency is increased, the pic gets smaller, larger and shifts towards higher temperatures (the frequency displayed here are 2.6 Hz (△), 10.4 Hz (×), 234 Hz (○) and 1.33 kHz (□)). From [49].

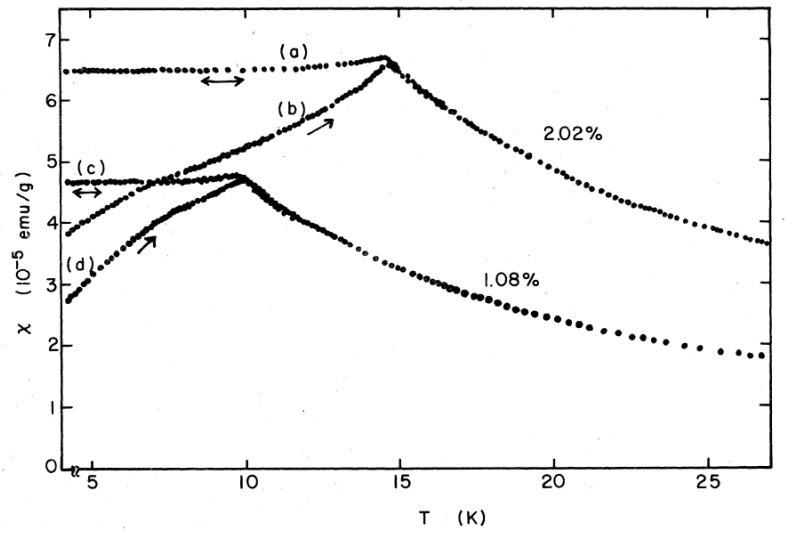

Figure 1.15: Magnetic susceptibility as a function of the temperature $\chi(T)$ in CuMn samples for doping contents of 1.08% and 2.02%. For curves (b) and (d) no external magnetic field applied during the cool down (ZFC procedure), then the susceptibility is recorded heating up under a field of 6G. For the curves (a) and(c), the sample is cooled down under a field of 6G (FC procedure) and the curves are recorded heating up. A strong irreversibility is observed just by applying 6G, which is remarkable. From [52].

It has to be noted that this effect is visible even with $h \approx 5$ Gauss, which is far below any energy scale of the system.

Temperature-based effects: memory and rejuvenation Those strange effects are not only shown by manipulating the field but also the temperature.

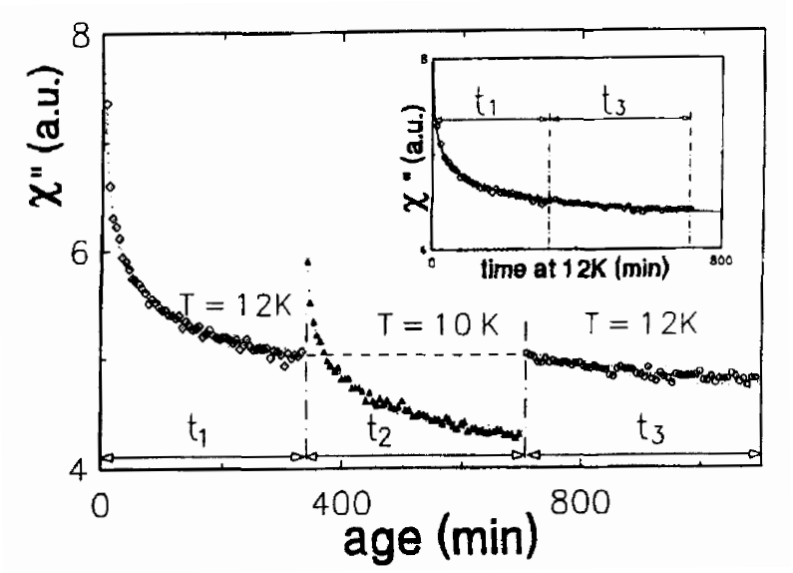

Figure 1.16: Imaginary part of the magnetic susceptibility as a function of time χ''. We observe a relaxation when the sample is brought to T=12K. When it's set to T=10K, the precedent relaxation stops and a new one restarts from the beginning as if the system never relaxed before: this is rejuvenation. However, as shown in the insert, when taken back at T=12K, the system resumes its relaxation from exactly the same point it was interrupted precendently: this phenomenon is called memory. From [69].

Indeed, by changing suddenly the temperature from $T_1 = 12K < T_g = 16.7K$ to $T_2 = 10K$ and coming back to T_1 (as presented in Fig.1.16), Lefloch and al.[69] highlighted the existence of rejuvenation and memory in spin-glasses. The ***rejuvenation***, in this context, can be seen in the transition from T_1 to T_2. The out of phase measured susceptibility is relaxing while staying at T_1 (it 'ages') but, when we suddenly change the temperature, the susceptibility jumps up! This is unexpected since the thermal energy is lower and thus, one would expect a simple slowing down of the relaxation. This appears like if the system had never relaxed before coming at this temperature, like if it hadn't aged: it is young again!
The second (even more) stunning effect appears when the sample is brought back to T_1. As seen just previously, changing the temperature seems to 'erase' the system history. However, if one comes back to an already visited temperature, the relaxation restarts exactly where it stops at the first visit. In the inset of Fig.1.16, it is very clear: there is no discontinuity when one aggregates the two curves taken at $T = 12$ K. The system

'remembers' it already relaxed in this state: it is a ***memory*** effect!

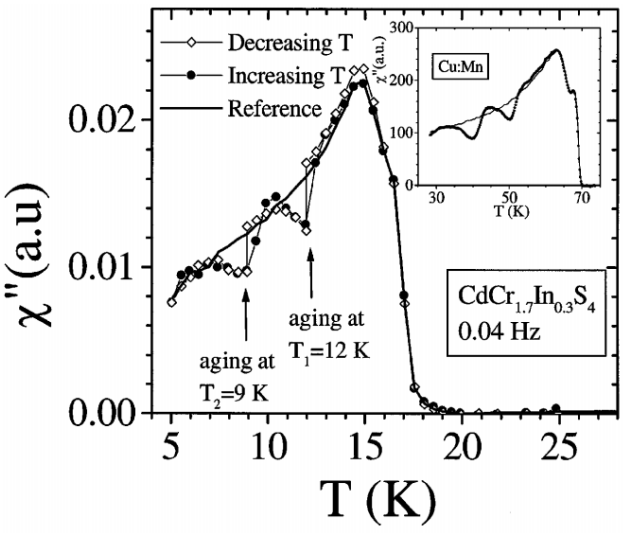

Figure 1.17: Imaginary part of the magnetic susceptibility as a function of time $\chi^{''}$. In this experiment the sample is cooled down from 25 K to 5K with two stops at $T_1 = 12K$ and $T_2 = 9K$. The system thus ages at those temperatures creating deeps in the data compared to the reference. When brought back from 5K to 25K **without** stops, the curves still follow the deeps created when cooled down. The system remembers it passed through two distincts stops and relaxed. This is called double-memory. From [39].

One can then wonder if this memory is valid for several temperature. The answer has been given by Jonason[39] and is pictured in Fig.1.17. In this experiment, we have three parts. In the first one, the sample is warmed up at a fixed rate of 0.1 K.min^{-1} from T= 5 k to 25 K. The resulting out of phase susceptibility is in solid line. The second part consists in decreasing the temperature at the same rate until $T_1 = 12$ K, where the cool down is stopped for a time t_{w1}. The sample then 'ages' at T_1 for a time t_{w1}, resulting in a relaxation of χ''. Then we continue cooling down until $T_2 = 9$ K where we wait during a time t_{w2} before cooling again to 5K.
And here comes the interesting third part. The system is warmed up ***continuously*** from 5 to 25 K and, despite this, the measurements follow perfectly the dips experienced at T_1 and T_2 when cooled down, even with the same amplitude! We can then conclude than the system remembers two successive ageing. The inset shows the same experiment for another spin-glass material (here CuMn), proving that this property is shared by every spin-glass.

1.3 Conclusion

In this section we have presented the main theories and experiments related to spin glasses. As we saw, this field has been at the centre of intense research both theoretical and experimental but those works leave us with many open questions.
On the one hand we have a mean field theory developed by EA, sophisticated over the years

by EA and finally Parisi, and on the other hand, a phenomenologically based scaling theory namely the droplet theory developed by Fischer and Huse. Even if some experiments tends to point at one or the other theory, both of them have forces and weaknesses that make difficult to decide among them.

The mean field theory predicts a phase space with a specific hierarchical order (ultrametric) composed of many states. Moreover the order parameter developed corresponds to the overlap between those states and, in relation with the ultrametricity, is continuously distributed between 0 and 1. Concerning the transition, it is always possible even with an applied magnetic field. However this theory is valid only in infinite dimension and for states at equilibrium.

The droplet model, on the opposite, is valid in dimension 3 and introduce well dynamical effects explaining some experiments. This theory, though, allows no spin glass state to survive when a magnetic field is applied. The order parameter is here much more simple and usual since it has only one value q_{EA} representing the fact that there is only one unique ground state.

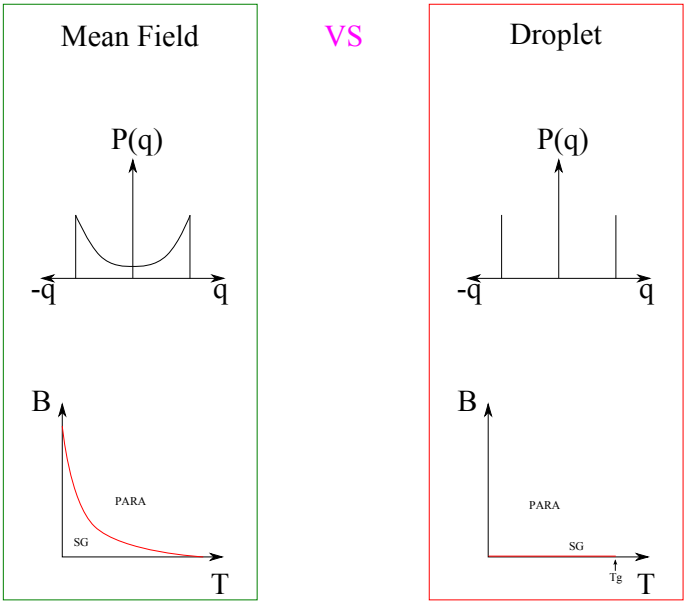

Figure 1.18: Comparison of the distribution for $P(q)$ and Paramagnetic-spin-glass transition line in the mean field model and droplet one. In the mean field model, $P(q)$ is continuous in between $-q$ and $+q$ because of the multiple ground states predicted, whereas it is only either $-q$ or $+q$ in the droplet model since only two ground states are available at equilibrium. Moreover, on the one hand, the mean field model predicts a transition line even with a magnetic field while, in the other hand, the droplet model tells us that a spin-glass state cannot exist under any magnetic field.

The main issue in the spin glass problem is to find an observable in order to chose

between both theories. As seen before, measuring the overlap q directly would give clear informations! However this quantity is hard to measure for several reasons:
- q is defined for systems at equilibrium. Yet the glass relaxes slowly towards equilibrium and one could observe dynamics instead of the wanted states.
- to measure this overlap we need to have access to the microscopic details of the spin configuration which is impossible with classical magnetic measurements . For now, only numerical simulations and some studies in our group enabled us to achieve such measurements.

In this thesis we will use coherent electronic transport as a probe for the microscopic configuration inside a mesoscopic spin glass. This probe allows us to investigate a microscopic configuration by measuring a macroscopic signal, as we will explain in the next chapter.

CHAPTER 2

Coherent electronic transport in mesoscopic systems

In the present work we use quantum transport as a probe for the spin configuration inside spin glasses. In this chapter I will introduce the theoretical elements needed to understand how the coherent transport can be used for our measurements.

2.1 Characteristic lengths and regimes in electronic transport

2.1.1 The Fermi wavelength

In a metal at equilibrium, the conduction electrons are well described by the semi-classical theory[11]. The ensemble of electrons can be seen as a free electron gas (Fermi liquid theory) whose interactions are taken into account by renormalizing their mass (m becomes m^*). This ensemble is described by fermionic properties. The energy of the gas is given by the Fermi energy $E_F = \hbar^2 k_F^2/2m^*$ with $\hbar$ the Planck constant, m^* the renormalized mass and $\overrightarrow{k_F}$ the Fermi wave vector. For $T \ll T_F \sim 10^4$ K (with $T_F = \frac{E_F}{k_B}$) the electron gas exhibits quantum properties. Thus the relevant characteristic length to be considered here is the wavelength defined by k_F i.e the Fermi wavelength

$$\lambda_F = 2\pi/k_F \tag{2.1}$$

It can be seen as the spatial extension of the electron quasiparticle. In a metal this distance is about a few Ångströms, meaning that, for a sample much larger than that, the previously explained description in terms of free electron gas is valid.
Furthermore one can link the electron density to this wavelength by

$$n_e \propto \left(\frac{1}{\lambda_F}\right)^d \tag{2.2}$$

where d is the dimension of the system.

2.1.2 The mean free path

In the previous section we talked about electron gas in which electrons only interact with each others. This is valid for an ideal material but, in a real one, the electrons can diffuse on impurities. Two types of diffusion can then happen : an elastic diffusion, in which no energy is exchanged, or an inelastic one, where some energy is transferred.

The elastic mean free path

Usually an elastic diffusion happens when an electron hits static defaults (in the lattice for example) or impurities. One can define the mean distance l_e travelled by an electron between two of those collisions. If $\lambda_F \ll l_e$, the electrons propagate freely between defaults and one can define an elastic collision time τ_e (Drude time) via the Fermi velocity v_F

$$l_e = v_F \, \tau_e \tag{2.3}$$

For a sample much larger than l_e, the electron motion is thus diffusive and one can define the diffusion coefficient as

$$D = \frac{1}{d} \, v_F \, l_e \tag{2.4}$$

with d the dimension of the system. Moreover, for any process in which a diffusive behaviour takes place (i.e $\tau_{process} > \tau_e$), one can associate a diffusion length[24]

$$L_{process} = \sqrt{D \, \tau_{process}} \tag{2.5}$$

It is important to stress that, since the electron doesn't lose any energy in an elastic diffusion, ($\left|\overrightarrow{k}_{incident}\right| = \left|\overrightarrow{k}_{diffused}\right|$) and the process is fully reproducible, this static disorder doesn't affect the coherence of the electron wave.

The INelastic mean free path

The other possible kind of interaction are inelastic ones. We stress that, unlike elastic processes, some energy is exchanged and thus, the diffuser (and the electron) may have changed its state after one collision. Then, it appears clearly that the inelastic collisions are an issue in preserving the electronic coherence and thus destroy the electronic interferences. This usually happens when an electron hits anything else than a static default. The main inelastic processes we may encounter are the electron-electron interaction (with l_{e-e} the associated length travelled by the electron between two electron-electron interaction), the electron-phonon one (associated to l_{e-ph}), the electron-photon one (associated to $l_{e-\nu}$) and, finally, the electron-magnetic impurity one (associated to l_{e-m}). One can thus define the inelastic mean free path l_{in} as the characteristic length of the most prominent process[78] i.e.

$$l_{in} \equiv \min(l_{e-e}, l_{e-ph}, l_{e-\nu}, l_{e-m}) \tag{2.6}$$

As done in the previous section, and under the same conditions, it is once more possible to define an inelastic collision time τ_{in} such that $l_{in} = \sqrt{D \, \tau_{in}}$.

2.1.3 The phase coherence length

Let's talk about maybe the most fundamental length for our study : the phase coherence length L_ϕ.
L_ϕ represents the average distance over which an electron keeps its phase well defined i.e. the distance over which the interferences between electrons are possible!
One can define τ_ϕ the phase coherence time related to L_ϕ, and, in the limit where $L_\phi \gg l_e$

we have :

$$L_\phi = \sqrt{D\,\tau_\phi} \tag{2.7}$$

τ_ϕ represents the lifetime of a quasi particle before coming back to the Fermi level via relaxation processes.
In this thesis, the experiments are based on electron interferences and thus require a large enough phase coherence length over sample length ratio. L_ϕ is mainly limited by inelastic processes and thus we want to increase l_{in} as much as possible. Moreover, the phonon-electron interaction is usually the prominent source of decoherence at high temperatures ($T > 1K$) and the electron-electron one at low temperatures ($T < 1K$). Since both of those couplings decrease with temperature, our aim is to reach the lowest possible temperature[1]. To fulfil this requirement, we use a dilution fridge allowing us to go down to $T \approx 50\,\mathrm{mK}$. Thus, going to really low temperatures seems to be a good idea to enhance L_ϕ[64], but not only ! Indeed, another issue can prevent us from measuring interferences : the thermal length.

2.1.4 The thermal length

To understand this effect we now have to think a bit more about the electron energy.
Let's consider an electron with energy E. While propagating, it will acquire an extra phase ϕ directly related to this energy E and the time of propagation t by

$$\phi(t) = \frac{E}{\hbar}\,t \tag{2.8}$$

However, in a metal, not all the electrons have the same energy. Thus, an electron with energy E_1 and another with energy E_2 will acquire a different extra phase leading to a dephasing $\Delta\phi = \dfrac{E_1 - E_2}{\hbar}\,t = \dfrac{\varepsilon}{\hbar}\,t$ between them.

Now, let's suppose those two electrons propagate into a sample of size $L < L_\phi$, such that the electrons remain coherent inside the sample. In a diffusive regime, we already defined D the diffusion coefficient. Then one can imagine to define a time τ_D for which the electron will visit the entire sample i.e. the time it will take them to pass from one side of the sample to the other :

$$\tau_D = \frac{L^2}{D} \tag{2.9}$$

called the Thouless time[71].

Thus, while passing through the sample, the two electrons will acquire a dephasing $\Delta\phi = \dfrac{\varepsilon}{\hbar}\tau_D$.

1 The other effects responsible for decoherence, especially magnetic diffusion, are not affected by lowering the temperature and can thus become prominent once at very low temperatures ($T < 10mK$).

For the moment it does not look like a big deal for interferences... Since the sample is coherent, the two electrons can still interfere and are just dephased. But, in a realistic sample with temperature T, there are not only two electrons but a **continuum of electrons** whose energy ranges from E_F to $E_F + k_B\,T$! And here comes the problem...
When the electrons interfere, their phases are added and can give rise to quantum features. Thus if the sample is long enough we end up in a situation for which all the phases average to 0 i.e. no quantum effect can be seen! It has to be noted that the interferences are not destroyed as for decoherence effect but simply blurred by the temperature.

Moreover, one can calculate the maximum length L_T of the sample to avoid that blurring. Indeed, we can see that the phases average to 0 when the two most dephased waves are π-dephased. Those two electrons are obviously the more energetically separated: the electron with energy E_F and the one at $E_F + k_B\,T$. Their phase difference $\Delta\phi_{max}$ is thus:

$$\Delta\phi_{max} = \frac{k_B\,T - 0}{\hbar}\,t \tag{2.10}$$

If this equals π at the end of the sample we have:

$$\Delta\phi_{max} = \frac{k_B\,T - 0}{\hbar}\,\tau_D = \pi \tag{2.11}$$

leading to

$$L_T = \sqrt{\frac{\hbar\,\pi\,D}{k_B\,T}} \tag{2.12}$$

This length is called **the thermal length!**
We calculated the maximum length for a given temperature T but, experimentally, we're often looking for the opposite, namely the maximum temperature we can use for a given sample length L. This gives the maximum temperature T_{max} that is equal to

$$T_{max} = \frac{\hbar\pi D}{k_B\,L^2} \tag{2.13}$$

2.1.5 The system dimensions: different regimes for different sizes!

In the previous sections we defined the relevant distances or energies in a system for electronic transport. But, as we saw, some of them become relevant only in certain conditions. From a general point of view, the system behaviour will be governed not by the absolute value of its dimensions but by their relation to certain parameters.

If we care about electronic properties (like the density of state), we have to compare λ_F

with the system dimensions:

$$\begin{aligned} \lambda_F \ll t < w < L \quad &\Leftrightarrow \quad \text{3D} \\ t \ll \lambda_F \ll w < L \quad &\Leftrightarrow \quad \text{2D} \\ t < w \ll \lambda_F \ll L \quad &\Leftrightarrow \quad \text{1D} \\ t < w < L \ll \lambda_F \quad &\Leftrightarrow \quad \text{0D} \end{aligned}$$

where t,w and L are respectively the thickness, the width and the length of the sample

However, if we care about coherence properties in electronic transport, the relevant dimension to consider is L_ϕ:

$$\begin{aligned} L_\phi \ll t < w < L \quad &\Leftrightarrow \quad \text{3D} \\ t \ll L_\phi \ll w < L \quad &\Leftrightarrow \quad \text{2D} \\ t < w \ll L_\phi, L \quad &\Leftrightarrow \quad \text{1D} \end{aligned}$$

2.2 Theory of coherent transport

2.2.1 Landauer Formalism

If we consider quite big samples (meaning that every physical quantity can be considered as homogeneous and in a diffusive regime), we can use the Drude formalism. However, when we want to take into account coherent properties, one has to consider a different approach. Indeed, if the physical quantities cannot be considered as mean values over the sample, the conductivity in the sense of Drude is no longer usable. One needs to describe the conductance in a different way. For that reason, in the 60's, Landauer proposed a new paradigm[41, 42] by describing the conductance as a transmission coefficient between two reservoirs.
To explain that theory, let's consider a current flowing perfectly into wires from one reservoir to another. Between those two, a barrier with a transmission coefficient T and reflection one R is set as in Fig.2.1.
In the simplest case, the current flowing from reservoir 1 (with a chemical potential μ_1) to reservoir 2 (with μ_2) is defined by $I = (\mu_1 - \mu_2)\,\rho(E_F)\,e\,v_F\,T = 2\dfrac{e^2}{h}\,T\,V$ in which $(\mu_1 - \mu_2)$ represents the chemical potential difference between the reservoirs and can be seen as the voltage V applied on each side of the sample, $\rho(E_F)$ the density of states at the Fermi level, e the fundamental electronic charge, v_F the Fermi velocity inside the sample and T the previously defined transmission coefficient.
From there it comes naturally that the conductance G is :

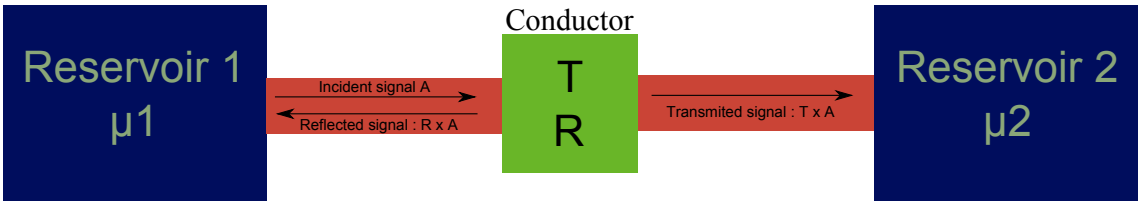

Figure 2.1: Representation of a current flowing between two reservoirs (in blue). In between those two reservoirs the current flows inside wires (in red) with perfect transmission and enters a quantum conductor (in green). This quantum conductor is considered as a "barrier" with a transmission coefficient T allowing to go to the second reservoir, and a reflection one R reflecting the electrons back to their original reservoir.

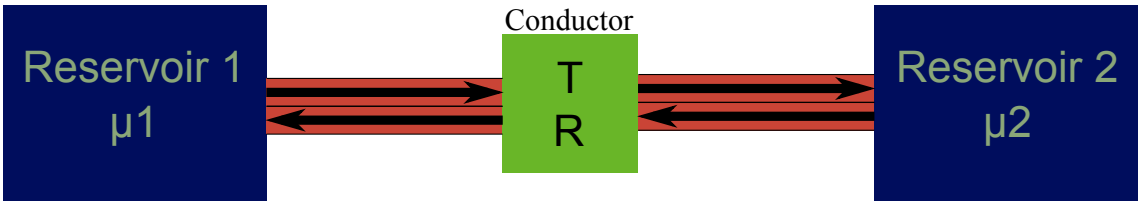

Figure 2.2: Same picture as in Fig.2.1 but the wires are more described. Here the wires are considered as roads with one lane for each direction, allowing electrons to go only one-by-one using this unique lane to access the sample.

$$G = \frac{I}{V} = 2\,\frac{e^2}{h}\,T = G_0\,T \tag{2.14}$$

with $G_0 = 2\,\dfrac{e^2}{h}$ the quantum of conductance.

So this is the formula if all the electrons encounter the same barrier in the sample i.e.

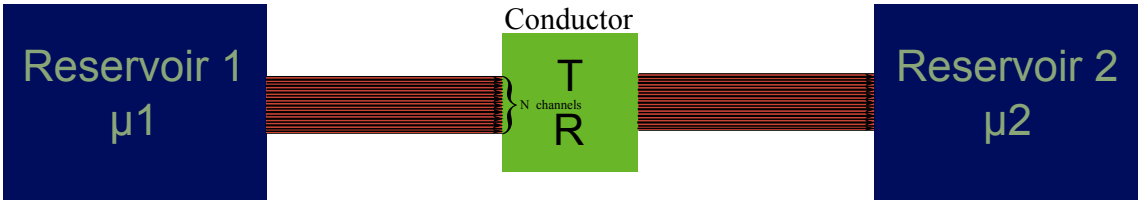

Figure 2.3: Same picture as in Fig.2.2 but the wires and electron channels are given a size! Electron channels have a size λ_F^2 and it is then possible to have many channels in a wire if its section S is large enough. More precisely we have N channels in the wires with $N = S/\lambda_F^2$.

if they all follow the same way one after the other from one reservoir to the other, as on a road with only one lane as in Fig.2.2. However, real wires are usually large enough to be considered as highways with many traffic lanes. Indeed, a sample of section S contains $N = S/\lambda_F^2$ "traffic lanes" called **channels** (which is simply the surface of the wire divided by the size of a channel $\sim \lambda_F^2$, with $\sim \lambda_F$ the Fermi wavelength representing the spatial

extension of an electron). The situation can now be pictured as an highway with N lanes or channels, each of them carrying electrons at finite temperature (according to the Fermi distribution). This is represented in Fig.2.3. We can now rewrite the previous conductance formula with the many channels pictured as:

$$G = 2\,\frac{e^2}{h}\,N\,T = G_0\,N\,T \tag{2.15}$$

However this formulation sets aside the possibility for an electron to pass from one channel i on one side of the barrier to another channel j on the other. From a more general point of view we can consider all the channels being independent with a certain probability T_{ij} for the electron of being transmitted in channel j (rhs) while entering in channel i (lhs). The opposite scenario is of course possible and is defined by the probability R_{ij} of entering in channel i and being reflected in channel j (with j not necessary different from i). Since electrons can enter from both direction in the channel, we also define the same values for electrons entering from rhs with T'_{ij} and R'_{ij}. In this way we can define a matrix representing the conductor transport properties, namely a scattering matrix S

$$S = \begin{bmatrix} r & t' \\ t & r' \end{bmatrix}$$

with $t = \sqrt{T_{ij}}$ and similarly for r.
Using this formalism, the conductance can be written[18] :

$$G = 2\,\frac{e^2}{h}\sum_{i,j}|t_{ij}|^2 = 2\,\frac{e^2}{h}\,\mathrm{Tr}\,tt^\dagger \tag{2.16}$$

2.2.2 Quantum diffusion

After presenting the Landauer formulation, it seems natural to ask how the transmission coefficients are defined.
Actually one has to focus on what happens in the sample itself and consider the real paths[25] electrons are following[1] inside to go from channel i to channel j on the other side. And as can be pictured on figure 2.4, there are many way to do so !
Now let's talk about electrons. At this level, electrons have to be considered as waves and can be written in terms of wave function. From that statement it is natural to speak in terms of quantum mechanics for the electronic transport : to go from one side to the other, the electrons will explore ***ALL the possible paths at the same time !***

To understand in a deeper way, we define the electrons as waves following a path p with the form

$$A_p = |A_p|\,\exp(i\,\frac{L_p}{\lambda_F}) \tag{2.17}$$

1 Obviously, the electrons do not "follow" those paths. Here we talk about electron probability waves propagating along those paths. But the model is simpler to understand if we consider in-phase electrons following different trajectories.

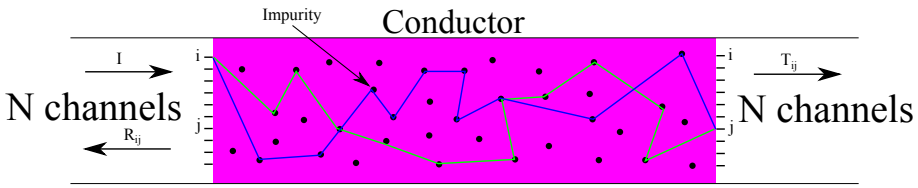

Figure 2.4: Detailed representation of the quantum conductor. Electrons can enter in any channel i and go out in the same or in another channel j. Inside the conductor they can follow many different paths to pass from channel i to channel j (two examples are in blue and green). The electrons taking those different paths will, in the end, interfere to give the transmission value t_{ij} for those channels.

with $|A_p|$ the amplitude of the wave, $\exp(i\,\frac{L_p}{\lambda_F})$ expressing its phase and L_p representing the effective length of the path.
Then the total probability to pass through the sample from point r to point r' is defined by[2] :

$$\begin{aligned} P(r,r',t) &= \left|\sum_p A_p\right|^2 = \sum_p |A_p|^2 + \sum_{p\neq p'} A_p A_{p'}^* \\ &= \sum_p |A_p|^2 + \sum_{p\neq p'} |A_p|\,|A_{p'}| \exp\left(ik_F\left(L_p - L_{p'}\right)\right) \\ &= \sum_p |A_p|^2 + \sum_{p\neq p'} |A_p|\,|A_{p'}| \exp\left(i\ \delta\phi_{p-p'}\right) \\ &= P_c + P_q \end{aligned} \tag{2.18}$$

with $P_c = \sum_p |A_p|^2$ the classical part of the conductivity (in the Drude sense i.e. the mean value used in everyday life) and $P_q = \sum_{p\neq p'} |A_p|\,|A_{p'}| \exp\left(i\ \delta\phi_{p-p'}\right)$ the quantum part of the conductivity rising from the interferences between waves exactly like the double-slits experiments with photons or electrons[37]!

This quantum part is usually negligible since the phase shift for each path is not correlated to others and should vanish on average for large samples. Actually one can prove that contribution not to be zero but of the order of one conduction channel ! This means that if we have a large conductor with many channels, the contribution ratio $\frac{P_q}{P_c}$ will be really small. But in small samples ($\sim \mu m$ large and $L \sim L_\phi$), i.e. with only a few channels, this contribution is not negligible at all and is responsible for many quantum features[10].

2.2.3 Phase coherence and quantum signature

To understand how this quantum part acts on the conductivity, let's focus on the formula itself.

We presented before the value L_p as the effective length of the path to explain easily the interference process. But L_p contains actually two parts : a part concerning the real geometrical length of the path and a second one taking into account the possibility of an applied magnetic potential. This allows us to rewrite the phase difference for two paths p and q with length L_p and L_q as follow :

$$\begin{aligned} \delta\phi_{p-q} &= L_p - L_q \\ &\approx k_F(l_p - l_q) + 2\pi\frac{\Phi}{\Phi_0} \\ &\approx \delta\phi_{disorder} + \delta\phi_{flux} \end{aligned} \tag{2.19}$$

$\delta\phi_{disorder}$ represents the real length difference between the two paths, depending only on the disorder inside the system. Φ represents the flux applied on the surface delimited by the two paths and $\Phi_0 = h/e$ is the flux quantum. $\delta\phi_{flux}$ then represents the phase shift induced by an hypothetical magnetic flux applied on the system.
This leads to some new quantum behaviour : since $\delta\phi_{p-q}$ depends on the disorder configuration, it appears that even two samples created to be identical will have different conductance because the disorder will be unique in each sample !
Moreover, when a magnetic field is applied, a phase shift is induced, leading to a Φ_0 periodic oscillation in the conductivity ! This term gives rise to many features including the famous Aharonov-Bohm (AB) effect[1].

The Aharonov-Bohm effect

In 1985, Webb et al.[76] made the following experiment : they took small metal rings whose intern diameter was $d_{in} = 784$ nm and branches are 41 nm large in order to mesure their resistance while sweeping a perpendicular magnetic field. This experiment gave evidences of $h/e = \Phi_0$ and $h/2e = \frac{1}{2}\Phi_0$ periodic oscillations in the resistance as can be seen in Fig.2.5.

The ring is thin enough (compared to the diameter) to consider that there is only one conduction channel in the ring[1] and that both parts of the ring have the same length.
Under that statement, the resistance behaviour can be explained simply by the quantum part of the resistivity described in the previous section. Indeed, electron can thus take only two paths (namely p and q) to go from one side of the ring to the other, one in each branch.
As seen before $\delta\phi_{p-q} = \delta\phi_{disorder} + \delta\phi_{flux}$. We can already say that $\delta\phi_{disorder} = k_F(l_p - l_q) = 0$ since we supposed the paths being equally long. However, by applying a magnetic field inside the ring (i.e. a flux), a dephasing $\delta\phi_{flux} = 2\pi\frac{\Phi}{\Phi_0} = \pi^2\frac{B \times d_{in}^2}{2\Phi_0}$ is created between the two paths !
As the phase is 2π periodic, a Φ_0 periodic oscillation is expected. With the dimensions of the ring, a Φ_0 flux corresponds to an applied field of $\Delta B = 0.0078$ T and, as frequency in the Fourier transform $1/\Delta B = 131$ T^{-1}. This corresponds exactly to what is observed in

1 Actually there are many channels in the ring but it is thin enough to consider them all equivalent with the same length.

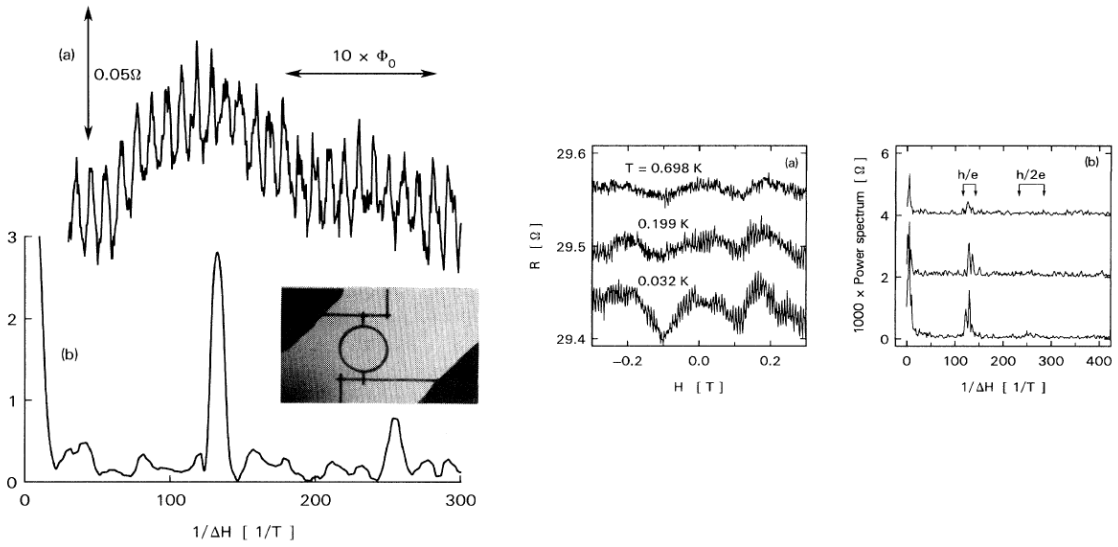

Figure 2.5: Sample and results of the experience of Webb et al. in 1985. The picture represents the sample which is a metallic ring with inside diameter $d_{in} = 784$ and whose wires are 41 nm large. The Fourier transform of resistance measurements as a function of the magnetic field shows two distinct pics for fluxes exactly equal to $h/e = \Phi_0$ and $h/2e = \frac{1}{2}\Phi_0$ showing that oscillations of the resistance with precise frequencies. From [76].

Fig.2.5 !
Those oscillations are thus due to a **dephasing between two electron paths** with a magnetic field! But, as said earlier, there are also evidences of $\frac{1}{2}\Phi_0$-periodic oscillations. So where do they come from ? One could argue that it is simply the first harmonic of the Φ_0-periodic oscillations (that will be referred later as AB oscillations). This seems to be a good guess, right? We'll see later in this chapter that it's not totally right. But first, let's have a look at some other quantum interferences effects in larger samples !

Universal Conductance Fluctuations (UCF)

As seen previously, quantum effects appear to be relatively stronger for samples with only few channels (i.e. with a small cross section) since it is of the order of one conduction channel. But there is also another condition ! In the previous sections we talked about interferences of electronic plane waves but that assumption stands only if we consider there is only elastic diffusion i.e. $L \leq L_\phi$.
If we are in this regime, the conductance will be changed by the quantum corrections. It has to be noticed that, at the end of the previous section 2.2.3 about quantum diffusion , I took into account only two interacting paths, but there are usually many of them ! The general idea, however, doesn't change. And, since the length of each possible paths will differ from a sample to another (due to different disorder configurations as said earlier), it will lead to fluctuations in the conductivity between samples. Altshuler (1985)[9] and, separately, Lee and Stone (1985)[43], calculated that the amplitude of such variations is

surprisingly **constant** for a given dimensionality and, moreover, does not depend at all on the mean conductance nor on any microscopic details of the disorder !
They are thus universal.

Ergodicity and magnetic field

Now let's apply a magnetic field. We've seen that we have a Φ_0 periodic oscillation in an "Aharonov-Bohm" ring (that can be seen as an interferometer). But what about a conductor with many channels in a disordered system ?

Actually the situation is a bit more complex. We can see this system as ***many "Aharonov-***

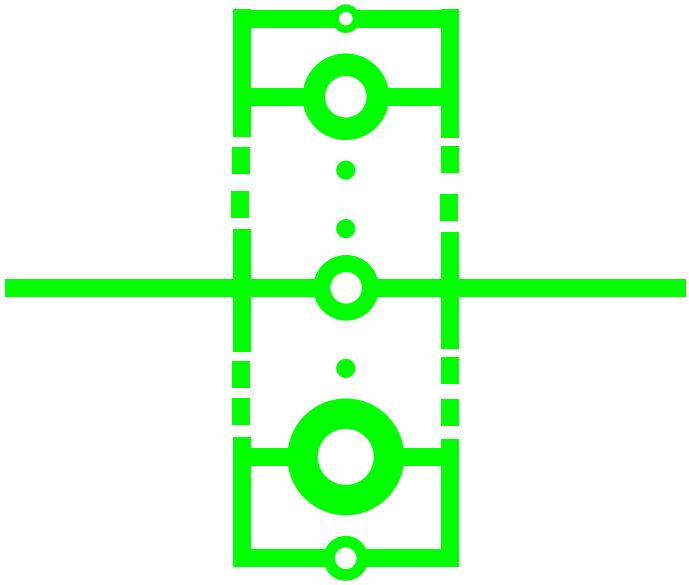

Figure 2.6: Modelisation of a sample of size $L < L_\phi$. Many AB rings are set in parallel to represent the different paths the electrons can follow crossing the sample. Each of those rings are of different size, showing that the magnetic field will generate different flux for each of the paths.

Bohm" rings in parallel with different surfaces as can be seen in Fig.2.6, each of them representing two interfering electron paths. Since the flux Φ is proportional to the surface, each of them will have a different magnetic-field period. This leads to the fact that if one changes the magnetic field, not all the rings will dephase the electron paths by the same amount. However, each of the rings still have a Φ_0 period and it it **always** possible to know how much it dephases for a given field. Thus, the electron paths are dephased with a different amount in each rings but in a reproducible way since each ring can be considered independent! From that, we can deduce that the conductivity will still be **fluctuating but with no period**[1] since the different frequency of the rings are superimposed!
But now, one question comes naturally in mind : can those fluctuations be related to the

1 Actually, one can observe that there is a "main" period which corresponds to rings of size L_ϕ^2. This is due to the fact that most of the paths participating in the UCFs have a size close to L_ϕ.

UCF we talked about ?
The answer is yes according to the Ergodic hypothesis[6]. In our case, ergodicity means that modifying the magnetic field is exactly equivalent to changing the disorder configuration i.e. the average over the field, is equivalent to the average over the disorder ($\langle \delta G \rangle_B \equiv \langle \delta G \rangle_{disorder}$).
This hypothesis has been experimentally confirmed by Mailly et al.[23] in 1992 on Si doped GaAs wires. In this experiment, they measured the magneto-resistance of a wire 46 times at 45 mK, with thermal cycling to room temperature between each measurement to change the microscopic disorder configuration.

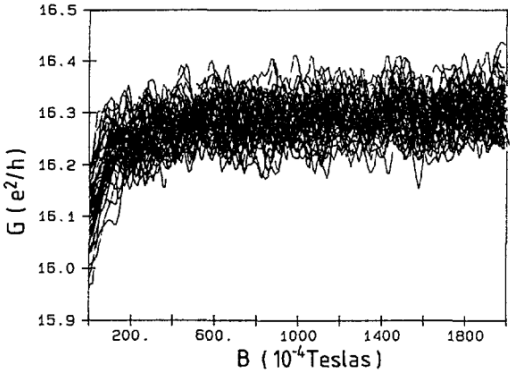

Figure 2.7: Conductance as a function of the magnetic field on Si doped GaAs wires at 45 mK. 46 curves corresponding to different measurements are displayed. Those 46 measurements were made on the same sample. A thermal cycling to room temperature is made between them to change the microscopic disorder configuration in the wires. The difference between the curves show that the change in the disorder configuration has a huge impact on the magneto-resistance measurements and thus on the UCFs. From [23].

Those magneto resistance measurements allowed them to determine the mean value $\langle \delta G \rangle_B$ taken over 0.2T and also the mean amplitude of those oscillations.
Moreover, for a given field, each measurement exhibits a different conductance proving that the disorder configuration has indeed been changed due to the thermal energy as can be seen in Fig.2.7. It is possible to determine the mean value averaged over the disorder $\langle \delta G \rangle_{disorder}$ (also called $\overline{G}$) on the same range of field.
And what we observe in Fig.2.7 and Fig.2.8 is that $\langle \delta G \rangle_B \equiv \langle \delta G \rangle_{disorder}$! This leads to a very important conclusion : ***Changing the magnetic field is totally equivalent to changing the disorder configuration to observe UCFs***[43].

However, the magnetic field has to be swept over a certain range to be equivalent to a complete change in disorder configuration. It is then possible to determine a field B_c for which $G(B)$ and $G(B + B_c)$ are decorrelated (meaning that it is equivalent to a complete disorder change).
This has been calculated by Lee et al. in 1985 and they proved that $B_c \propto \dfrac{\phi_0}{wL_\phi}$. Experi-

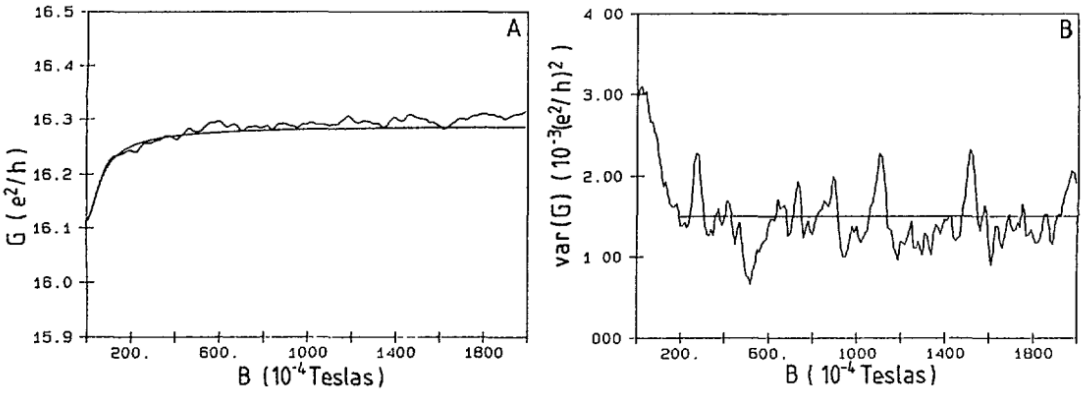

Figure 2.8: Figure A : Average of all the 46 curves displayed in Fig.2.7. A theoretical fit that doesn't take UCFs into account is also displayed. The fact that the fit corresponds well to the experiment reveals that the UCFs amplitude, once averaged over all the disorder configurations goes to zero. Figure B : Variance of the conductance calculated with the 46 curves as a function of magnetic field. The variance of the UCFs changes by a factor of two after 300 G as predicted by the weak-localization theory we'll see in the next section. From [23].

mentally, it means that to have a good equivalence between disorder averaging and field averaging, one has to sweep the field at least over a few B_c.

Mesoscopic effects in a conductor : Length dependence and weak localization

In the previous section we have seen that the magnetic field has an effect on the phase of the electrons and we related this to UCFs. But this field-dependent interference effect leads to another remarkable feature.

Remember when we talk about Aharonov-Bohm effects in metallic rings? We said that we would come back to it in order to explain the $\frac{\Phi_0}{2}$-periodic oscillations. The time has come! Those $\frac{\Phi_0}{2}$-periodic oscillations, as said before, could simply be the first harmonic of the Φ_0-periodic (AB) oscillations. But let's have a look at another experiment before making a definitive conclusion.

Imagine a chain of several **identical** Aharonov-Bohm rings as in Fig.2.9(left figure) and check on the conductivity as a function of an applied magnetic field. What would we expect? This question is pretty complex and has been experimentally addressed by C.P. Umbach et al. in 1986[73].

In their experiment, they measure the conductivity of several arrays with different lengths (ranging from 1 to 30 loops). The results are displayed if Fig.2.9.

The first observation is that the behaviour of $\Delta G = \delta G/G$ as a function of the number of rings is completely different for the $\frac{\Phi_0}{2}$-periodic and the AB oscillations! As we can see, the AB oscillations amplitude fades out as $\sqrt{N}$ (with N the number of rings) while the other is

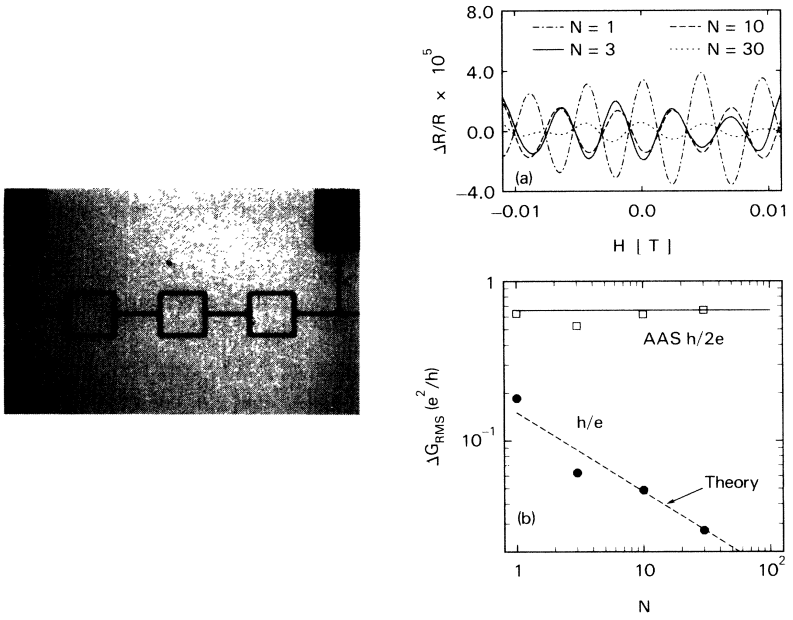

Figure 2.9: Left picture : SEM image of the sample. Several metallic loops with the same size are set in series. Right curves : Relative amplitude of the AB and AAS oscillations as a function of the number of loops N in series. The AAS relative amplitude remains constant because of the robustness of the time-reversal invariant paths over the disorder. On the opposite, the AB relative amplitude decreases with N because of the randomness of the electron phase between the loops. From [73].

constant. Those results are thus incoherent with our previous explanation of harmonics. It must have another origin. Actually, those $\dfrac{\Phi_0}{2}$-periodic oscillations were predicted by Al'tshuler,Aronov and Spivak (AAS) in 1981[10] and arise from another interference effect. The AB oscillations come from the interferences between two different paths. But what about "self interacting" paths? Let me be clear: of course a wave cannot interact with itself but it can interact with the one going through the same path but in the opposite direction (clockwise and anti-clockwise)! This is pictured in Fig.2.10. Those paths are called **time-reversal invariant paths**.

Those probability waves interfere constructively, strengthening each other and thus the probability for the electron to remain in the loop (instead of going out) is enhanced. Mathematically, it can be proven that the transmission of this kind of path is reduced by a factor of 2, leading to a net reduction of the ring total conductivity: this phenomenon is called **coherent retrodiffusion**! But why isn't it reduced with the number of rings then? In the experiment of Umbach, the rings are coherent ($L_{ring} < L_\phi$) but the length *between* rings is longer than L_ϕ, meaning that the rings are not coherent one to another. In the case of AB oscillations, it means that the variation of resistance of each ring ΔR_0^{AB} cannot simply be added. Indeed the correction to the resistance depend on the initial phase of the electron entering the ring. Since the phase is randomized in between the

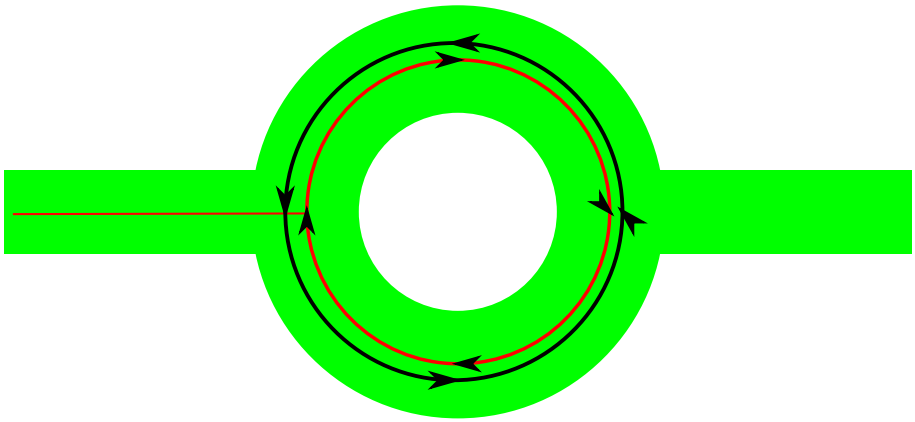

Figure 2.10: Aharonov-Bohm ring with a example of time-reversal invariant path. The paths going clockwise and anti-clockwise always interfere constructively and are dephased only by applying a magnetic field in the loop. Thus, even if the the whole sample is not coherent, as long as the two paths are coherent, the AAS oscillations relative amplitude remains constant.

rings, the correction ΔR_0^{AB} is then random for each ring. Thus, to obtain the total variation of resistant ΔR_{total}^{AB}, one has to add N random terms (one for each ring) whose average value ΔR_0^{AB} is the same. Mathematically, the variance (or "size") of the addition of random terms grows as $\sqrt{N}$. Thus, for AB oscillations, $\Delta R_{total}^{AB} = \sqrt{N} \times \Delta R_0^{AB}$ i.e. $\frac{\Delta R_{total}^{AB}}{R_{total}} = \frac{\sqrt{N} \times \Delta R_0^{AB}}{N \times R_0} = \frac{1}{\sqrt{N}} \times \frac{\Delta R_0^{AB}}{R_0}$: QED!
Moreover, we saw earlier that the UCFs are intimately related to AB oscillations. Then, can we say something about UCFs from what we've just said. The answer is clearly yes! In Umbach experience, each ring can be said L_ϕ long. Adding several rings can thus be seen, in the case of a real sample, as increasing the length of a sample. We can then deduce that the UCFs size will be reduced by increasing the size of the sample.
In 1D-sample samples like ours with many channels leading to UCFs, the general idea is then that **UCFs amplitude is reduced by length** of the sample (if $L > L_\phi$, obviously)!

Let's come back to AAS oscillations now. As explained before, the correction to the resistance is due to paths making a full loop. It also means that we do not care about the initial phase of the electron since, whatever the initial phase is, the two paths always interact constructively! The effect can thus just be considered independent in each ring and we can simply add the corrections of each of them: $\Delta R_{total}^{AAS} = N \times \Delta R_0^{AAS}$. We now have $\frac{\Delta R_{total}^{AAS}}{R_{total}} = \frac{N \times \Delta R_0^{AAS}}{N \times R_0} = \frac{\Delta R_0^{AB}}{R_0}$: **the amplitude of AAS oscillations is** thus remarkably **robust over the disorder**!
This explanation was quite detailed but important to understand what happens in more complex samples as metallic wires. In a sample such that $L \gg L_\phi$, you can "cut" it into L_ϕ long samples. We previously said that we can model such coherent part as "Aharonov-Bohm" rings in parallel. It thus seems reasonable to model larger samples as several arrays

of parallel "Aharonov-Bohm" rings put in series exactly as in Fig.2.11.
With that model, we end up with a situation very similar to the one we've just described!

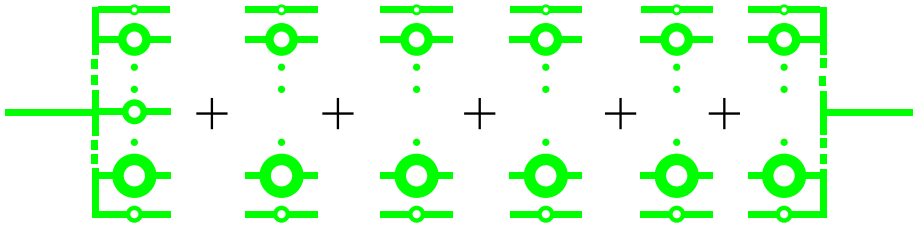

Figure 2.11: Representation of a sample thanks to AB rings. A coherent sample can be described as seen in Fig.2.6 with AB rings in parallel : we can see that as a fundamental brick. Thus, to describe a longer sample we just add several of those bricks in series. This model allows to account for coherence effects in mesoscopic samples and is simple to visualize.

And indeed, in addition to the UCFs we described earlier thanks to the AB oscillations (that will "disappear" for long enough samples as seen before), we observe an equivalent for the AAS ones : the **weak localization** effect!
The time-reversal invariant paths we observe in rings can also be found in pieces of metals as pictured in Fig.2.12. The "non-looping" paths are responsible for the average resistance and are called **diffusons** [1] while the time-reversal invariant ones are responsible for the weak localization and are called **cooperons**.

However, this weak localization effect is valid only for a field $B = 0$. Indeed, since in a real metal every loop has a different size and since the doubling probability of being retrodiffused is $\Phi_0/2$ periodic, when one applies a magnetic field the effect is destroyed. To be totally exact, to put the clockwise path and the anti-clockwise in antiphase, one has to apply a field equivalent to $\Delta\phi = 4\pi\dfrac{\phi}{\phi_0}$. Thus, it has to be noticed that the effect is totally killed first in larger loops and then destroyed progressively in smaller ones[2]. Concerning the relative amplitude of the effect, if we take the problem with all the channels (not only the time-reversal invariant ones) , as in any quantum conduction effect, it is possible to show that it is of the order of $\dfrac{2e^2}{hG_D} = \dfrac{2G_0}{G_D} = \dfrac{1}{N_c}$ with $G_0 = \dfrac{e^2}{h}$ the quantum of conductance, G_D the classical part of the conductivity (also called Drude conductance) and $N_c = \dfrac{G_D}{G_0}$ the number of conduction channels.

1 The attentive reader will have realized that UCFs are due to interferences between several diffusons.
2 Of course each loop still have a $\Phi_0/2$ period and thus, for a given field B, it is always possible to find loops for which $B \times S_{loop} = n \times \Phi_0/2$. The two interfering paths are thus in phase and the weak localization effect still appear. However the proportion of loops with paths in phase for $B \neq 0$ is totally negligible and so their effect on the resistance.

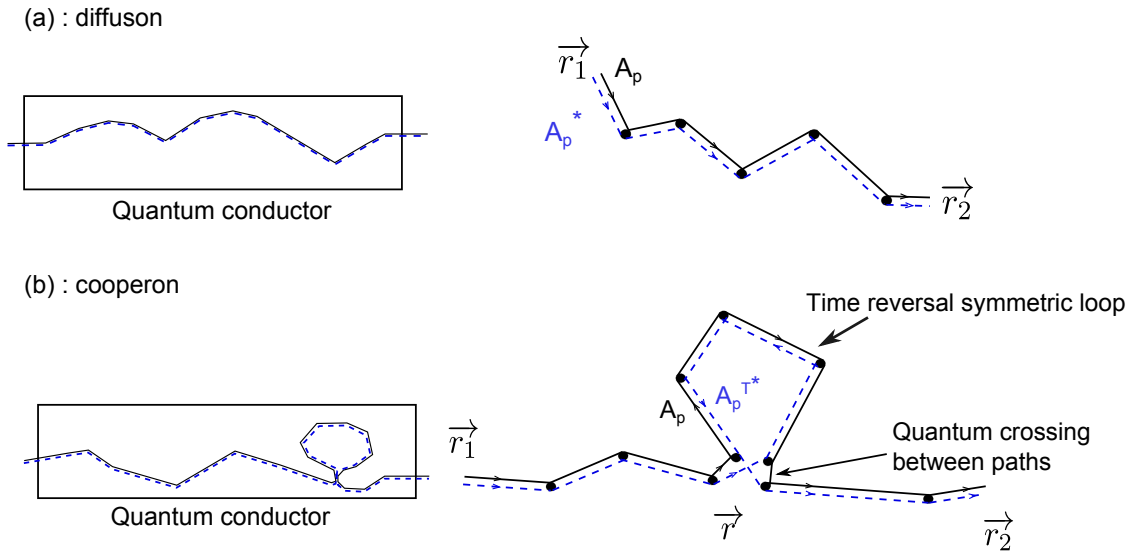

Figure 2.12: Schematic representation of (a) a diffuson and (b) a cooperon. The diffuson corresponds to the classical part of the conductivity in which the amplitude A_p along a trajectory interfere with the its conjugate A_p^*. On the other hand, the cooperon includes a loop and thus a time-reversal invariant path along its trajectory. The cooperons are thus responsible for the weak-localization effect due to the the interference between A_p and A_p^{T*}, doubling the reflection probability of the path.

Thus the total conductivity can be written (at zero magnetic field) as :

$$G = G_D - G_{wl} \propto P_{diffusion} + P_{Cooperon} = P_{diffusion}(1 - \frac{P_{Cooperon}}{P_{diffusion}}) = P_{diffusion}(1 - \frac{1}{N_c}) \tag{2.20}$$

where G_{wl} is the weak localization correction.
We can then see that the main component of the conductance corresponds to the Drude one with only small corrections due to the weak localization.
In quasi-1D wires (as we will use in our experiments) one can show that this correction is directly related to the ratio between L_ϕ and L : $\Delta g_{wl} \propto -\frac{L_\phi}{L}$

Moreover, we've just seen that the effect is killed when one applies a magnetic field. The limit is thus obtained when the field is high enough to break the reversibility in the smallest loops, i.e. with a surface of the order of l_e^2 [1]. In which case we finally recover the Drude conductivity[44].

We'd like to finish this part by saying a word about the temperature influence on the previously explained mesoscopic effects. Indeed, we did not speak at all about how

1 It is the smallest possible path to create a loop.

important is the temperature at which the experiment are performed but it is crucial! If we consider what happens with the temperature, the process occurring is the thermal averaging. We saw earlier that the relevant length for such process is the thermal length L_T. So if the sample is longer than L_T, the UCF amplitude will be reduced.
Moreover, those experiments are performed at low temperature because L_ϕ is enhanced due to the reduction of the phonon modes number, allowing us to avoid the previously described averaging effect on disorder.

2.2.4 Onsager relations

Now that we presented the main features of mesoscopic samples and the formalism adopted to explain the conduction properties, let's focus on the measurements themselves.
When we talked earlier about Landauer formalism, we considered only the case in which the wires are used for both sending current and measuring the potential i.e. the so called "2-points" measurement. However, if the distance between probes is smaller than L_ϕ, some particular symmetries rule the magneto-conductance measurement and separating the voltage probes and current wires becomes crucial. In most cases, however, we experimentally use "2-points" measurements, even when two wires are used to send current and two others to measure the voltage. Indeed, if the two measuring probes are separated by a distance superior to L_ϕ, the current and voltage wires are undistinguishable for the electronic transport: in terms of electron phase there is no difference between the wires.
In his 1986 article, Büttiker[17] considered a fully coherent sample with four wires, each of them being connected to well separated perfect reservoirs. A hole is created in the middle of the sample such that a magnetic flux can be applied.
Since the wires are considered having only one conduction channel, and because of time reversal symmetry[1], we can expect some particular relations. Thus, the probability $T_{i,j}$ of transmitting (reflecting) an electron from wire i to wire j and the probability of reflecting an electron in the same wire $R_{i,i}$ can be proven to obey to the following relations[22, 56]:

$$T_{i,j}(\phi) = T_{j,i}(-\phi) \qquad R_{i,i}(\phi) = R_{i,i}(-\phi) \tag{2.21}$$

With 4 wires, it is then also possible to define four points resistances between wires $R_{mn,kl} = \dfrac{(V_k - V_l)}{I_{mn}}$ with the wires k and l measuring the voltage and m,n sending the current. It can also been expressed through the previously defined probabilities:

$$R_{mn,kl} = G_0(T_{km}T_{ln} - T_{kn}T_{lm})/D \tag{2.22}$$

1 A time reversal symmetric variable or process is defined as being identical if the time t is changed to $-t$. For example, the mass of a particle is time reversal symmetric but the velocity is not. In our case, the coherent electronic transport is symmetric upon time reversal but decoherence processes are not. Thus if $L > L_\phi$, the electronic transport cannot be considered as a time reversal symmetric process.

with D a known mathematical coefficient independent from the indices.
From Eq.2.21, it is then possible to prove the so-called Onsager relations:

$$R_{mn,kl}(\phi) = R_{kl,mn}(-\phi) \tag{2.23}$$

This relations expresses that the measured resistance, when a flux ϕ is applied, is the same than the one with a flux $-\phi$ providing that we exchange the current and voltages contacts ! This has been experimentally shown in 1986 by A.Benoit et al.[13] in a gold ring as can be seen in Fig.2.13 where $G_{14,23}(B) = G_{23,14}(-B)$
This is a general result that can be used for Aharanov-Bohm oscillations but also, as we've just seen and this is important in our case, for UCF's.

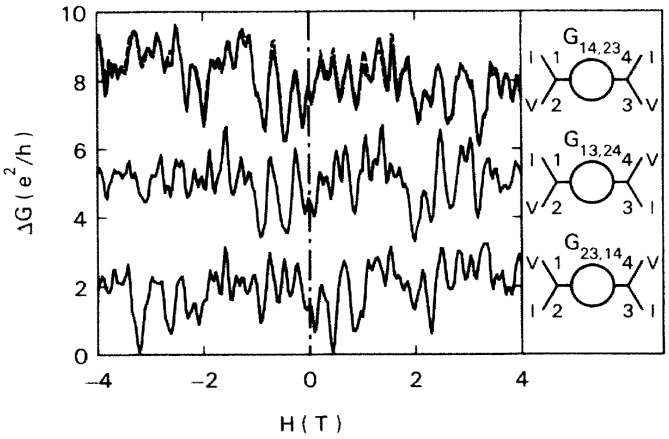

Figure 2.13: Magneto-conductance measurements on Au rings with different wiring configurations (shown in the right part of the figure). $G_{ij,kl}$ corresponds to using wires i and j to send current and wires k and l as voltage probes. We observe that the the first and the third configurations give mirror results i.e. $G_{14,23}(B) = G_{23,14}(-B)$, giving evidences of the Onsager relations. From [13].

Now that the Onsager relations have been established, let's see what kind of informations can be extracted from them.
It is now possible to define two quantities δG_s and δG_m such that :

$$\delta G_s = (G_{14,23}(B) + G_{23,14}(-B))/2 \tag{2.24}$$

$$\delta G_m = (G_{14,23}(B) - G_{23,14}(-B))/2 \tag{2.25}$$

Those values inform us about the symmetries in the system. Indeed, if the system is time-reversal symmetric, then equation 2.23 holds and thus, $\delta G_s = G_{14,23}(B) = G_{23,14}(-B)$ while $\delta G_m = 0$. However, if the system breaks that symmetry, $\delta G_m \neq 0$. But when will that breaking happen ?
The simplest example is to take a magnetic sample. When a field B is applied, a magnetization M is created. As the field is reversed to -B, the magnetization has to become -M if one want to preserve the symmetry. It is the case for example in paramagnetic samples.

The Onsager relations thus become : $G_{14,23}(B,M) = G_{23,14}(-B,-M)$.
However, if the system has a preferential direction for the magnetism, (as in ferromagnets or spin glasses), $M(B) \neq -M(-B)$ and $\delta G_m \neq 0$. Usually this value is thus used to measure the magnetic contribution in the conductance and δG_s to determine the orbital one.

CHAPTER 3

Mesoscopic physics and spin-glasses: a recent love story

As we mentioned in the the first chapters, this PhD has been dedicated to the study of spin glasses by the mean of mesoscopic physics tools.
I presented the remarkable properties of glasses and particularly spin-glasses as well as notions of coherent electronic transport in metals. This was necessary to understand the real subject of this thesis which is an overlap between those two fields: coherent transport and mesoscopic spin glasses.
Surprisingly, those two fields have been rarely studied together except in our group. The main point of this new approach is that coherent transport is a powerful probe to establish the phase diagram as well as, potentially, the topology of the spin glass phase space as we will see later.

3.1 Kondo effect

Spin glasses are magnetically disordered material with frozen impurities. But above the freezing temperature T_g, those impurities are free (i.e energy degenerated) and a peculiar effect comes into light : the Kondo effect.
It is necessary to understand this effect to interpret the behaviour of the resistivity when $T > T_g$ and thus detect when it deviates from the expected one, showing the onset of the spin glass phase.
If magnetic impurities are present in a material, the resistivity is strongly modified at low temperatures. While decreasing the temperature, resistivity in this kind of material decreases as well until reaching a minimum and, finally, increases again logarithmically.
The first who described this effect was J. Kondo in 1964[36]. In his model he considers the interactions (noted J) between *free* up-down energetically degenerated spins ($\pm S$) and conduction electrons spins (s). He finds out, after a perturbation calculus to the third order, that the dominant diffusion process at low temperature is due to those interactions, increasing the resistivity. Indeed, while travelling, electrons can diffuse on magnetic impurities by swapping their spin i.e if $S = 1/2$ and $s = -1/2$, we can end up with $S = -1/2$ and $s = 1/2$: this is called “Kondo spin-flip".
Finally he gets the Kondo contribution to the resistivity:

$$\rho_{Kondo}(T) = \frac{3\pi J^2 S(S+1)}{2e^2\hbar\varepsilon_F}\left(1 - 4J\nu(E_F)\ln\frac{k_B T}{D}\right) \tag{3.1}$$

with e the electron charge and $\nu(E_F)$ the density of state at the Fermi level.
Considering also the T^5 dependence to phonons and the effect of all impurities, Kondo

gets the total resistivity for $T > T_g$:

$$\rho(T) \propto \alpha T^5 + c_{imp}(\rho_\alpha - \rho_\beta \ln T) \tag{3.2}$$

with α, ρ_α and ρ_β being constants and c_{imp} the impurity concentration.

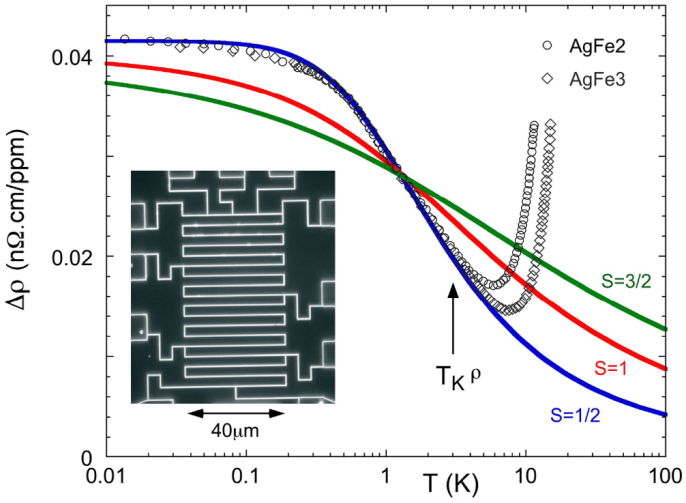

Figure 3.1: Variation of the resitivity as a function of the temperature for AgFe2 and AgFe3 wires comparable to ours. As can be seen on the raw data (∘ and ⋄), a logarithmic rise in the resistivity is observed as the temperature is lowered. Moreover, they can perfectly be fitted by the Kondo formula for S=1/2 (blue curve), proving that this rise comes from the Kondo effect. From [47].

This formula works pretty well in explaining the usual shape of the resistivity as can be seen in Fig.3.1 for AgFe wires similar to our samples[47]. However, the assumptions taken are quite restrictive. First there should not be any impurity-impurity interactions meaning that the concentration cannot be too high, otherwise impurities get too close one to another and will interact. Second, he used the perturbation approach meaning that the coupling J has to remain weak to keep on using that formula.
But the most clearly visible problem of that formula comes from the fact that the resistivity diverges for $T \to 0$. This issue comes from the fact that J becomes way too strong at very low temperatures and this perturbation method falls. The temperature for which the approximation falls is called "Kondo temperature" (T_K)
To solve this problem, Nozières[54] supposed $\lim_{T\to 0} J = \infty$ (idea taken from Anderson) and proposed to use the Fermi liquid formalism instead of the perturbation approach. Indeed, for J really high, impurities always have an electron cloud coupled to them, resulting in an effective magnetically neutral complex. Thus, for $T \ll T_K$, it can be considered as a non-magnetic impurity for which the usual Fermi liquid description holds.

A second important feature, but not critical in our case, is the creation of a so-called

Kondo cloud. The magnetic impurities also have a long range interaction with the electrons by the same RRKY process than for creating a glass. Thus not only one unique electron is forming a complex with the impurity but many electrons are attracted and form a cloud[34] around it. This cloud is going larger with the temperature, and is of the order of $\frac{1}{T_K}$ at $T = 0$.
When an impurity is totally surrounded by this Kondo cloud, we say that it is *screened* and this complex appears as globally neutral. Our problem in that case is that we need impurities to "see" each other since we want a spin glass! And if two impurities are too far away ($d > \frac{1}{T_K}$), they can't see each other because of the screening... Thus no RKKY interaction and no glass...
This can become a real problem at really low temperature ($T < 1mK$) where impurities start to be almost fully screened. Experimentally we'll never reach that limit and Kondo cloud will not be a problem in our conductance measurements.

3.2 Universal conductance fluctuations in spin glasses

As seen in the previous chapter, Universal Conductance Fluctuations (UCF) can be considered as fingerprints of the disorder inside samples since they depend strongly on the disorder configuration. The idea of using them in spin glasses as a probe to investigate the spin disorder configuration thus came naturally and was first proposed by Al'tshuler and Spivak[9] in 1985. Practically, it means that we should see changes in the UCF if the spin configuration changes but it will remain the same if it does not change at all.

3.2.1 First works on conductance fluctuations

In 1991, De Vegvar, Levy and Fulton[75] performed the first measurements of UCF as a function of the magnetic field (what I will call a "UCF trace") as it is displayed in Fig.3.2. In their experiment, they measured UCF traces on mesoscopic (2 x 0.42 x 0.9 μm) 1000 ppm CuMn spin glasses at different temperatures. As can be seen, clear quantum fluctuations are present! Moreover, we can use the amplitude of those fluctuations to determine the phase coherence length in the sample since they are directly related. Below the glass transition (expected to be around $T_g \approx 1K$), we can clearly see a rise in the fluctuations amplitude, showing that in the glassy phase the coherence length is much longer. Indeed, in the glassy phase, the spins are not degenerated anymore since they are frozen and, consequently, the effective concentration of degenerated impurities c_{imp} decreases. The Kondo effect is thus killed as the spins get frozen, diminishing the diffusion processes of electrons in the sample. And since this process was dominant, L_ϕ is enhanced compared to the paramagnetic (Kondo) phase. In the glassy phase, they estimate $L_\phi \approx 1\mu$m, which is quite large.

From those measurements it is also possible to extract the magnetic contribution to the conductivity G_m defined in Chapter 2 thanks to Onsager relations. We remind the reader that G_m is only sensitive to fixed magnetic contributions such as the frozen spins in a spin glass. Here, the magnetofingerprints are highly reproducible below the expected T_g, suggesting that the spin configuration remains the same once the transition is reached. The disorder is *frozen*.

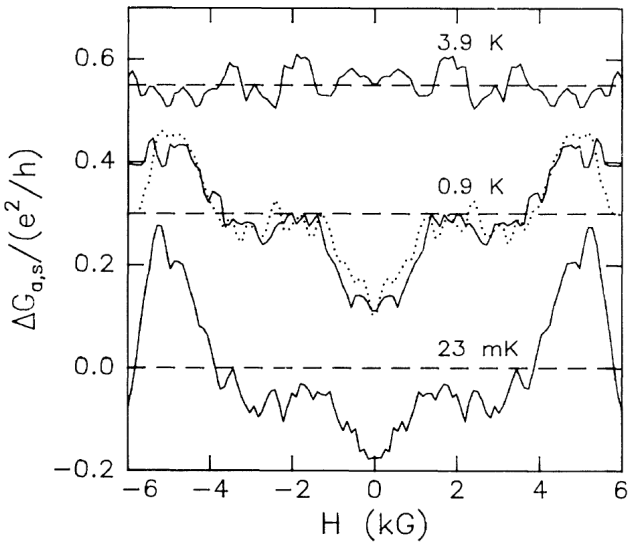

Figure 3.2: Magnetic part of the conductivity as a function of the magnetic field for different temperatures on a 1000 ppm CuMn spin glass. As the temperature is lowered, the amplitude of the variation increases, proving an enhancement of the phase coherence length L_ϕ due to the progressive freezing of spins. Moreover, the reproducibility of the traces proves that even for $B \gg \frac{k_B T_g}{\mu_B}$, the spin configuration is not affected. From [75].

Another remarkable property is that even upon cycling the magnetic field up to ten times the typical exchange field $B_g = \frac{k_B T_g}{\mu_B}$, we see no decorrelation between traces as can be seen in Fig.3.2! This is indeed surprising since we would expect the spins to be polarized by such a large field. It thus suggests that the spin configuration is invariant even if one applies large magnetic fields.

This pioneering work displays important results for our studies. First, it shows that the UCF are reproducible below T_g even with low concentration spin glasses (0.1%!), proving that the disorder is frozen. Second, the glass appears being insensitive to the application of large fields (up to ten times B_g), proving that UCF traces can be used over a large range of magnetic field without perturbing the spin configuration.

However there are also unsolved questions. The calculated correlation between two G_m traces after thermal cycling above T_g should be close to zero since the configuration will totally change. But the correlation stays quite high ($C > 0.40$) even after a heating at $T = 2T_g$. This could be explained by the presence of clusters, resulting in different freezing strengths inside the sample[77].

To go further in the understanding of the glassy phase with this UCF probe, a deeper insight on the UCF in the spin glass phase is necessary. Several recent works have been recently conducted theoretically as well as experimentally in our group to shed some new light on how tu use this new technique.

3.2.2 A renewal

In our group, Thibaut Capron and Guillaume Forestier made the first steps for a new experimental exploration of spin-glasses, a few years ago.
As explained just before, the amplitude of the UCFs increases when we reach T_g because of the freezing of spins that kills Kondo effect and thus increases L_ϕ. But there is also another way of lifting the spins degeneracy: magnetic field!
Indeed, when a magnetic field is applied, it will be more favourable for the spins to align with it, lifting the degeneracy. Moreover, we saw that, even for strong field, the frozen spins are not affected by the field since the traces are reproducible. Then, deep in the glassy phase, once everything is frozen, we would expect to have a constant amplitude for the UCFs.

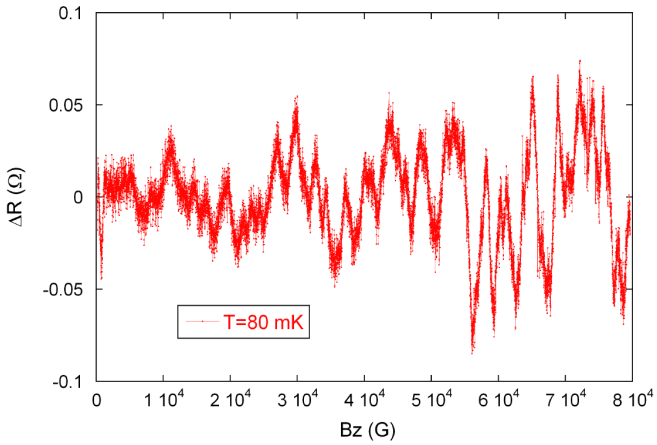

Figure 3.3: Variation of the resistance as a function of the perpendicular magnetic field on a 700ppm AgMn spin glass wire at 80mK. The amplitude of the UCFs is not constant and increases with the magnetic field despite the fact that $T \ll T_g$. This proves that some magnetic spins remain unfrozen (and can be polarized) even at temperatures T as low as corresponding to $T/T_g = 0.2$. From [20].

However, T.Capron[20] proved that, even for $T \ll T_g$, the amplitude of the traces increases as the magnetic field goes higher as pictured in Fig.3.3! And, as presented just before, this means that L_ϕ increases. It confirms that some *free* magnetic impurities are present and can be polarized by the field, acting on the coherence length. Thus, it still exists free spins in the glassy phase even for $T = T_g/10$, which is really surprising!
More quantitatively, we can relate the amplitude of the UCFs at low field with L_ϕ. Thus, $\tau\phi$, which is proportional to the number of free spins, can be deduced. And, even more surprisingly, the results show that even at $T/T_g = 0.2$, 20% of the spins are free! This is totally at odds with the previously accepted idea that all the spins get suddenly frozen at T_g.
This also unveils the fact that many spins do not participate in the formation of a spin glass and that they have to be taken into account when one wants to consider electronic transport in those magnetically disordered systems.

At this point some people may argue that we are in small systems and that we're extrapolating results taken on bulk materials. I would answer that G. Forestier et al.[29] showed that, even in small systems like ours, the T_g, the $R(T)$ and $R(B)$ (Fig.3.4) are totally equivalent to the ones measured in bulk materials!

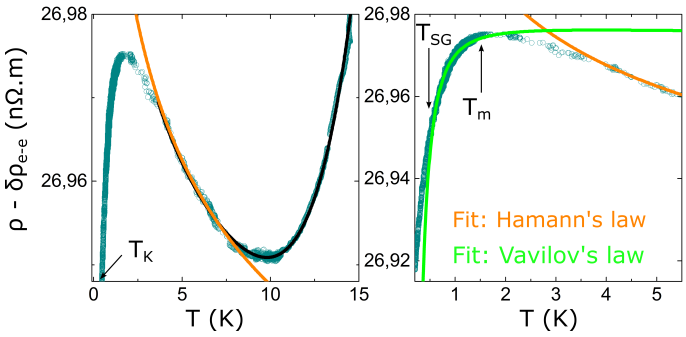

Figure 3.4: Resistivity without the electron-electron interaction contribution as a function of the temperature for a 500ppm AgMn spin glass wire. On the left panel, we can clearly see the decrease of the resistivity with the temperature until reaching 10K, due to the electron-phonon interaction being killed (black fit). Then a logarithmic rise appears until 2K because of the Kondo effect as shown in Fig.3.1 (orange fit). On the right panel, we present a zoom on the low temperature part. After reaching the maximum at T_m, the resistivity decreases again due to the apparition of the glassy phase. As the spins get frozen, the Kondo effect is killed resulting in this decreasing. From [29].

Thus it means that the electronic transport in small systems and in bulk are the same. We can then easily transpose the data we get from our systems to more "standard" spin glasses.
From that, what else can we say about our measurements?
Actually, the main aim in our work is to precise more quantitatively how much the spin configuration changes between two quenches. In order to do so, we base our further conclusions on a quite recent article by D. Carpentier and E. Orignac[21]. In that paper, they propose a theoretical expression allowing to connect directly the mathematical correlation between UCF traces and the overlap between the real equilibrium states those UCFs represent.
As seen in Chapter 1, we can define an overlap $q_{\alpha\beta}$ between the different states in the spin glass phase and, from that, a distance $d_{\alpha\beta}$ which is more easy to handle. Indeed, if two states are almost identical the normalized distance is $d_{\alpha\beta} \approx 0$ and if they are really different, they are "far" so $d_{\alpha\beta} \approx 1$. What is impressive is that those theoreticians proved that comparing different UCF traces corresponding to different states allows to exactly know *quantitatively* how far those two states are!
It can then give us information about the structure of the phase space as defined in the Chapter 1.
Also, they propose an experimental process pictured in Fig.3.5

Basically, it consists in measuring the UCFs at a given temperature T_0, heat up the

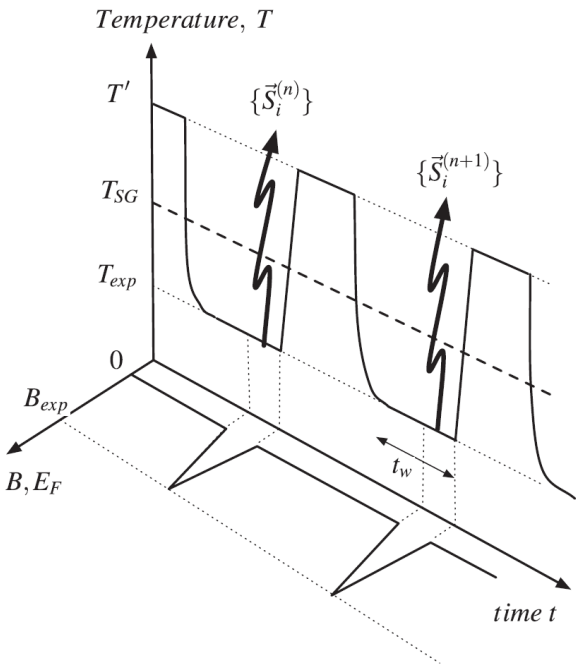

Figure 3.5: Representation of the proposed protocol by D.Carpentier. A UCF trace n representing the configuration $S_i^{(n)}$ is taken by sweeping the magnetic field at a temperature $T_{exp} \ll T_g$. The field is then brought back to zero. After that, the system is heated up to a temperature $T' \gg T_g$ during a time t_w and then brought back to T_{exp}. A new UCF trace $n+1$ representing the configuration $S_i^{(n+1)}$ is then taken. This process is repeated over and over. At the end, the correlations between the traces are calculated, leading to having a statistical distribution of correlation values, giving informations about the phase space structure. From [21].

measured sample at a temperature $T_1 \gg T_g$ during a given time t and then compare the UCFs taken before and after the protocol. By repeating this process a large number of times, statistics can be made and a distribution of the correlation values can be displayed. From that, we can get the distribution of the overlap values $P(q,C)$, for this spin spatial distribution C, but not directly the $P(q)$ as defined before. Indeed, the $P(q)$ is defined as the average of $P(q,C)$ over all the possible configuration i.e. $P(q) = \langle P(q,C)\rangle_C$. We thus would need to experimentally get $P(q,C)$ for many different spatial distributions by warming up the sample to a temperature such that spins can move in the sample and repeat the previously defined protocol.
If the structure of the phase space is standard, as pictured in the droplet model, the $P(q)$ should have a standard distribution whereas in the case of a mean-field model as Parisi's one, the distribution would be totally different as pictured in Chapter 1, Fig1.9.

You have now all the keys to understand why the investigations on coherent electronic transport in mesoscopic spin glasses are relevant to contribute to one of the biggest question

in condensed matter physics: the nature of the spin glass phase!
And since we are really interested in addressing that question not only theoretically but for real, I will now expose the different methods and equipments required to experimentally answer it.

CHAPTER 4

Experimental setup

If one wants to study coherent electronic transport, many requirements are to be fulfilled in the setup. First of all, L_ϕ must be comparable to the length of our samples[1]. Two strategies seem available to achieve this point : the first one is to reduce the sample size as much as you can to be close to L_ϕ while the second one, on the opposite, consists in enhancing L_ϕ in the sample.
Another issue lies in being able to detect those quantum variations that are, as we have seen, of the order of e^2/h. In systems like ours (typically a few tenth of ohms), it corresponds to very small resistance variations. This requires our measurement lines to add as less parasitic noise as possible. Indeed, we have two major sources of noise in our experiments, electronic noise and thermal noise.
This chapter will be dedicated to the presentation of the experimental techniques allowing us to fulfil all those requirements.

4.1 Sample fabrication

During my Phd I measured several kinds of samples made by different people. Some of them were boron-doped diamond (Bousquet et al.), others were superconducting samples (CEA Leti). Here I will focus on the samples used for my thesis main subjects: mesoscopy and spin glasses.
The geometry of our samples are made in such a way that we are in a quasi-1D regime, allowing us to have a better contrast $\left(\frac{\Delta G}{G}\right)$ to see quantum effects. Indeed, when are in this regime, the resistivity in enhanced as only a few conductions channels are present. And since we've seen that those variations are of the order of e^2/h (i.e. one conductance channel), it means that the smaller the conductance (the less conduction channels), the more contrast we can get.
But other conditions have to be taken into account ! When we'll measure UCFs, we need to sweep the magnetic field over a few $B_c \approx \frac{\Phi_0}{w\, L_\phi}$ (defined in Chap.2 as a critical field to be in the ergodic limit). The main problem here is that B_c is defined as the field needed to put a quantum flux into a surface of size $L_\phi \times w$ (in the limit where $w < L_\phi$). Thus w has

1 A strong notable exception is the weak-localization feature that is totally robust to the length of the sample.

to be large enough to make B_c experimentally reasonable[1].
In the end we chose to make samples that are 100 nm large, 50 nm thick and few microns long as shown in Fig.4.1.
Since those samples are of nanoscopic size, we need specific techniques to produce them,

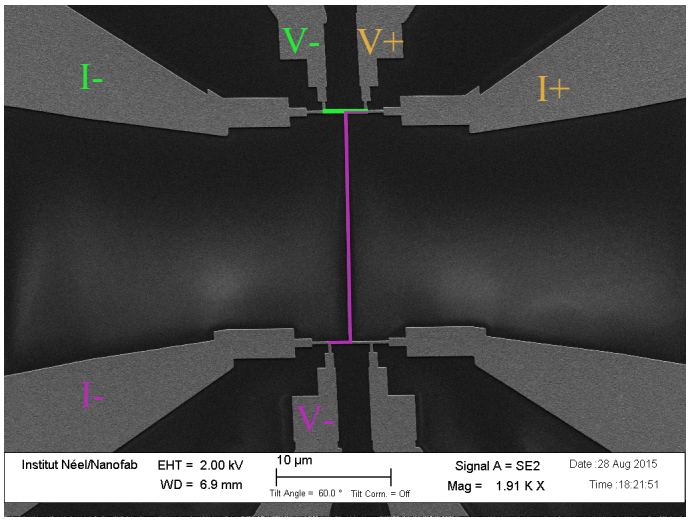

Figure 4.1: SEM image of a typical sample. The sample can be measured with two configurations with the contacts in orange being unchanged. The first one is depicted in green. It allows to measure the 3μm sample (green). In violet is the second configuration that allows us to measure the 25μ sample.

like electronic lithography for example.
The samples I used were made by the previous PhD student that worked on the subject (Dr. Guillaume Forestier) at the PTA (CEA Grenoble) with the following procedure : Some resist is applied on a silicon wafer. Then a focused electron beam is used to draw the desired pattern. Afterwards, the wafer is set into a developer fluid that will remove the insulated resist (positive resist). Next, we simply have to deposit the desired material in the holes we made and remove the remaining resist (lift-off process).

Now we got “pure" samples. In order to make spin-glasses, we have to dope them with magnetic impurities. To do so, we use an ion implanter in Saclay (near Paris, France), in which we irradiate our samples with a focused ion beam at a fixed power designed to dope them uniformly with the desired concentration.

Once the samples are made, it is now time to measure them! For that, we need, as previously explained, to enhance L_ϕ and thus cool them down to very low temperatures.

1 By reasonable we mean that we should be able to sweep over at least $10B_c$. And since $B_{max} = 6T$ in our experiments, it gives a maximum limit of $B_c = 0.6T$.

4.2 Cryogenics

In order to go to low temperatures, we use a so-called “dilution" fridge.
The principle of this kind of fridge is to use a peculiar property of helium isotopes[45]. Indeed, helium can be naturally found with two different isotopes, namely ^4He (99.9999 % of the total helium) and ^3He (0.0001%). When a mixture of those two elements is set around 870 mK, it undergoes a phase separation between a poorly concentrated ^3He phase (with a lot of ^4He) called “diluted phase" and a highly concentrated ^3He phase (with few ^4He). Moreover, as can be seen on the phase diagram in Fig.4.2, the concentration in the diluted phase is directly related to the temperature of the mixture.

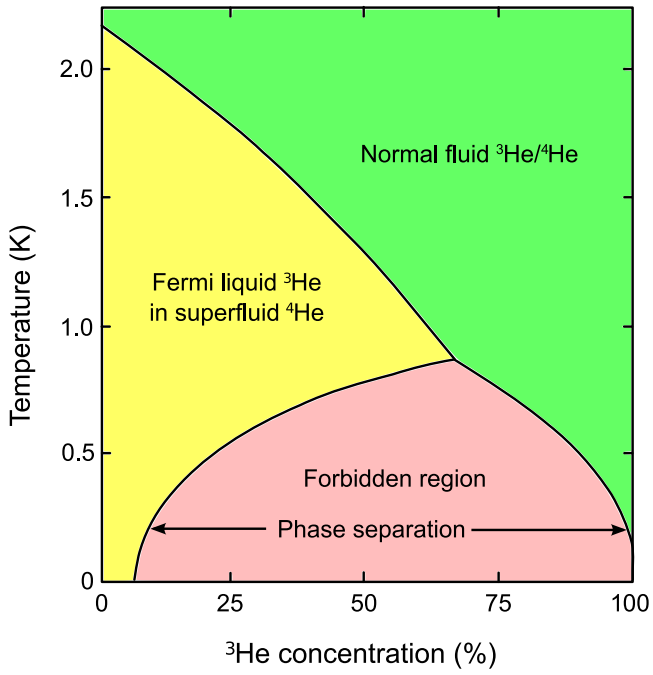

Figure 4.2: Phase diagram of a mixture of ^3He and ^4He. Below 870mK, a phase separation appears between a poorly concentrated ^3He phase (left branch on the diagram) and a highly concentrated ^3He phase (right branch on the diagram).

In a dilution fridge, this mixture is in a close pumping circuit as shown in Fig.4.3. The proportion of each element is set such that the interface between the two phases appears in the so called mixing chamber. This mixing chamber is simply a box whose section is much larger than the tubes to increase the surface over which we can pump, and thus the quantity of pumped mixture. As ^3He is lighter than ^4He, the concentrated phase will be on top of the mixing chamber and the diluted one on the bottom. The cooling process is thus the following : if we manage to lower the concentration of ^3He in the “diluted phase", a disequilibrium will appear and will be offset by ^3He migrating from the concentrated phase to the diluted phase! This process is endothermic (meaning that it absorbs thermal

energy from the environment) and is responsible for the cooling process. In the fridge this is achieved by directly pumping on the diluted phase. ^3He being lighter, in proportion it will be pumped more than the ^4He and then the concentration of ^3He decreases.

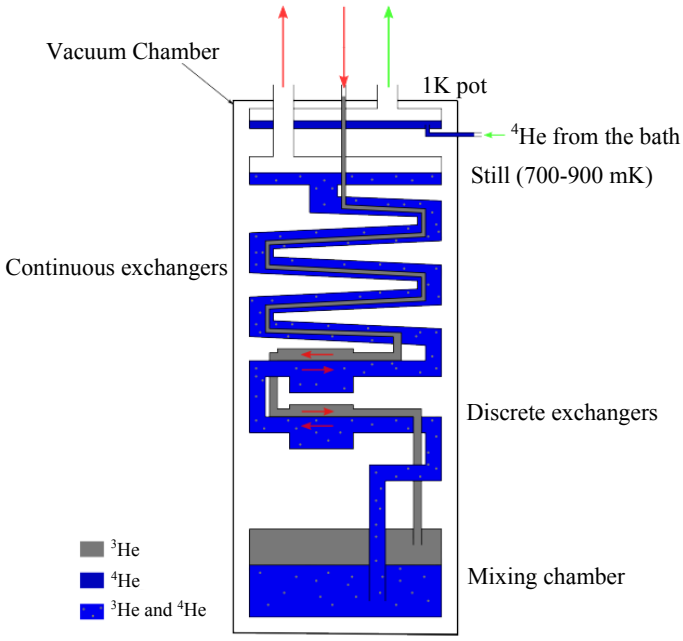

Figure 4.3: Representation of a dilution fridge. The ^3He is going in and gets cooled down by the ^4He bath, the 1K pot, and then by the outgoing mixture in the exchangers (continuous and discrete). The mixture is pumped out of the fridge from the still. Pumping ^3He from the mixture is easier than ^4He, making a disequilibrium and starting the dilution process.

The pumped ^3He then goes up in the fridge to the pump that is at room temperature and is then reinjected, closing the circuit. And actually, if everything is done right, the main heat flux comes from this reentering mixture, leading to a major problem to cool down as you cannot avoid it. Indeed, in a cryostat, we cannot afford to have such a huge entering heat when we already have leaks as the fridge is never perfectly isolated and thermalized. Moreover, as we're going down in temperature, the cooling power of our fridge decreases as T^2 (which is really fast!). However, since the ^3He going out of the mixing chamber is really cold, it would be a shame not to use it to cool down the reinjected mixture coming from room temperature! To do so, several heat exchangers are placed along the circuit to maximise the efficiency of the process by pre-cooling the entering mixture with the one going out.
It has to be noted that in order to be able to make this dilution process work, the mixture has to be pre-cooled around 870mK to provoke the phase separation. This seems already a big gap to cross since we're starting from 300K...
But in reality it is not such a big deal!
First, we simply place the dilution circuit into liquid Helium at 4K placed in a dewar. This

allows to pre-cool the whole system and mixture to 4K. Then, as we need to go below that temperature, we need to isolate the sample and mixing chamber from that “warm" environment. This is achieved by placing the sample chamber (IVC) into vacuum once it is at 4K. That way, it won't be in thermal contact with the 4K bath and can be cooled down well below that temperature. Then, by making a Joule-Thomson expansion thanks to a compressor in the dilution circuit, we bring the mixture temperature from 4K to 1K. But we're not yet to 870mK, we have one last step.
To go from 1K to the phase separation temperature, we just have to let the pumping system do all the work! Indeed, at 1K we are pumping on a real mix of ^3He and ^4He as it didn't undergo its phase separation yet. The mixture can then be seen as a ^3He gas on which we pump. And since the temperature of ^3He at low pressures can go down to 200mK, we have some cooling power to bring the whole system to 870mK!

4.3 Wires

Now that we are able to cool the sample down to very low temperatures, it is necessary to ensure that nothing will bring extra heat and warm it up. Indeed, if the cryostat is empty with no wire and only the sample we can go down to 10 mK. But, since we actually want to measure the sample, we need to connect it with wires that will go up to our measurement devices at room temperature. Unfortunately, when one connects something warm (here at 300 K) with something cold (10 mK) some heat is exchanged... Our goal is thus to minimize this exchange due to the wires.
Moreover, those wires have an electrical resistance and add some thermal noise on the voltage measurements via the Johnson-Nyquist[38, 55] noise as well as they conduct hot photons.
Those two issues lead us to adapt our setup in a particular way. First, we have to thermalize our wires as much as possible on the different stages of our fridge. That way, once they arrive on the sample, the wires will carry minimum heat because it will have been dissipated all along the fridge before. To minimize even more the heat flux, we can use longer wires to have more length and then increase the heat resistance (Wiedemann-Franz law)!
However, here we considered only heat flux coming from 300K directly into the wires. Another source of heating comes from the surrounding environment via radiative processes[30]. Indeed, any matter irradiates photons whose energy is proportional to their temperature (black body). Thus, those photons can be absorbed by any other matter and, in our case, by the wires or directly the sample. And if those photons are “hotter" than the sample (for example coming from the IVC walls which are at 4K since touching liquid helium), they will heat it up! To prevent that, the sample is shielded with some metal box that is connected to the mixing chamber and thus irradiating only low temperature photons. Concerning the wires, we use thermocoaxes between 4K and the sample. They proved themselves to be excellent high frequencies filters[81] (perfect for photons) and do not carry much heat. Moreover, we need long lines to thermalise the electrons. Indeed, the dissipation via phonon is so reduced at low temperature that long wires are needed for electrons to have time to thermalise. To summarize we use two meters-long wound thermocoaxes wires in between 4K and the sample.

From now on, you know everything to wire a cryostat from 4K to 10 mK.
However we didn't say a thing about wires going from 300K to 4K. Actually this is much simpler and the only problem resides in the thermal noise that they could bring. To prevent that Johnson-Nyquist noise (scaling as $\sqrt{R}$) and parasitic electromagnetic one, we simply use shielded coaxial wires with very low resistance (few ohms per meter).
Well, now that we are able to electrically measure our samples at low temperatures, let's see the external setup!

4.4 Heating the samples

In most of my experiments, I need to be able to heat the sample at temperatures way higher than 4K. And as we've just seen, the cryostat allows me to go to very low temperatures but hardly higher than 4K. Of course we can still isolate the sample and then heat it up by passing current into a resistor placed on the mixing chamber. This allows us to heat all the fridge and thus use the usual thermometer to know the temperature. This technique is, however, really time consuming as you can't use high currents and the heat has to propagate through a mass whose calorific capacity increases with temperature. For example it would take about a day to warm the fridge up to 50K without burning the wires...
Moreover, we are not interested in warming up the whole fridge! We just need to heat up the sample. Thus we could just pass some current through it! The other interesting point in doing so, is that it allows us to quench the sample fast after heating. Indeed, when one stops passing current, the sample, since heated very locally, will rapidly recover its initial temperature[1]

The crucial point here is to calibrate precisely this process. To do so, we rely on the resistance variation of our sample as a function of the temperature. Indeed, we measure once the R(T) of our sample by heating the whole cryostat and then compare it with the one we get by heating with a current. Both curves are displayed on Fig.4.4. It is then possible to identify which temperature corresponds to a given current, and thus, once calibrated, to use the current to heat up the sample.
However, it has to be noticed that, below 1K, the electrons are really badly coupled to phonons. Thus, passing current is not an efficient way to heat up the sample below 1K. Hopefully, for those temperatures we can still heat with the dilution on, and that's what we will do.

1 Of course this requires a local heating only. If the environment is also heated the sample cannot relax the heat properly.

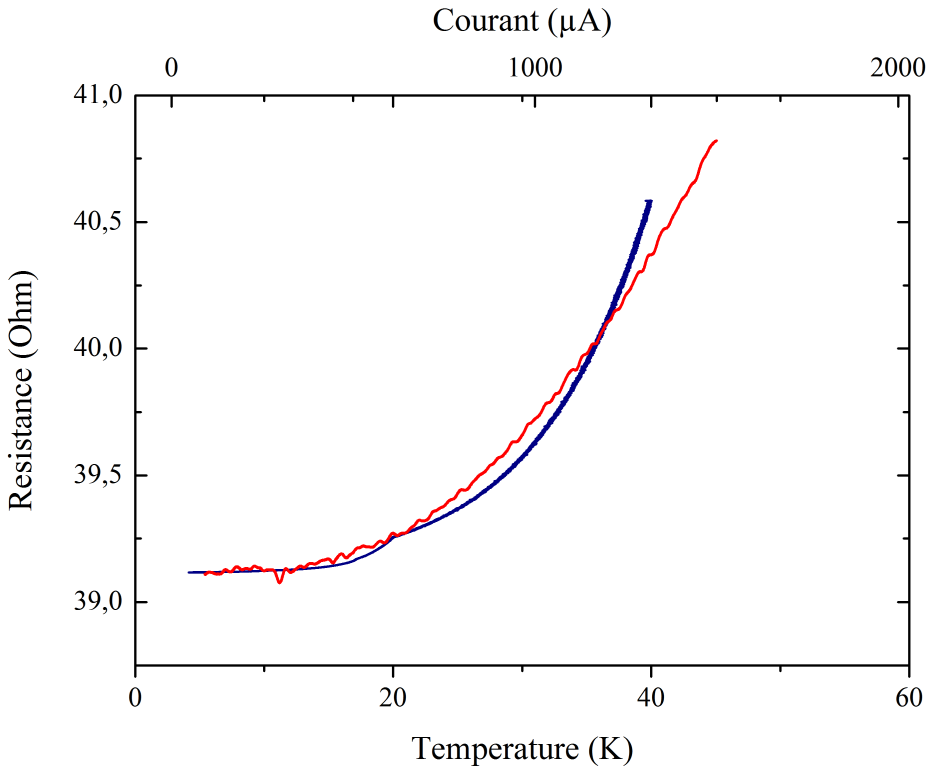

Figure 4.4: Calibration of the sample heating. In blue, the resistance as a function of the fridge temperature is displayed. In red, the resistance as a function of the current sent in the sample is shown. To calibrate the heating in the sample, we just make a comparison between the two curves, allowing us to have the Heating Temperature as a function of the Current sent.

4.5 Magnetic field measurements

As explained in the previous chapters, most of my work will be based on magneto-resistance measurements. In order to make those measurements, we need to sweep the magnetic field applied on the sample. To achieve that, we use a 2-axes superconducting coil. It is constituted of two separated parts : the first one is simply a solenoid allowing to apply a field perpendicular to the sample and whose maximum value is 8 T; the second one is situated around the solenoid allowing us to make an in-plane field with a maximum value of 1.3 T thanks to two Helmholtz coils.
The first choice we had to make was to choose the span over which we would sweep the field. This has been a heavily debated subject and after some tests (that will be explained later on) we chose to sweep in between 0 and 6 T.
This is quite simple but, during my PhD I faced a major problem while sweeping the magnetic field. Indeed, during my first year some strange features appeared at low field (< 1000 G) while sweeping. I later discovered that those features were undesired effects due to a huge extra heating on the sample. The main question then was to discover where

it was coming from. The first idea was a problem of spikes in the current sent into the coil. But despite changing the power supply twice and recording the current sent to the coil to check for anomalies, the problem was still there. I thus removed one by one every piece of the setup. Upon close inspection, it appeared to be a problem inside the sample holder and, actually, was the soldering...
To solve the problem I thus needed to design a new sample holder in which the soldering wouldn't be based on tin. The solution I opted for was to use silver-based epoxy as solder. One of the main quality of that choice is that it is pretty easy to use since it is not necessary to mix several components in that version. Moreover, even on small soldering the contact resistance is really low (only 1 to 2 ohms). The counterpart of this, is that it is mechanically weak and it has to be manipulated with caution.
Once the soldering problem was solved, we had to care about mechanical problems such as the size of the sample holder, the length of the cables, etc..
The protective screen of the sample has a diameter of 28 mm, limiting the sample holder size. We thus decided to design the sample holder as a PCB circle of diameter 26 mm on which a metallic circuit is printed.
After the sample is glued, it is important to properly connect it electrically in order to measure. First step, we obviously have to connect it to the sample holder. We just simply bound it with Aluminium wires from the sample pad to a metallic part on the holder. Second step, it is necessary to connect the sample holder to the measuring lines in the cryostat. Moreover, we want to be able to disconnect the entire sample holder from the cryostat to connect easily the sample and manipulate it before cooling down the fridge. Thus we have to imagine a system in which we can plug the holder in the cryostat. For that, we chose to use Omnectics connectors because it has been already used in cryogenics without any noticeable problems or deterioration (as far as we know) and because of their really small size allowing us to have two rows of twenty contacts on such a small surface. Male connectors are set on the holder and female ones are set on the cryostat side. The only problem with it, is that the connectors are so small that the pins are really close and soldering them without bad contacts between them is not easy. Third (and final) step, we have to connect the female connectors to the wires. For that the female connectors are set on another PCB placed in a copper box. On this PCB the connectors are connected to metallic tracks and then to the wires soldered with the previously cited silver epoxy.
Finally, this whole system allowed to reduce extra heating by, at least, a factor of ten. The residual heating is probably due to some tin which is still present in the wires themselves.

Now that we solved that issue, we are able to send current into the sample and to measure the voltage. However, we cannot simply measure the resistance with some usual everyday devices as, for example, voltmeter: we wouldn't be precise enough. We thus need to use some special schemes that I will now describe.

4.6 Low noise measurements

As seen in the previous chapters, the typical variation of conductance we're looking for is of the order of G_0. So what does it mean for the *resistance* variation? Let's take $G = G_m + \Delta G$, with G_m the mean value of the conductance and ΔG the variation of it.

Respectively we define $R = R_m + \Delta R$. We thus have:

$$\begin{aligned} R = \frac{1}{G} &= \frac{1}{G_m\left(1+\frac{\Delta G}{G_m}\right)} \\ &= R_m\left(1+\frac{\Delta G}{G_m}\right)^{-1} \\ &\approx R_m\left(1-\frac{\Delta G}{G_m}\right) \\ R &\approx R_m - R_m^2 \Delta G \end{aligned}$$

From here we get that

$$\Delta R = R_m^2 \Delta G$$

So now, if $\Delta G = G_0$, as we expect we have that $\Delta R = R_m^2 G_0$ and is thus dependent on the absolute value of the resistance!
In our system, since the resistance of the samples is typically of 100 Ohms, this variation will be roughly of 0.4 Ohms maximum if we are in the best conditions (like having $L < L_\phi$). Of course this is (unfortunately...) never the case and if we want to have a short sample, the resistance will be way lower and the variations will be of the order of 0.01 Ohms... It thus becomes clear that we need very precise devices.
To do so, we use a bridge configuration to increase the dynamic of our devices. By dynamic, we mean the variation of signal over the total signal the device receives. Indeed, on digital devices, it is much more difficult to see a variation of 1Ω over $1\text{G}\Omega$ than 1Ω over 10Ω because of the discretization. If you have 16 bits and measure a $1\text{G}\Omega$ signal, the lowest variation ΔR_{max} you can see is $\frac{10^9}{2^{16}}$ representing 15258 Ohms... There is no way you can see a 1Ω variation... Whereas if your signal is of 10Ω you get $\Delta R_{max} = \frac{10}{2^{16}} = 1.5 \times 10^{-4}\Omega$ making your 1Ω variation visible!
The bridge configuration allows us to add a negative signal to what we measure to compensate its mean value. For example, if we are watching at the variation around a 40Ω signal ($\Delta R_{max} = \frac{40}{2^{16}}$), we will "subtract" 39 Ω and get a $\Delta R_{max} = \frac{1}{2^{16}}$, which is much better!
But another point has to be considered. Having instruments with a high dynamic is of course important but what about noise? Because if the signal is lower than your noise, even with the best possible dynamic you'll never be able to measure anything. We could answer that to measure a resistance we could simply send more current and, just by Ohm's law, we would get a higher voltage and thus the Signal to Noise Ratio (SNR) would be really high as the noise is constant no matter which current strength we send.
However, we face another issue here. If one sends a current in a resistive sample, some Joule heating will appear. And, as we saw before, we made a lot of efforts to avoid extra heating on the sample...
Actually, at the mesoscopic scale, we are less concerned by the sample temperature than

by the electrons one (knowing that the electrons can be hotter than the sample but not the opposite) but the idea remains. Actually our samples are smaller than l_{e-ph} when at low temperatures such that we cannot count on the phonons to cools down our electrons. In our case, the limit we have is then that the energy the electron can give to the sample is lower than the thermal energy of the phonon bath i.e. $eV = eRI \leq k_B T$ with V the voltage across the sample, I the current and R the resistance[61].
This gives us a strong limitation on the current we can send into the sample and brings directly back on the table the question of noise.
Another solution to reduce the measured noise is to reduce the frequency window (bandwidth) in which we measure. Indeed, that way, all the noise out of this window will be excluded from the measurement. This can be achieved by using lock-in amplifiers.
Lock-in amplifiers are widely used in voltage measurement for their ability to exclude most of the noise sources such as 50 Hz or high frequency noise.
In my case, the lock-in is used as a sinusoidal voltage source (ranging typically from 10 Hz to 100kHz) and also as a measurement device. In short, it will multiply the signal sent to the sample with the one measured, which will, based on a mathematical principle about sinusoidal function, suppress any signal which is not at the same frequency as the exciting signal. The bandwidth is then really small and the signal less noisy.
To enhance again the SNR, another simple trick would be to average the signal longer by increasing the integration time of the lock-in (also called time constant). The lock-in averages the signal longer, which reduces the final noise as the square root of the integration time. This is even the simplest way actually... But of course when something is too simple, there is a counterpart.

4.7 Setup calibration

And this counterpart is that averaging your signal can make you loose a lot of information! On a general point of view, just imagine that your signal varies sinusoidally on time with a temporal period of T as on the blue curve in Fig.4.5. If one averages over a time which is between 0 and T, the result will be a curve whose amplitude is reduced and that will be shifted as shown on the green curve of Fig.4.5. And even worse, if we average over a time superior to T what you'll recover will just be zero...

An example on my measurement is displayed in Fig.4.6 for a given magnetic field sweep speed. It is clear that when averaging, the data look smoother but also highly shifted and that the amplitude is reduced.
As we have just seen, this problem is due to the fact that the signal changes too fast compared to the integration time. The strategy here is then to keep a long integration time (to increase the SNR) while making the signal change slower (from a temporal point of view) by sweeping the magnetic field at a lower rate. This can be seen in Fig.4.7 where the sweep rate is changed while keeping the integration time constant.

Of course this lengthens the measurement duration in a not negligible way... Moreover, it has to be noticed that we're not talking about minutes or seconds, but hours! And if the duration is too long, we then recover the well-known 1/f noise that mainly comes from the

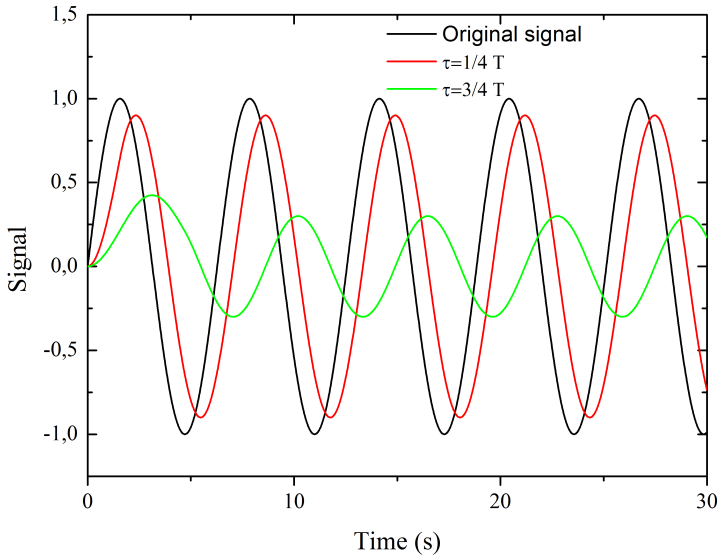

Figure 4.5: In black, an example of a sinusoidal signal with a period T. In green, the same signal but averaged over a time $\tau = \frac{3}{4}T$, like would do a lock-in with a time constant τ. We clearly can see that the amplitude of the oscillations is lowered and that the signal is shifted. However, if the time constant is reduced, we recover a signal much closer from the original one (red curve).

drift of the instruments over time. Unfortunately, that can be really annoying for our data post-treatment...
As you can see, when improving the SNR, we have to face many problems. Indeed, when we increase the integration time, we have to reduce the sweep speed and thus increase our measurement duration leading to having 1/f noise.

It becomes now pretty clear that we need to find a good balance between all those parameters to find the optimum ones for our experiments.
Let's then start by the end: the 1/f noise. The noise curve is displayed on Fig.4.8

To keep the 1/f noise level at a reasonable level, we cannot afford experiments that last more than 8 hours. Meaning that we have to sweep at a speed of $60000/8 \times 3600 \approx 2G/s$ as the lowest speed. From that, we can deduce, from the previous measurements displayed in Fig.4.6 , that we can average up to 20 seconds without loosing too much information. Actually, the gain that you get by passing from 10 seconds to 20 seconds average is quite negligible (we gain only a factor of $\sqrt{2} \approx 1.4$)... We thus decided, for the obvious reason of making experiments faster, to speed up the sweeping to 5G/s with an integration time of 10 seconds leading to a roughly 4h long measurement.

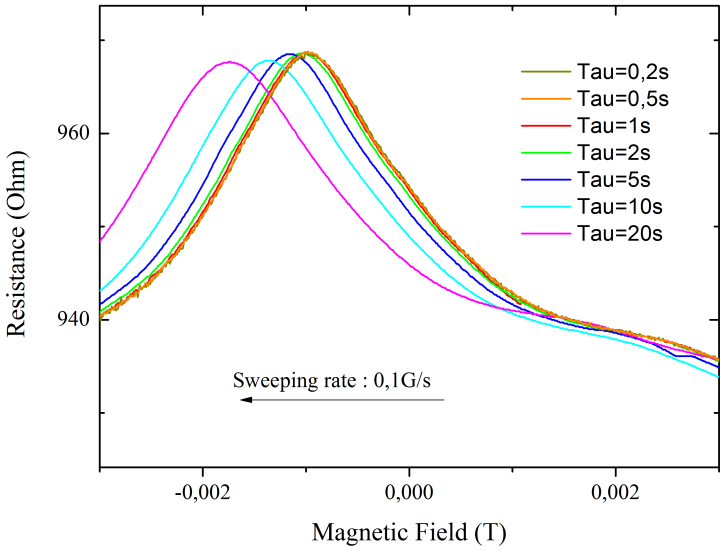

Figure 4.6: Resistance as a function of the magnetic field for different lock-in time constants and a fixed magnetic field sweep rate (0.1 G/s). With low time constants we ensure to get the expected signal. As the time constant is increased, we see that the signal gets shifted and looses its amplitude, as also shown in Fig.4.5.

You may have also noticed that I did not say a word about the frequency at which the samples are measured. Indeed, we measure our samples at a really low frequency ($\approx$ 12Hz), which prevents us from any capacitive effects[1] and allows us to measure at a frequency at which the environment noise is at the lowest.
Now that we made our setup calibration clear in order to have nice raw data, let's see how the post-treatment is done.

1 The capacitance between our wires and the ground is $\approx$ 5nF and the total resistance of the wires and the sample is $\approx 200\Omega$, leading to a cut-off frequency around MHz...

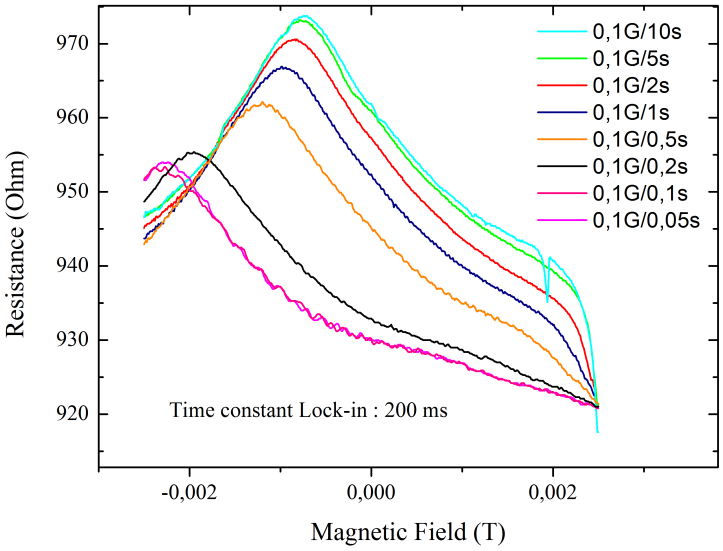

Figure 4.7: Resistance as a function of the magnetic field for different magnetic field sweep rates and a fixed lock-in time constant (200ms). As seen in Fig.4.6, the lock-in time constant and the magnetic field sweep rate have to be consistent with the variation speed of the signal. Here, we see that when the field is slowly swept i.e. when the signal changes *slowly*.

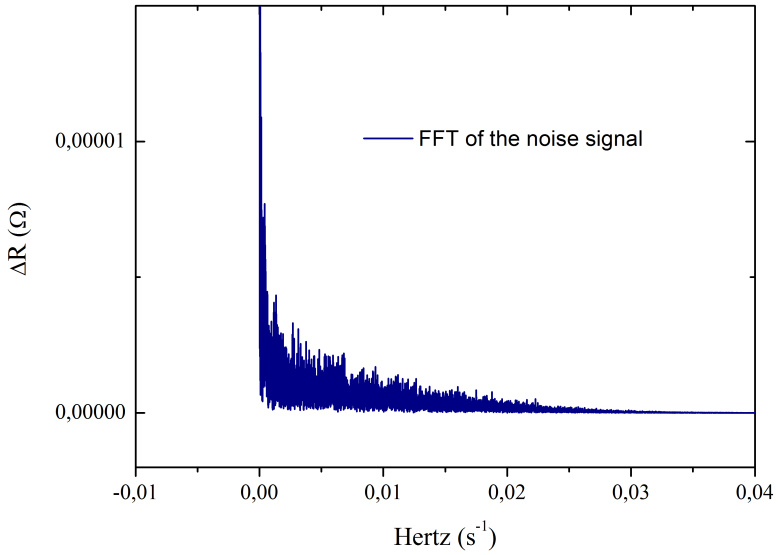

Figure 4.8: Fourier transform of the noise signal. The resistance of a sample has been measured during 36 hours at a constant field. The signal measured is then the noise of our setup. One can see that to keep the noise at a reasonable level, we need to keep the measurement time below 8 hours.

4.8 Data post-processing

We all know that post-processing is very important to obtain comprehensive results. But the usual pitfall with it, is that you can make almost anything appear with a good post-treatment[1]...
I thus want to explain how my data are treated such that there is no concern about it and then about the results.
First, as seen before, we chose good parameters to have our raw data with all the informations we need (not smoothing artificially or loosing amplitude). Then we obtain magneto-resistance curves such as presented on Fig.4.9

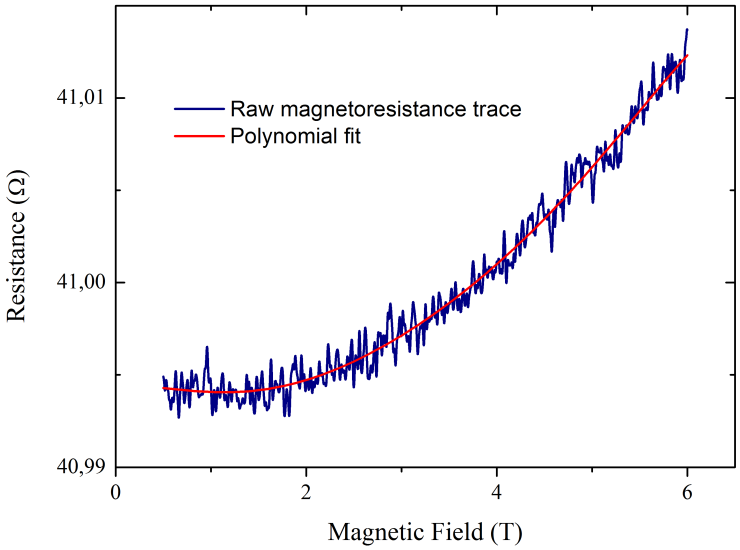

Figure 4.9: Resistance of a pure silver sample as a function of the magnetic field. The signal consists in two different parts, a classical one and a quantum one. The first one is fitted by a polynomial fit that is subtracted afterwards.

Since we're more concerned by the UCFs, it is crucial to remove the classical part of the resistivity.
Two approaches were considered. The first one was to opt for a fixed band-pass filters that would remove high frequency noise (that are not physical) and also the classical low-frequency part of the resistivity. The problem with that option is that, because of the low frequency noise, the measurements for two supposedly identical curves would be different... Moreover, some of the low frequency components of noise (1/f noise, classical

1 As John Von Neumann said:"With four parameters I can fit an elephant, and with five I can make him wiggle his trunk".

part,..) have the same frequency than some signals we're looking for!
We thus opted for the second option, namely to fit our data with a high-order polynomial fit and subtract it. The counter part of this method is that the fit you take is slightly different from one curve to another but it is also its strength! Indeed, as we've just said, low frequency noise can change over time. Thus, the fit can adapt to that change and provide a good subtraction of low-noise and classical part.
Thanks to that, we end up with exploitable UCF as can be seen in Fig.4.10

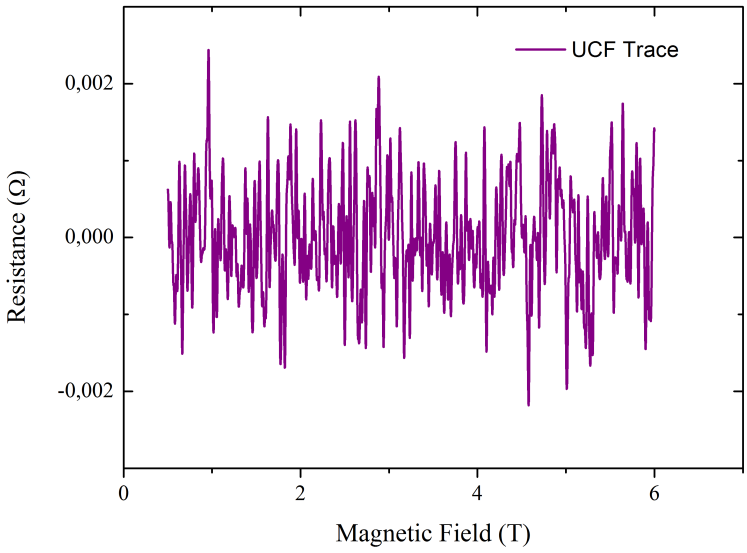

Figure 4.10: Quantum part of the resistance of a pure silver sample as a function of the magnetic field. The date are the same as the ones of the Fig.4.9. The polynomial fit is subtracted from the raw magnetoresistance data. We thus simply observe the quantum part of the resistance, namely the UCF.

Now that this has been explained and that we can agree that nothing has been hidden or that post-treatment will not interfere in our physical discussion, let's get into it in the next chapter!

CHAPTER 5

Experimental study of mesoscopic silver wires: changing disorder at low temperatures?

All along my PhD I have been trying to implement an experimental setup to test the idea developed in the previous chapters, namely using the electronic coherent transport to probe the disorder inside metallic samples and more precisely spin-glasses.
In this chapter I present some experimental results that I managed to obtain during my thesis on pure and manganese-doped mesoscopic silver wires.

5.1 Characterization of the samples

5.1.1 Geometry

The samples we used are 3 and 25μm-long silver wires made by electronic beam lithography (see Chapt.4 for more details), with a width of 200nm and a thickness of 50nm. Both samples are part of the very same wire but measured with two different configurations. One of the sample is left unimplanted (99.9999% pure silver) while the other is doped at 500ppm with Manganese (AgMn 500ppm). Those are depicted on Fig.5.1.
The first thing to do before performing any measurement is to precisely characterize our samples in terms of electronic transport.

5.1.2 Temperature dependence of the resistance

The resistance of both types of sample is thus measured as a function of the temperature. The results are displayed on Fig.5.2
The behaviour of the pure sample (a) is pretty simple to describe. When lowering the temperature the resistance decreases due the lowering of electron-phonon interaction[2]. Once arriving at 10K, the resistance saturates and is not anymore limited by this electron-phonon interaction but by the scattering on static impurities. Then, below 1K, another phenomenon comes into light: electron-electron interactions[7]. From those interactions result a $\frac{1}{\sqrt{T}}$ increase of the resistance below 1K to zero temperature.
We also get the resistivity at low temperatures (4K) $\rho_{pure} = \frac{R \times S}{L} = \frac{39.12 \times 2e^{-7} \times 5e^{-8}}{25e^{-6}} = 1.564e^{-8} = 15.64n\Omega.m$.
And from that we get the elastic mean free path $l_e^{pure} = 54nm$, taking the Fermi velocity $v_F = 1.39 \times 10^6 m.s^{-1}$.
On the doped sample (b), on the other hand, the behaviour is much more complex. At first, the resistance decreases from 300K to 10K because of the same processes happening

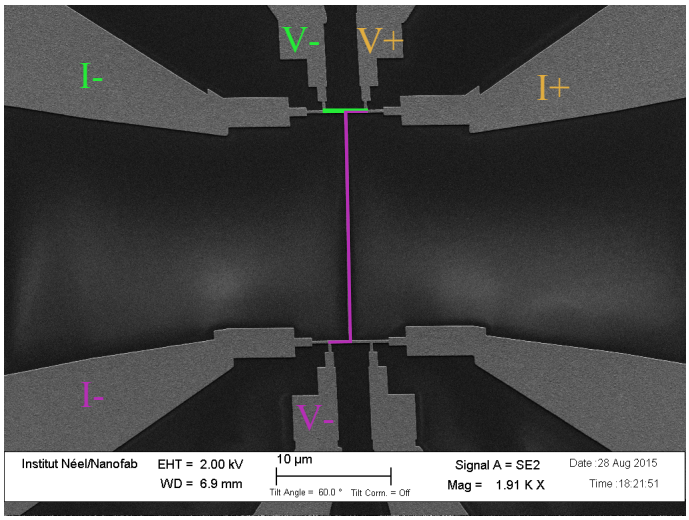

Figure 5.1: SEM image of a typical sample. The sample can be measured with two configurations with the contacts in orange being unchanged. The first one is depicted in green. It allows to measure the 3μm sample (green). In violet is the second configuration that allows us to measure the 25μ sample.

in the pure sample, namely the decreasing of electron-phonon interactions. But then, one can see a large increase that was not present in the pure sample curve. So what happens? Actually we already described this behaviour in the Chapter 3. Indeed, we are dealing here with a metal in which magnetic impurities are present. We are thus in the perfect situation to see the Kondo effect appear: the resistance increases logarithmically as the temperature is lowered due to the interactions of the electrons with the magnetic impurities.
Again, we can get the resistivity at 4K $\rho_{AgMn} = \dfrac{R \times S}{L} = \dfrac{18.1 \times 2e^{-7} \times 5e^{-8}}{3e^{-6}} = 60.3n\Omega.m$ and the elastic mean free path $l_e^{doped} = 15.7nm$.

At this point we can already be sure of the presence of magnetic impurities in our sample because of that behaviour. But what about the formation of a spin glass state? Shouldn't we be able to see it in the R(T)?
As can be seen in the inset of Fig.5.2(b), around $T = 1K$, the logarithmic increasing of the resistance stops and a sudden drop is observed. As seen previously, for the Kondo effect to happen we need ***free*** magnetic impurities. So if there is a sudden drop, it means that something suppressed the Kondo effect i.e. something froze the impurities that are thus not free anymore. We interpret that behaviour as the emergence of a spin-glass state that freezes the spin in a certain configuration, diminishing the number of free spins and thus killing the Kondo effect.
This global behaviour has been addressed theoretically by Vavilov and Glazzman[74]. They indeed predict a competition between a Kondo phase and a spin-glass one, with the latter being prominent at very low temperatures. From that, they predict the appearance of a

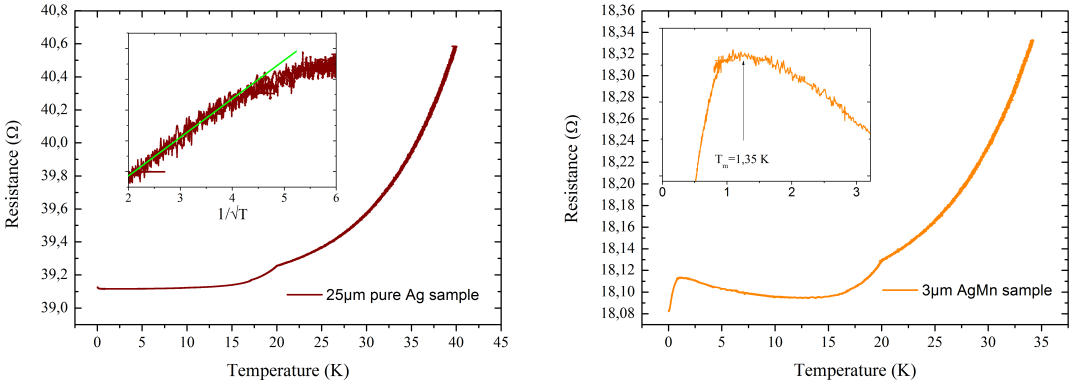

Figure 5.2: Resistance as a function of the Temperature for the pure sample (a) and the doped one (b). We can clearly see on (a) and (b) that both resistance behaviours above 10K are equivalent, decreasing as phonon modes are getting inaccessible. At low temperatures, (a) exhibits a standard behaviour for pure metals: it is flat between 10K and 1K and then a $\frac{1}{\sqrt{T}}$ increase of the resistance is observed due to electron-electron interaction as shown in the inset of Fig.5.2(a). The deviation from the linear fit comes from the saturation of the electron temperature below 50mK. The doped sample on (b) has a different behaviour: a Kondo logarithmic increase is observed until 1.5K, followed by a fast decreases due to the rise of the spin glass state.
In both curves, the anomalies that can be seen at exactly 20K are due to a change of sensibility on thermometer measurement and are thus not physical.

maximum in the resistivity at a temperature T_m that is directly related to the freezing temperature T_g by

$$T_m = \frac{\alpha_s}{2} T_g \ln\left(\frac{T_g}{T_K}\right) \tag{5.1}$$

with α_s being a constant depending on the spin and T_K the Kondo temperature. In AgMn, $\alpha_s = 2.33$ and $T_K = 40mK$[28, 62]. Here, extracting $T_m = 1.35K$ graphically and replacing it in their formula, we get a freezing temperature of $T_g = 470mK$. This value is very consistent with the expected concentration of 500ppm that would give $T_g^{expected} = 500mK$. From now on, we are sure that a spin-glass is present and that we doped with the right concentration while the pure samples behave exactly as expected as a function of the temperature.

5.1.3 L_ϕ measurement: the weak anti-localization

Another important point to characterize in our samples, since we will use coherent transport, is the electronic phase coherence length L_ϕ.
To measure L_ϕ in a mesoscopic sample, we can see two different ways. The first one is to use the weak localization[14] (or, in our case, anti-localization) process or the amplitude of

the UCFs[3]. The latter needs much more parameters and assumptions to properly work. In our system we thus decided to use the first one, namely, weak anti-localization.
As explained in chapter 2, this is an interference effect that results in a peak (or a dip) in the resistivity around zero field. The width and height of the peak are directly related to the dimensionality of the sample in terms of electronic transport, its geometry (that is perfectly known from SEM imaging) and to L_ϕ.

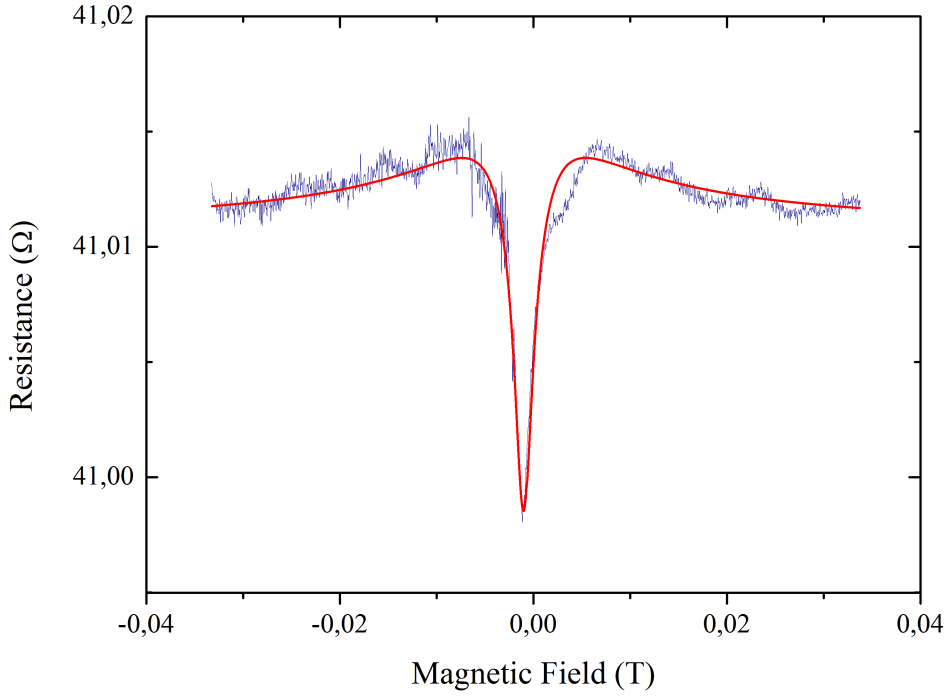

Figure 5.3: Resistance as a function of the magnetic field around zero field on the 25μm-long pure silver sample. This corresponds to a weak anti-localization measurement. The magnetic field is swept between -350G and +350G, exhibiting a strong dip in the resistance around zero field. By fitting this dip with known geometry parameters we can retrieve the value of L_ϕ. Here $L_\phi = 8\mu m$.

In our sample, we know that we are in the case of 1D electronic transport since L_ϕ is of the order of micron, whereas width and thickness are much smaller. Thus, by precisely measuring the resistance around zero field for 50mK, 100mK, 200mK, 600mK, 900mK and 4K, and fitting our curves with the 1D weak anti-localization formula, we can obtain $L_\phi(T)$. One typical curve taken at 200mK and its 1D weak anti-localization fit are displayed on Fig.5.3. We retrieve values ranging from 2 microns at 4K to 9.5 microns at 50mK with a spin-orbit length L_{so} of 1.1 micron.
Those values are coherent with what is usually observed in such samples. The variation of L_ϕ as a function of temperature can easily be explained by the fact that, when one rises

the temperature, more energy is available and thus more scattering processes are allowed to happen. However, here, L_ϕ does not follow the expected $T^{-1/3}$ dependence[8] as shown in

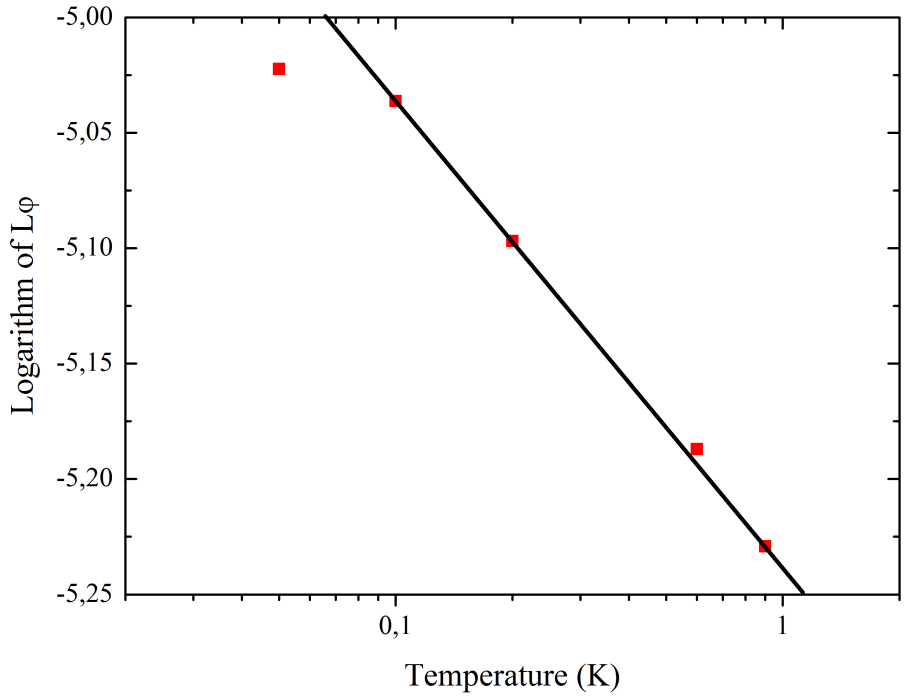

Figure 5.4: Logarithm of the L_ϕ values as a function of the temperature. The linear adjustment taken above 100mK shows a $T^{-1/5}$ dependence instead of the expected $T^{-1/3}$ one.

Fig.5.4. Why is that? Unfortunately, at low temperatures, we had to make a compromise between not over heating our sample and being able to precisely measure. We thus needed to use slightly higher current that we should have done to respect the $eV = k_B T$ rule. Our sample is then heated slightly over the fridge temperature and its behaviour deviates from the theory.
We stress that every single experiment that I will show later was made with the exact same set of parameters, namely same time constant, magnetic field sweep speed, and, crucially the same current as the one used to calculate L_ϕ. Those values can thus be used to interpret our further results without any restrictions.

5.2 Magnetoresistance and Universal Conductance Fluctuations (UCFs)

5.2.1 Magnetoresistance of the samples

Now that we fully characterized our samples in terms of size, shape, temperature dependence and coherence parameters, we can start trying to extract the UCFs. To do so, we

sweep the magnetic field between 0 and 6 teslas with a speed of 5 gauss per second at 100 mK, temperature for which we are deep in the glassy phase.
Data are plotted in Fig.5.5.

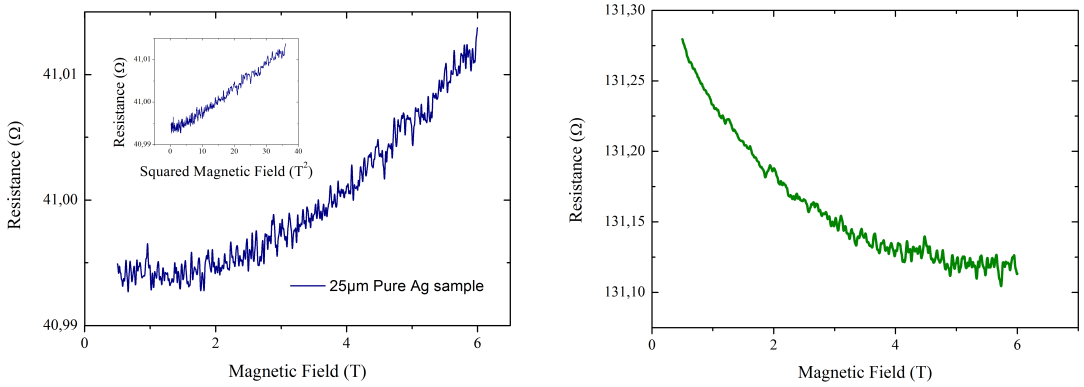

Figure 5.5: *Left panel*: Resistance of the 25μm-long pure silver sample as a function of the magnetic field. We observe an increase of the resistance as the field gets higher. This is coherent with the free-electron model under the low-field assumption. *Right panel*: Resistance of the 25μm-long AgMn sample as a function of the magnetic field. We observe a strong decrease of the resistance as the field gets higher. This is explained by the fact that we polarize spins with the field, diminishing the number of free spins and thus killing Kondo effect.

We can already see that, depending on the samples, the magnetoresistance behaviours are really different.

Pure sample

It is theoretically pretty difficult to model the resistance behaviour of metals under field. It depends on many parameters such as its composition, its crystallographic orientation, etc...[11] But in most cases, by assuming the free-electron model in metals and under the assumption of low-field, it is possible to prove that the resistance evolves quadratically with the field[80].
And indeed, on the pure Ag sample, one can see that we recover the expected quadratic behaviour as can be seen in the inset of Fig.5.5(a) in which it is plotted as a function of B^2.

Doped sample

Concerning the spin glass sample, things are different. We observe a strong decrease in the resistivity as we increase the field. As seen in the pure sample, in a metal without magnetic impurities, we would expect an increase. But, here, in a spin glass, we have to deal with many magnetic impurities which are not frozen as I explained in Chapt.3, even for $T \ll T_g$. Thus, if we increase the field, some magnetic impurities will get polarized[12, 53]. And so, as if we were lowering the temperature, diminishing the number of free magnetic spins will result in lowering the resistance due to the weakening of the Kondo effect[29].

5.2.2 Universal Conductance Fluctuations

Now that we understand the “classical" behaviour of our samples, we can extract the UCFs following the protocol explained in Chapt.4: we fit our data to remove this classical part and retrieve only the UCFs. One typical trace for the doped sample is shown in Fig.5.6.

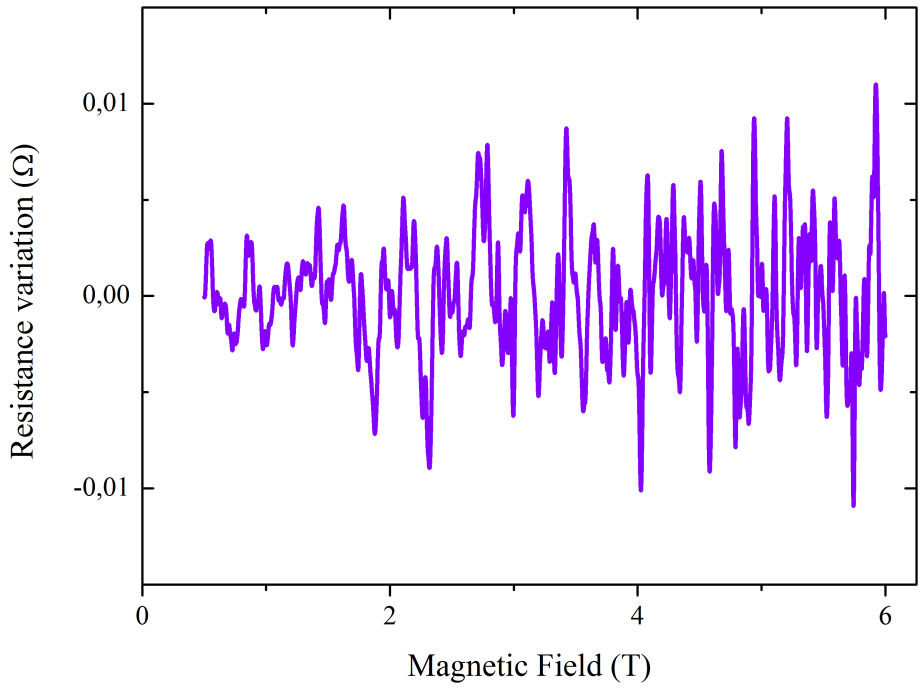

Figure 5.6: Resistance variation of the AgMn sample as a function of the magnetic field after removing the classical part. We thus retrieve only the quantum contribution to the resistance i.e. Universal Conductance Fluctuations (UCFs). This kind of curve will now be called a “UCF trace".

Since we explained earlier that UCFs are magneto-fingerprints of the disorder in the sample and want to use this property to probe disorder changes, the first experiment to consider is then to carry out the measurement of the UCFs twice with a ten minutes interval without doing anything to the sample. This way we should be able to determine if our protocol is destructive or not. If it is, the UCFs will change between two consecutive measurements since it would have changed the disorder. If not, it will be perfectly reproducible.
We thus do two consecutive measurements on the doped sample to verify this hypothesis. And, as we can see on Fig.5.7, those traces are perfectly reproducible!
This reproducibility with fields going above 6T is completely at odd with the energy scales involved in the formation of our spin glass. Indeed, the energy to be considered in such a case is $E_g = k_B T_g$, which corresponds roughly to a magnetic field B_g around 0.1T for

$T_g = 500mK$. This field should then represent the critical field over which the spin glass would be destroyed, the spins being progressively polarized by the field. What is strange here is that it is clear that the disorder has not changed since we recover the exact same trace...
However, this behaviour has already been observed in previous experiments as the ones of De Vegvar or even the ones of T. Capron in our group. This problematic has also been addressed by D.Petit using torque measurements, showing that the critical field when one is well below T_g cannot be extracted so easily and is way higher than B_g. This could be explained by the existence of cavity fields that can be hundred times higher than B_g in spin-glasses.
The conclusion at which we arrive is then that our measurement process does not change the spin configuration in the glassy phase or, at least, not enough to be noticeable in our traces.
This reproducibility is visually very clear but we need need a better way to compare the different traces we will obtain.
The method we have used to quantify the reproducibility between UCF traces is to calculate the correlations between the traces using the the Pearson coefficient C. It is the same coefficient than the one proposed by Carpentier et al.[21] and explained in Chapt.3. The correlation between two UCF traces $UCF1$ and $UCF2$ can be written as:

$$C_{1,2} = \frac{\sum_{i=1}^{n}(UCF1_i - \overline{UCF1})(UCF2_i - \overline{UCF2})}{\sqrt{\sum_{i=1}^{n}(UCF1_i - \overline{UCF1})^2}\sqrt{\sum_{i=1}^{n}(UCF2_i - \overline{UCF2})^2}} \tag{5.2}$$

in which $UCF1_i$ (respectively $UCF2_i$) are the data points from the trace $UCF1$, $\overline{UCF1}$ is the mean value of $UCF1$ and n is the number of points.

For two identical traces (same data) we will get $C = 1$ whereas it will be 0 for two totally independent, decorrelated traces. It follows that two curves taken consecutively without doing anything to the sample should have a correlation $C = 1$. But, as shown in Fig.5.7, we only retrieve $C = 0.95$. We interpret this difference by considering that our measurements are not perfect. This problem can be reduced to one word: noise.
For our measurements, we can set $UCF1 = UCF1_0 + \Delta UCF1$ and $UCF2 = UCF2_0 + \Delta UCF2$, with $\Delta UCF1$ and $\Delta UCF2$ representing the noise contribution to the UCF traces. Since both traces are taken with the same parameters and same setup, we can infer that both noises $\Delta UCF1$ and $\Delta UCF2$ have the same spectral density and thus the same standard deviation σ_n BUT are uncorrelated. From those assumptions we can get

$$C = \frac{\sigma_0^2}{\sigma_0^2 + \sigma_n^2} \times C_0 = \frac{1}{1 + \left(\frac{\sigma_n}{\sigma_0}\right)^2} \times C_0 \tag{5.3}$$

with C_0 being the Pearson coefficient without noise and σ_0 being the standard deviation (so here, roughly, the amplitude) of UCF.
As can be seen, if we have noise (and it is always the case experimentally) it will decrease C and the more noise we have, i.e. the greater is σ_n, the more C is affected.

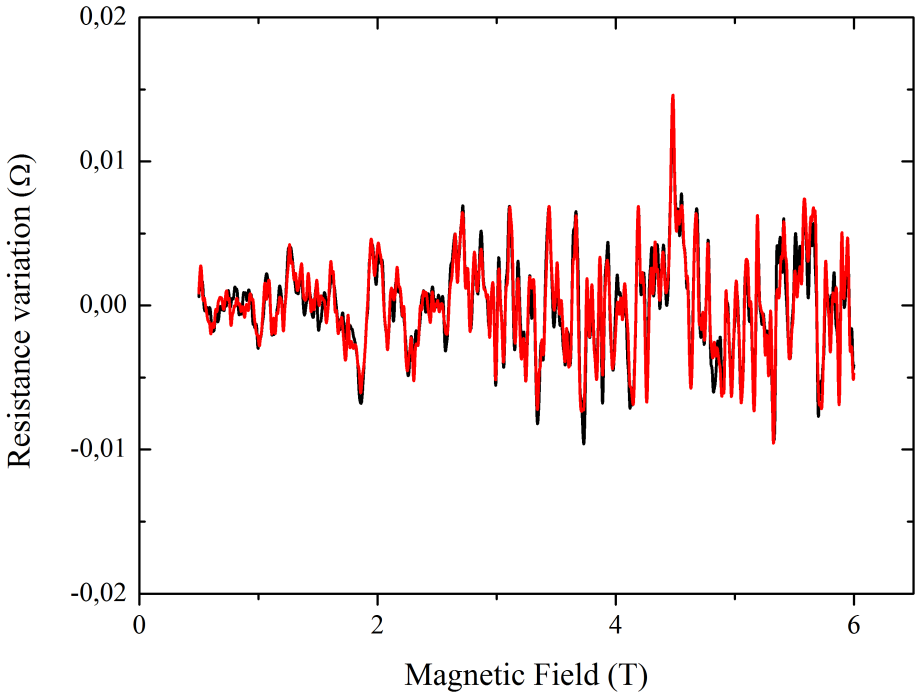

Figure 5.7: Two UCF traces taking on the same sample, one after another and few minutes apart. As can be seen the two traces look identical, proving that our experiments didn't alter the sample disorder. In reality, calculating their Correlation coefficient C, we get $C = 0.952$ instead of 1. We can easily attribute that small deviation to our experimental noise.

This correlation value between two supposedly identical curves, that we will call "Autocorrelation", can thus be seen as a really good measure of the experimental noise we get and its influence on the correlation calculation.
And even better, it directly gives us the SNR and hence the noise for our measurements! Indeed, since for the two previous curves, $C_0 = 1$, we get that $\frac{1}{1+\left(\frac{\sigma_n}{\sigma_0}\right)^2} = 0.95$ and thus $\frac{\sigma_n}{\sigma_0} \approx 0.23$. From that, we can calculate the noise V_n by knowing the measurement current I. Here $\sigma_0 \approx 5\times10^{-3}\Omega$, such that in volts it represents $V_0 = \sigma_0 \times I \approx 5\times10^{-3}\times2\times10^{-7} \approx 1nV$. We thus get $\frac{\sigma_n}{\sigma_0} = \frac{\sigma_n \times I}{\sigma_0 \times I} = \frac{V_0}{V_n} = 0.23$ and then $V_n = 230pV$. Since we have a time constant of 10 seconds on the lock-in, we thus get the noise $S_n = \sqrt{10} \times V_n = 730pV/\sqrt{Hz}$ which is consistent with the noise added by our amplifiers ($\approx 750pV/\sqrt{Hz}$).
Another important point has to be mentioned concerning the interpretation of this coefficient. In theory, it tells us precisely how much a disorder configuration is different from

another one. But for that to be perfectly true, the coefficient which is considered has to be taken over an infinite UCF trace, i.e. with a field which is swept over an infinite range. Why is that? Well, on a mathematical point of view, if one takes totally independent finite-sized samples[1] the correlation between them will not be zero as there are always coincidental correlations.
Practically, of course, such a trace is impossible to get[2] but an approximation can be made. Indeed, the problem here is to get a sample large enough to make those coincidental correlations completely negligible. But what means “large enough" in that sense? We can see that as a measure of how much information we have compared to what could call a “noise". Thus the relevant scale would be “how much information do I have". And for that we have to think about the field B_c that we defined as the field over which we have to sweep to be in the ergodic limit. In other words, it means that when we sweep over B_c we have a perfect fingerprint of the system disorder if the noise is null. But if we sweep only over B_c, comparing with another decorrelated sweep, they will not have a correlation $C = 0$ because of coincidences. Thus, we have to sweep over many B_c to be sure to have a significant number of fingerprint to be compared and for the noise to be averaged, otherwise C will be overestimated as can be seen if we take different spans of field to calculate C.
Now that we've been clear with the correlation coefficient and its limits, let's explain the experimental protocol we follow.

5.3 Temperature annealing measurements

5.3.1 Experimental protocol

The protocol is quite simple and is depicted on Fig.5.8. At first, we take a UCF trace of the sample at a given temperature $T = T_0$. Then, we heat the sample up to another temperature $T = T_1$ during a given time τ before coming back to T_0 again[3]. Another UCF trace is then taken at $T = T_0$ right after the temperature has stabilized. The previously defined Pearson correlation coefficient $C(T)$ is then used to compare them.
The first test is then to check that no evolution is visible over time at T_0 and that any change is only due to the annealing.
We thus measure two UCF traces with an interval of 24 hours between them. With those new measurements, we get $C = 0.96$, which is within noise level, meaning that no decorrelation can be observed over time.
Now that we have a comparison point, we can actually heat up the sample.

5.3.2 Manganese doped silver sample

On Fig.5.9 are shown two traces for the AgMn sample with a measurement temperature $T_0 = 50mK$ and heating temperature $T_1 = 600mK$.

1 “Sample" is here to understand in the sense of quantity of data
2 Infinity is rarely accessible when one deals with experiments.
3 Note that above 4K we heat up the sample with a DC current. As we can switch it on or off instantly, it allows us to heat and cool down the sample very fast.

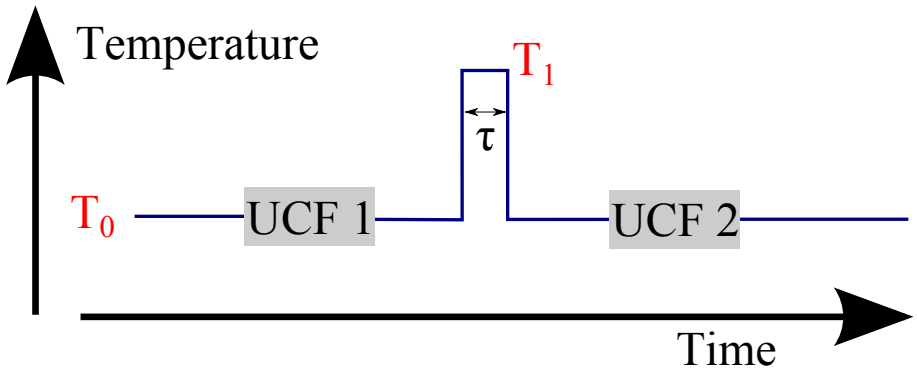

Figure 5.8: Schematic representation of the protocol used to calculate the correlations between UCF traces. First we get a UCF trace at the measurement temperature T_0, that we will call UCF1. We then heat up our sample to a heating temperature T_1 during a time τ. Finally we wait for the sample to come back to T_0 and take another trace, UCF2. The correlation coefficient $C(sample,T_0,T_1,\tau)$ is then calculated between those two traces.

As can be seen, they look pretty identical but let's calculate the correlation coefficient. Here we get $C_{doped}(0.6K) = 0.957$. Since T_g has been confirmed to be equal to 500mK, we face a big problem. We were expecting some significant decorrelation since we should change drastically the spin configuration when T_1 overcomes T_g.
Our first guess was to suppose that we did not heat the sample enough to really change the spin configuration. Indeed, the R(T) curve shows that the interactions between spins come to light already around 1.5 or 2K. So let's have a try at 4K (=$8T_g$). Result: we get pretty much the same correlation coefficient ($C_{doped}(4K) = 0.93$)... Maybe that was still not enough!
Thus we decided to heat up the sample way higher than T_g to be sure to change the spin configuration.
A first point is taken for $T_1 \approx 15K \ggg T_g$. Since T_g is 30 times lower than T_1, we expect the spin configuration to totally change when the sample is brought to 15 K.
And indeed, we finally see an effect! We get a correlation $C_{doped}(15K) = 0.87 \ll C_{doped}(0K)$ for the spin-glass wire. However, we see here that we didn't reach $C = 0$ whereas we are sure to have changed the spin configuration. So what happens?
To explain that behaviour we have to remember that our electrons do not diffuse only on magnetic impurities, such that the UCF traces are not only determined by the spin configuration but also by the static disorder in our sample. Our data has hence two contributions, one magnetic and one static. Thus, what happens if the magnetic disorder has totally changed but not the static one? If we come back to the Pearson coefficient C, our data can be rewritten as $UCF1 = UCF1^m + UCF1^o$, with $UCF1^m$ being the contribution of the magnetic disorder and $UCF1^o$ the static (or orbital) one. We can then

easily get that

$$C = \frac{\sigma_o^2}{\sigma_o^2+\sigma_m^2} \times C_o + \frac{\sigma_m^2}{\sigma_m^2+\sigma_o^2} \times C_m = \frac{1}{1+\left(\frac{\sigma_m}{\sigma_o}\right)^2} \times C_o + \frac{1}{1+\left(\frac{\sigma_o}{\sigma_m}\right)^2} \times C_m \quad (5.4)$$

with σ_o being the amplitude of the orbital contribution, σ_m the amplitude of the magnetic one, C_o the correlation between the static contributions and C_m the correlation between the magnetic ones.
We thus see that if the static disorder does not change (i.e. $C_o = 1$) whereas the magnetic one changes entirely (i.e. $C_m = 0$) , as expected in our experiments for $T_1 > T_g$, we get a minimum $C_{min} = \frac{1}{1+\left(\frac{\sigma_m}{\sigma_o}\right)^2}$ in the correlation values when the magnetic contributions, i.e. the spin configurations, are totally decorrelated. This value is thus directly related to the amplitude ratio between the two contributions.
So, here, we may have reached C_{min} by heating at $T_1 = 15K$. However, the difference between $C_{doped}(15K)$ and $C_{doped}(0K)$ is quite small, complicating the measurements if $C_{doped}(15K) = C_{min}$.
Then, to confirm that we reached the regime in which the magnetic part is totally randomized, we heat the sample slightly higher to see is there is any change in C. If not, it means that we actually are in this regime and $C_{doped}(15K) = C_{min}$.
The results for $T_1 = 26K$ are depicted in Fig.5.11
And, surprisingly, we find $C_{doped}(26K) = 0.74 < C_{doped}(15K)$!
Since we are sure that the spin configuration has entirely changed at 15K, nothing more should have happened at 26K... We thus need to conclude that something different is going on than just a simple change in the spin configuration! Maybe having a look at the pure sample could be useful.

5.3.3 Comparison between doped and pure samples

At first, we wanted to confirm experimentally that nothing was happening on UCFs in the pure samples, such that we can perfectly know what is the spin-glass contribution to the possible disorder change. Thus both doped AgMn and pure Ag wires were measured at the same time with exactly the same protocol.
As for the doped one, first, we have to check that we have a full reproducibility on the pure sample. Two typical traces for the pure Ag sample are displayed on Fig.5.12 with no annealing. We get $C = 0.969$, as expected for fully reproducible traces.
Since no magnetic spin is present in this sample, no change in the disorder should appear for heating temperatures as low as the ones we use and thus $C_{pure}(T)$ should be constant and close to 1 for any of those temperatures. With the same protocol we measured $C_{pure}(0K)$, $C_{pure}(16K)$ and $C_{pure}(27K)$. The results are shown on Fig.5.13.
Whereas, $C_{pure}(0K)$ is almost equal to 1 as explained just before ($C_{pure}(0K) = 0.97$), we find $C_{pure}(27K) < C_{pure}(16K) \ll 1$! Our first idea of an unchanged correlation coefficient

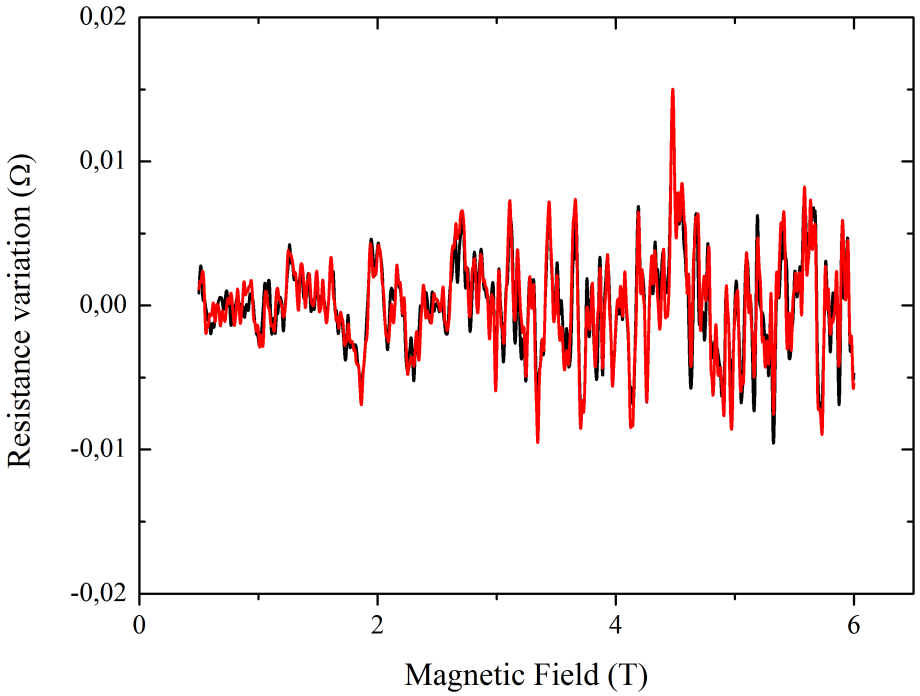

Figure 5.9: Two UCF traces taken following the protocol described in Fig.5.8. They have been measured at $T_0 = 50mK$ with a heating temperature of $T_1 = 600mK$.
As can be immediately seen, the two traces are really close and we can calculate $C(AgMn,50mK,600mK,10s) = 0.957$. The sample magnetic disorder has not changed at all!

at low temperatures on the pure sample is then proven to be totally wrong... End even more importantly, it means that the static contribution to the correlation is way larger than the magnetic one. Indeed, if we talk about spin-glasses, C_m should be 0 above a few T_g. The problem here is that $C_{doped}(4K) = C_{doped}(0K) = 0.95...$ Leading us to conclude that C_m is, in the best case, only as large as the noise in our system... Moreover, we can see that C_{pure} decreases even faster than C_{doped} as T_1 increases!
The change that we observe is thus mainly due to the static contribution C_o.
In a nutshell, we showed that the changes in the spin configuration cannot be measured via UCF studies (up to our sensitivity) but also that we can see an evolution in the sample disorder. This evolution is then due to structural changes at temperatures that are not usually associated to atomic movements.

We need to do tests to get more clues about this unexpected behaviour. And since the effect appears to be larger on the pure sample, we will focus on it.

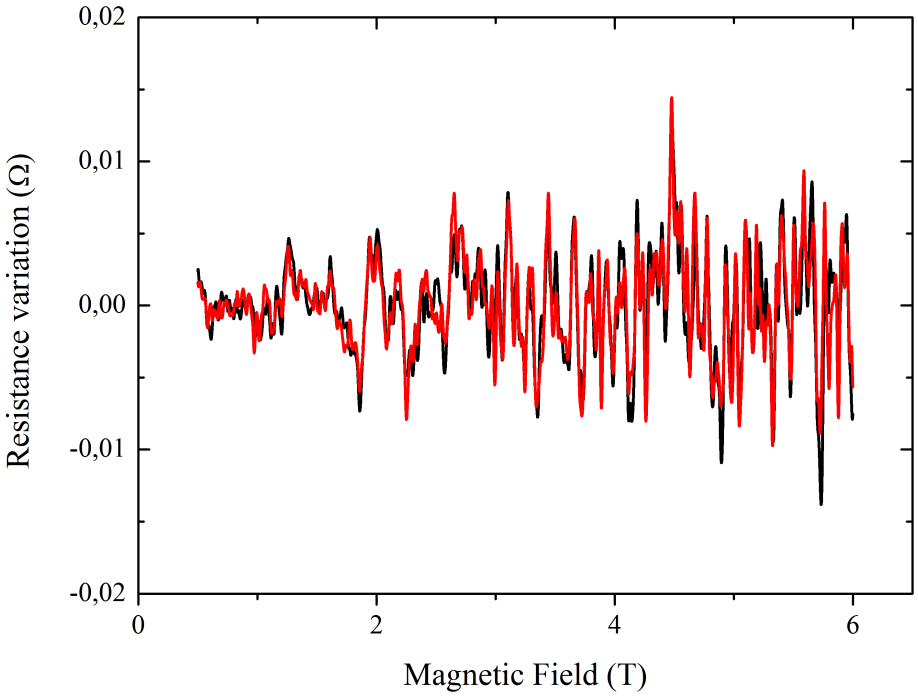

Figure 5.10: Two UCF traces taken on the same sample before and after a heating at 15K. We observe a slight change between them. And indeed, when calculating C, we get $C(AgMn,50mK,15K,10s) = 0.87$, which is out of noise level and the sign of a change in the disorder.

5.3.4 Pure silver sample

So what can we change in our protocol to have more insights? We have four different parameters in our protocol: T_1, T_0, the heating time τ and the length of the sample L. Since we are plotting all our curves as a function of T_1, its effect will not be considered separately.

Annealing time dependence

The easiest and most intuitive thing to change first is τ. We thus chose different τ ranging from 1 second to 30 minutes with the exact same protocol for each of them taking $T_0 = 50mK$ and $T_1 = 20K$ and $L = 25\mu m$.
The results are displayed on Fig.5.14.
As we can see there is a dispersion in the data but it is does not seem at all related with the time spent to heat the sample. Moreover, it has to be noticed that this dispersion remains

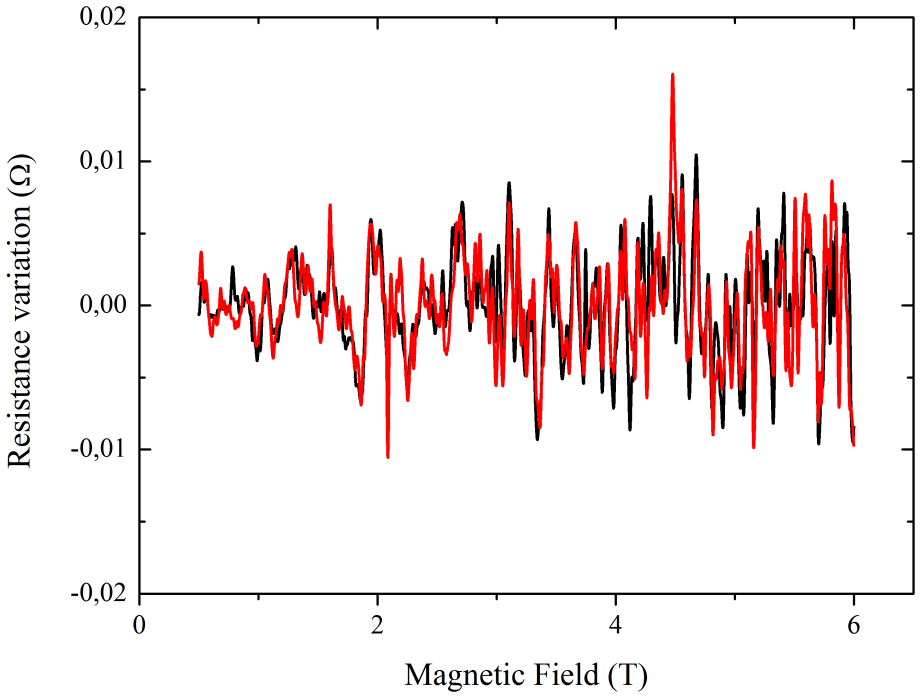

Figure 5.11: Two UCF traces taken on the same sample before and after a heating at 26K. We observe a even more distinct change than between the ones taken with $T_1 = 15K$. Their correlation coefficient $C(AgMn,50mK,26K,10s) = 0.74$ is indeed lower. It means that, between 15 and 26K, more disorder has changed, which is not expected for a spin glass in which $T_g = 0.5K$.

in an interval comparable to the noise of our measurement i.e. $\Delta C(\tau) \approx \Delta C_{noise} \approx 0.05$. The correlation can thus be said independent from τ for a given T_0, T_1 and length.
That study also allows us to conclude that whatever processes happen in our samples, it happens on a time scale of less than one second and does not evolve with time. Following that statement, we fixed $\tau = 6s$ for the rest of our studies.

Measurement temperature dependence

The second parameter to study is then T_0, the temperature at which we measure our sample before and after being heated up.
At first, we thought that this parameter would not change anything since all the changes in the disorder happen while being heated up and not at our measurement temperature T_0. But it is worth to check!
To measure at a given temperature, one has to be able to keep that temperature constant over the measurement time, which is close to 4 hours in our case. We are thus stuck over temperatures ranging from 50mK to 800mK, due to the limitations of a dilution fridge.

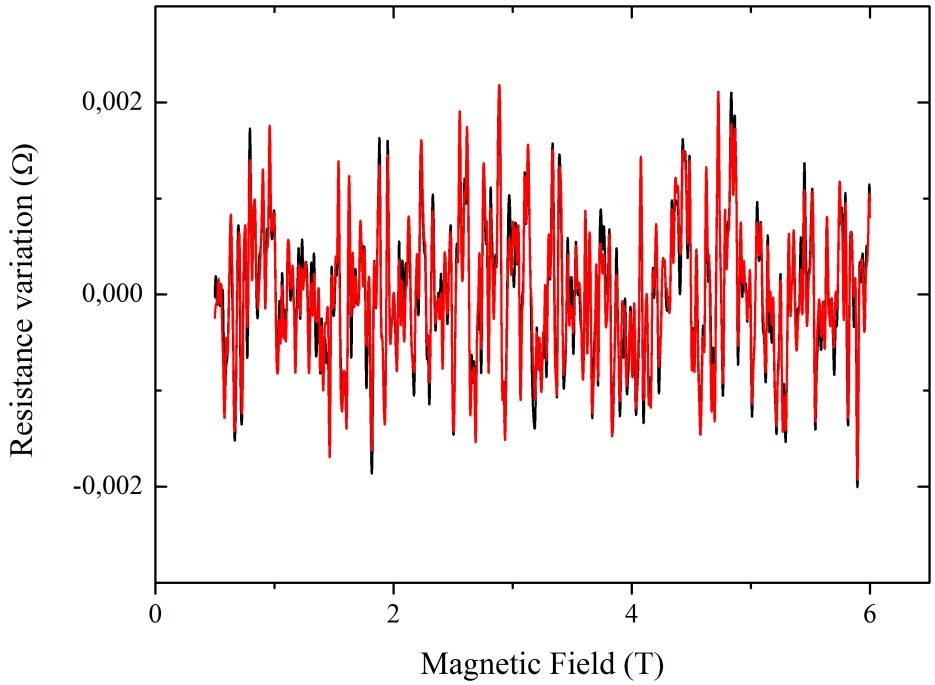

Figure 5.12: Two UCF traces taking on the same pure sample, one after another and few minutes apart. As previously explained with the AgMn sample, the two traces look identical, proving that our experiments didn't alter the sample disorder. Here, we get $C = 0.969$.

Another point of stability is obviously the one at 4 kelvins since we are using a wet dilution fridge. Above that temperature, the next stable point potentially available would be the one of liquid nitrogen (77K) but at such high temperatures it is impossible to see any UCFs due to the dramatically small value of L_ϕ above 10K...
We thus took three different values for T_0, namely $T_0 = 50mK$, $T_0 = 600mK$ and $T_0 = 4K$. What is pretty striking is that there are big differences between samples in the correlation coefficients for a given T_1! First let's see what happens when the measurement temperature T_0 is changed whereas the length is kept constant as in Fig.5.15.
We can see that, as T_0 is increased, the global behaviour remains the same (a decrease of C as we anneal at higher temperatures), but changes dramatically on a quantitative point of view.
Indeed, C decreases faster as the measurement temperature T_0 goes down.

Sample length dependence

Finally, we changed the only parameter left: the sample length.
We thus measured both long (25μm) and short (3μm) samples for all the T_0 we mentioned

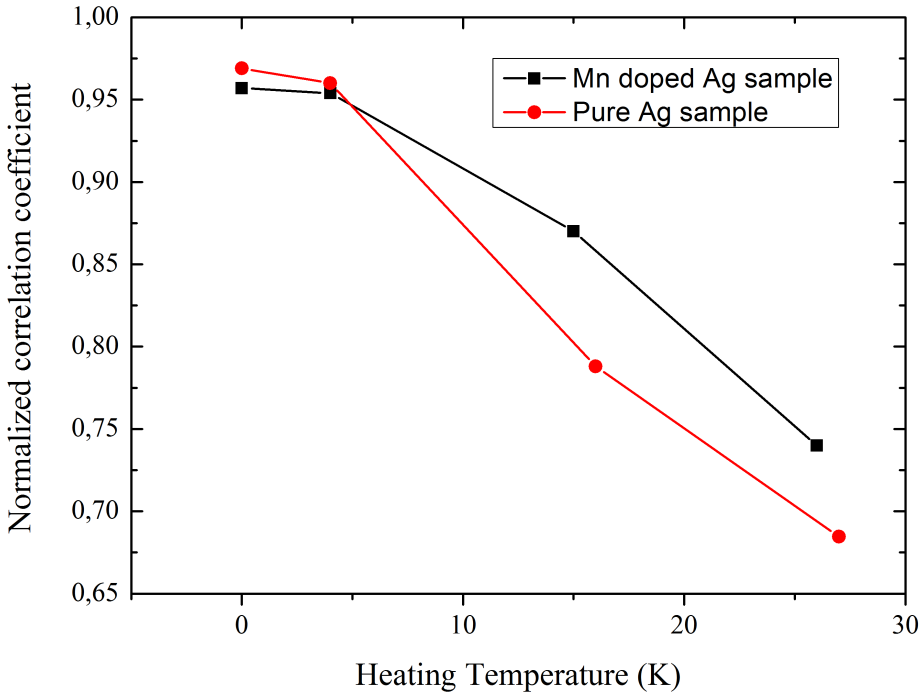

Figure 5.13: Correlation coefficient C as a function of the heating temperature T_1. In black, we see that the correlation for the AgMn sample drops for $T_1 > 4K$. Surprisingly, whereas there is no magnetic spins in the pure sample, its correlation (in red) drops also and even faster than the doped one!

before.
The results are displayed on Fig.5.16. As can be easily seen, when one reduces the length of a sample, the correlation coefficient remains higher!
It has to be noticed that this behaviour is robust for any temperature T_0 we explored.
It is clear that, with any set of parameters, the effect of increasing T_1 is always the same, namely decreasing the correlation. The rate is clearly not the same depending on the different parameters but qualitatively the effect of T_1 remains.
We now have a full panorama of the effects of our protocol parameters, explaining their limits and why we chose them that way.

Annealing at room temperature

The only parameter left without a proper explanation is then T_1. You saw that we did not go higher than $T_1 = 45K$ on our pure silver sample and might wonder why. The reason is that we heat up the sample with some DC current (as explained in details in Chapt.4). To go to $T_1 = 45K$ we already have to pass 1.5mA and if we would like to go higher we

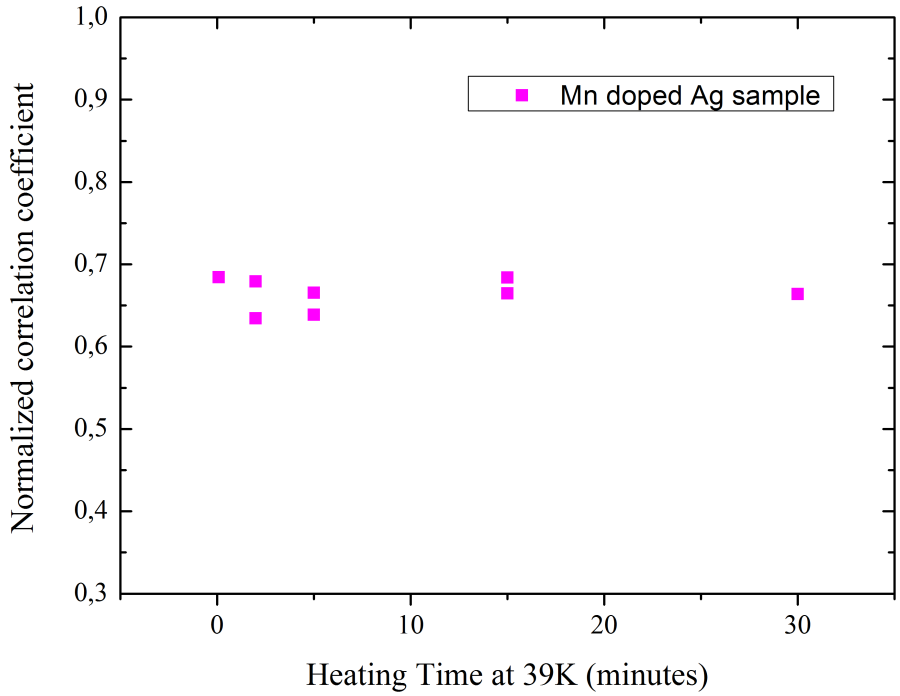

Figure 5.14: Calculated correlation coefficient for the same AgmN sample, with $T_0 = 50mK$ and $T_1 = 20K$, as a function of the heating time τ. We see that the distribution of the correlation values does not exceed the noise level. Hence, we can deduce that there is no effect of the heating time τ on the correlation values between 1s and 30 minutes.

would risk to exceed the electro-migration critical current and blow up our sample. The only way to increase T_1 higher than that is thus to warm up the whole fridge. And the only temperature easily available is $T_1 \approx 300K$ i.e. room temperature. The result for such a strong heat up is shown in Fig.5.17 and we can clearly see that the correlation is really close to zero ($C_{pure}(300k) = 0.052$). This is no surprise since Mailly et al. already proved that a thermal cycling to room temperature totally randomizes the UCFs. But this is a strong indication that we can reproduce previous results and go beyond them.

Repetition of heatings

Another way of characterizing our effects would be to see what happens when the annealings are repeated over and over.
At first, before doing the experiment, we intuitively thought that the disorder would be more and more changed as we repeat thermal cyclings. Indeed, we can easily imagine that, everytime we heat, we move a certain proportion of the disorder, and thus $C_{N,N+1}$ between the trace N and the following trace $N+1$ is a constant. But after two cyclings

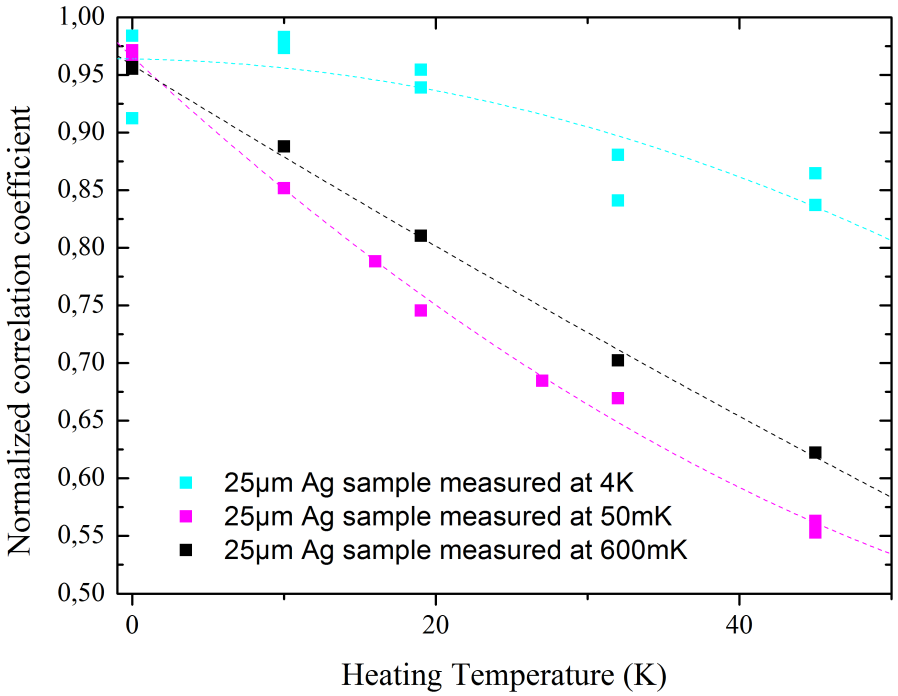

Figure 5.15: Correlation values for the same sample but for different measurement temperatures T_0 as a function of the heating temperature. As T_0 is increased we observe that C get closer to 1. We attribute this behaviour to the fact that L_ϕ gets lower as the temperature is increased, reducing the number of electronic paths that see a moved defaults on a L_ϕ distance.

we will have changed twice this proportion and thus $C_{N,N+2} < C_{N,N+1}$. Hence we decided to calculate all the correlations $C_{\alpha,\beta}$ for 6 consecutive and identical measurements. The results are depicted on Fig.5.18.
As can be seen, all the values are around the same value with a really small dispersion, such that we can say that $C_{\alpha,\beta}$ is constant! This result calls for another explanation that I will give in the next section.

In this one I presented you the results that I obtained on both pure silver and manganese doped mesoscopic silver wires. We will now discuss them and try to find physical explanations.

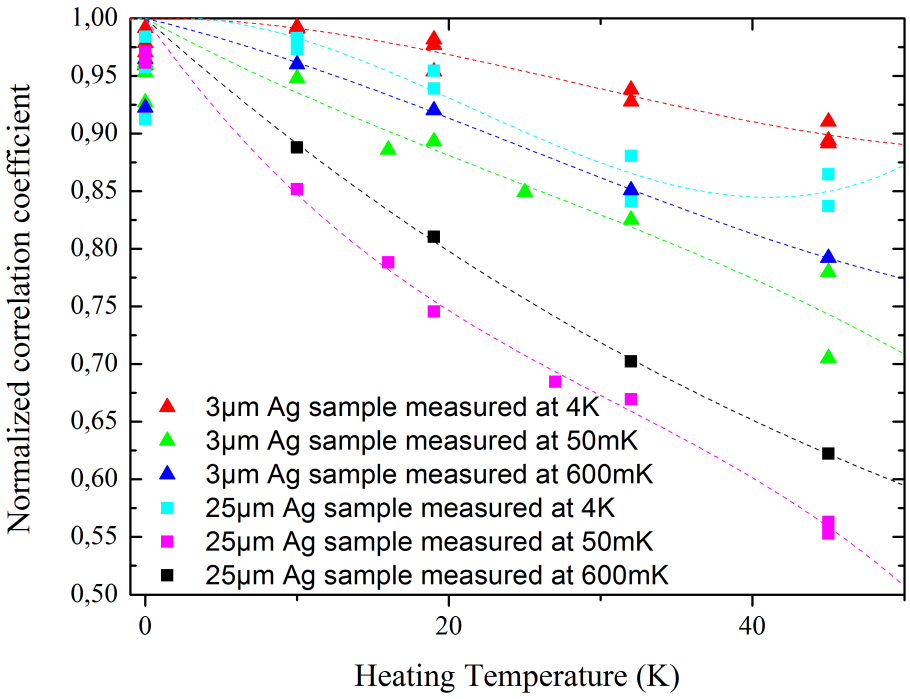

Figure 5.16: Correlation values for the different samples we studied at different measurement temperatures T_0 as a function of the heating temperature T_1. We see that all the behaviours and qualitatively the same: the correlation values drop as we heat more. But quantitatively, the length of the samples L and T_0 appear to have a strong effect.

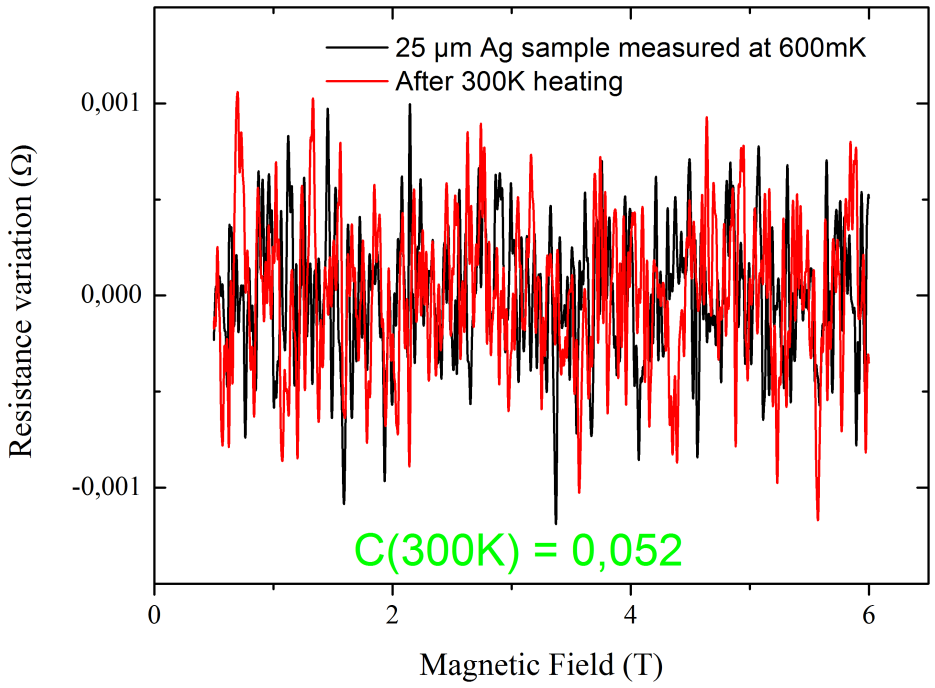

Figure 5.17: Two UCF traces taken on the 25μm long pure Ag sample before and after a thermal cycling to room temperature. In contrast with the previously presented curves, those two look very different, revealing a very strong change in the internal disorder of the sample, as expected according to the experiments of Mailly et al. Here we can even calculate that $C = 0.052 \approx 0$, meaning that the disorder configuration has totally changed.

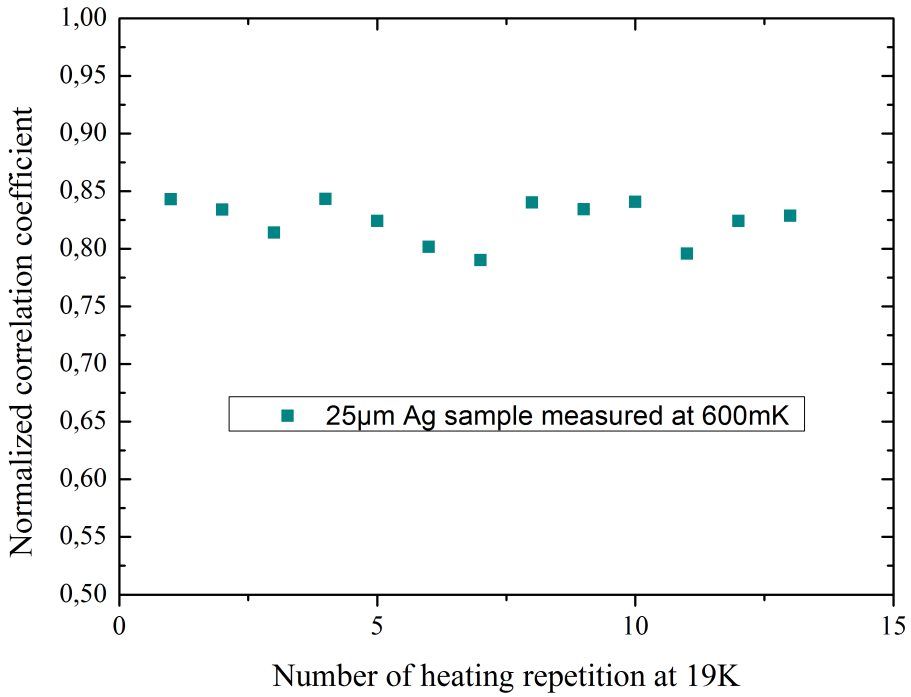

Figure 5.18: Correlation values taken between every UCF traces among a six of them taken after the same protocol. In this case we measured the UCFs on the 25μm long pure silver wire with $T_0 = 600mK$ and thermal cyclings at $T_1 = 19K$. We see that all the correlations $C_{\alpha,\beta}$ have the same value, meaning that, when heating, we always change the same set of defaults in the lattice.

5.4 Discussion and interpretation

5.4.1 Energy scales

The first thing to notice is that we are talking about changes that appear in the structural disorder of our wires i.e. atoms moving, vacancies and so on. The usual order of magnitude in energy when one talks about such moving atoms is the electron-Volt (eV) or a fraction of it. This might not sound like something big (electrons are small cute little particles and one Volt is not a huge voltage) but in reality this energy is equivalent to a temperature of more than 10 000 kelvins!
Even by taking a fraction of that we are roughly talking about temperatures of 1000 kelvins, which is three order of magnitudes higher than our heating temperatures
On the other hand, we are dealing with temperatures much higher than the ones expected to move the magnetic spins ($T_g = 500mK$) or even electron traps in the structure (of the order of 1K).
The scale of energy involved in our measurements is thus completely at odds with any of the processes expected to play a role in those samples.
Moreover, we see that there is a progressive decorrelation as we increase the temperature. We conclude from this behaviour that we are thermally exciting some processes that are widely distributed in energy. And since correlation values do not saturate until (at least) 45K, it means that we are not above their energies but, on the contrary, that their energy distribution extends toward even higher temperatures.
Then, the main question is to know what is happening. If the UCFs are changing, it means for sure that we change the structural disorder, that something is moving.

5.4.2 What is moving?

A first clue to answer this question could be found in the annealing repetition experiment we described earlier. As a reminder, we measured a UCF trace, annealed our sample to $T_1 = 19K$, took another trace and repeated this protocol 6 times.
We saw that this experience leads to a weird result which is that all the correlation values $C_{\alpha,\beta}$ taken between any of the six traces α and β are the same.
We can directly interpret this result as the proof that the same proportion of disorder is changed between any of the configurations represented by any trace α and β.
Moreover, this result also necessarily implies that everytime we heat, we change the **exact same set** of “impurities".
Indeed, let's imagine that we change 10% of the disorder between UCF N and UCF N+1 by heating up and then again 10% between UCF N+1 and UCF N+2. If those 10% represent entirely different sets of impurity it means that we change 20% of the disorder between UCF N and UCF N+2. Thus we would not have $C_{N,N+2} = C_{N,N+1}$.
Of course this is the worst case scenario (the two sets are totally distinct) but this demonstration holds for any hypothesis in which the two sets are not the same.
But it still does not tell us what is moving. The only thing we can say now is that those moving systems keep their energy even when their position changes. This peculiar property led us to think about oscillating systems such as Two-level-systems (TLS).

Shortly, TLS are two-level defects within a material (atoms, vacancies,...) that can oscillate between positions separated by energy barriers in disordered systems such as glasses. Studies showed that below 6-7K TLS can oscillate between positions without thermal activation needed, simply by tunnelling effect.
However, above this temperature, TLS start to be activated by the thermal bath. Typically those movement are associated with time constants on the order of the millisecond, which is coherent with our measurement showing no dependence in time above 1 second and, more importantly, moving defaults only above 4K[72]!
Moreover, those barriers do not change their energy as TLS oscillate, such that a TLS that will have moved for $T_1 = 20K$, will move again if we anneal again at $20K$.
Even though we have no direct proofs of the fact that we are probing TLS, this is an probability to consider.

5.4.3 Mesoscopic effects influence on the measure

So now, how to explain the behaviour we observed concerning the temperature and length dependences?
It is clear that the decorrelation is much smaller in short samples than in long ones! But why?
Since both samples are part of the very same wire, no change in the resistivity, diffusion coefficient or density of defaults can be used as an argument in this discussion. Moreover, we can easily assume that the proportion of defaults that are moved at a given temperature is homogeneous all along the wire. It seems clear that we cannot explain this decorrelation difference by a physical change between samples.
Thus if the answer is not to look for in a physical change, the answer necessarily lies in the measurement technique itself i.e. the electronic transport and the UCFs.
As explained in the previous section, the main length to be considered in terms of electronic transport in mesoscopic systems is the electronic coherence length L_ϕ. Now let's see how this can act on our measurements.
From a transport point of view, all the coherent features (such as UCFs) appear on a scale of L_ϕ, such that we are always keen to look for a $\frac{L}{L_\phi}$ dependence.
On the length dependence measurements, when we increase L, $\frac{L}{L_\phi}$ increases and we observe a drop in the correlation values as can be seen in Fig.5.16.
In a nutshell, it means that when $\frac{L}{L_\phi}$ increases, C decreases.
But, with that explanation, we face a problem.
Indeed, we also saw that on the temperature measurements, when one increases T_0, the correlation goes higher. We need to recall now that, when we increase the temperature, L_ϕ goes the opposite way and thus $\frac{L}{L_\phi}$ is increased.
This gives us that if $\frac{L}{L_\phi}$ increases, C increases as well.
We have here a contradiction between our two measurements when trying to explain them

using the $\frac{L}{L_\phi}$ ratio.
This parameter is then, for sure, not the relevant one, to explain our measurements.
It appears that we have a competition between two distinct effects and that we need to consider them separately.
Let's start by the temperature one.

5.4.4 L_ϕ dependence of the correlation

Considering only the T_0 temperature dependence, we have to focus on what happens to the UCFs correlation when L_ϕ is getting lower.
We've seen previously that their amplitude is strongly affected by L_ϕ but here this effect is irrelevant. Indeed, since the correlation is calculated at a given T_0, the two traces have the same amplitude and there is no reason for which a change in the absolute amplitude would change the correlation value since the coefficient is normalized.
Basically, C compares the only form of the UCFs, and hence, the change of the disorder in our samples. So maybe we should focus on how the moving defaults change the UCFs.
So, again, L_ϕ is the length to consider. We arrived to two different hypotheses concerning the effect of the moving defaults. The first one is to say that, to change entirely the UCFs (i.e. $C = 0$) we need to move a certain proportion of the static disorder e.g. 30%. The second one is to say that you need to change not a certain proportion of impurities but a given number of them in a L_ϕ long section of the wire.
With the first idea, we would get the same correlation for a given heating temperature T_1 whatever the value of T_0. Indeed, even if we increase T_0 and thus that L_ϕ is reduced, the proportion of defaults that are moved on the scale of L_ϕ is the same, under the assumption that the density of defaults is constant along the wire. However, this is in total contradiction with the results we obtained. Hence, it is not the case in our measurements. Hypothesis 2 is then the only one remaining on the table.
The idea behind this hypothesis is that $C = 0$ if all the electronic paths see at least one moved impurity on a scale of L_ϕ.[1]. This idea fits much better with our results. Indeed, on a physical point of view, we can see that problem as the probability for an electronic path to encounter a moved default over a length L_ϕ. If the transport is 1D as in our samples, an electronic path will pass through an average of N impurities, with N directly proportional to the length on our sample. So, if there is only a few impurities that moved on a size L_ϕ, the probability P_m for this path to see one moved impurity is quite low. However, with many impurities , this probability rises.
Indeed, if L_ϕ is reduced, the absolute number N of moved impurities inside it will be smaller. Thus, if L_ϕ is reduced by a factor of two, N will also be divided by two.
Let's consider a fully coherent sample ($L = L_\phi$) in which 30% of the impurities are moved. We can easily say that it is equivalent to considering that an impurity has 30% chance to have changed after the annealing. It is thus pretty natural to say that $P_m = 1 - (1 - 0.3)^N$. So if L_ϕ is large, N will also be large, i.e P_m will be close to one, meaning that almost all

1 We place ourselves in the strong coupling limit in which an electron scattering on an impurity is totally randomly dephased as expected for static disorder.

the electronic paths will have interacted with a moved impurity. The UCFs will thus be totally changed, and C will be low.
On the opposite, if L_ϕ is small, N will also be small and P_m will be close to zero. The UCFs will thus be only partially changed and C will be high.
So, as a conclusion, for the same proportion of moved defaults, if L_ϕ is small, P_m will also be and C will be high. On the contrary, if L_ϕ is large, P_m will follow and C will be smaller: QED!
Another effect that might be considered when one changes L_ϕ is related to the ergodicity. Indeed, here, we gave an explanation exclusively based on the internal disorder but when one changes L_ϕ, the value of the critical ergodic field B_c changes as well. Which means that, as L_ϕ diminishes, B_c rises and for a same field span we will have swept over less B_c, potentially giving us an ergodicity issue. This would also result in a higher C as the measurement temperature T_0 gets higher.
Those two effects are thus probably happening at the same time, but are impossible to distinguish with those measurements. For that we would need to measure samples with different L_ϕ but also the same $\frac{L}{L_\phi}$ ratio and sweep over the same number of B_c.

5.4.5 Length dependence of the correlation

Now let's consider the T_0 constant, such that, compared to the previous section, we will now work with L_ϕ being a constant.
We've just seen before what happens on a sample of size L_ϕ. But what would be the effect of having a sample whose size L is larger than L_ϕ?
As we saw earlier, for any mesoscopic effects, the simplest way of considering this problem is to "cut" the sample into sub-samples (or "blocks") of size L_ϕ and then see what happens when we aggregate them.
Imagine now that we can measure individually each of those blocks. We would retrieve UCFs traces for each sub-sample and could calculate the correlation on each of them.
From Chapt.2 we get that the UCF trace of the whole sample is simply the addition of each sub-sample traces.
We'll now make a strong assumption saying that each of those blocks taken individually, has the same correlation coefficient after heating. This can be justified by the fact that, since we have many electronic path[1] that encounter many impurities, the previously defined P_m can be seen not as a probability but really as the proportion of electronic path that have changed, which should be the same in every block.
We have several blocks of size L_ϕ, each of them having the same correlation coefficient $\bar{C}$, i.e. $C_{UCFi,UCFi'} = \bar{C}$ for two traces $UCFi$ and $UCFi'$ taken on the same block i before and after annealing.
However, if we make the calculations, we see that if we calculate the correlation between $UCF = UCF1 + UCF2 + UCF3 + ... + UCFN$ and $UCF' = UCF1' + UCF2' + UCF3' + ... + UCFN'$, we get that $C_{UCF,UCF'} = C_{UCFi,UCFi'} = \bar{C}$. Which is not at all what we

1 If we simply divide the section S by the "size" of an electron in a metal λ_F^2, we get that the number of electronic paths is of the order of 10^5.

measured...
Something in our interpretation must be wrong.
First, we have to take into account that, in our measurements, we are rarely in the limit where $L > L_\phi$. Indeed, for $T_0 < 4$K, even for $L = 25\mu m$, we are in a limit where L is of the order of L_ϕ[1], such that it is difficult to say that we can approximate the sample to an addiction of sub-blocks.
The only case where we could do that approximation would be for $T_0 = 4K$. However, here, we're dealing with another issue: L_ϕ is really small such that the number of defaults seen by each path over a length L_ϕ is really small[2]. This leads to the fact that we cannot say that P_m corresponds to the proportion of changed paths and thus the correlation for each block might not be constant.
An experiment that could allow us to conclude would then be to measure long samples for which we have the limit $L > L_\phi$ such that "cutting" the sample would be relevant.

5.4.6 Conclusion

Mesoscopic systems and alloys are believed to have two different disorder energy scales. The first one, close to zero, corresponds to the energy of spin flips, electron traps,... while the other one corresponds to very high energy (above 300K) excitations as moving atoms, clustering or electromigration. Between these two extremes, no disorder changes are expected to happen.
In this chapter, we measured UCF traces in metallic wires to probe the internal disorder of such systems.
We showed that upon a heating inferior to 4K, no major changes are to signal. But we cannot exclude the possibility of fast processes with low activation energy (e.g tunnelling systems) below this temperature. Indeed, they would be invisible in our measurements due to averaging.
However, after heating above 4K, modifications in the structure of the lattice can be observed. Those modifications appears to have a broad energy distribution as more and more changes are induced when the heating temperature is set higher, but with a characteristic time below the second. This behaviour would match with TLS measurement in which they retrieve the same characteristics.
Those measurements also provided results about mesoscopic effects that have a big impact on the correlations between UCFs and thus, on how they can be used as a probe for the disorder. Indeed, we have proved that those fluctuations are actually sensitive to the absolute number of disorder sites that moved on a scale of L_ϕ and not on the total proportion. Moreover, we showed that those moving disorder sites are always the same when we heat up at the same temperature, which is a total surprise!
We have also shown that the correlations between traces are sensitive to the length of the sample. We only have an incomplete interpretation of this effect but this leads to a stronger decorrelation.
To sum up, thanks to UCFs correlations, we proved that major changes in the structural

1 In the best case scenario, with $T_0 = 600mK$ and considering the $25\mu m$ sample, we have $L \approx 4L_\phi$.
2 We can approximate this number N by dividing L_ϕ by l_e^{pure}, which gives $N \approx 50$ impurities.

disorder of metals happen even at low temperatures (10-50K), on opposition to what is believed. Moreover, we also showed that this probe has to be handled with caution when one wants to interpret data as they are very sensitive to a large range of parameters.

CHAPTER 6

Ancillary works

After the previous chapters you have (or not!) read, you know the results I obtained on my main PhD subject: mesoscopic transport and spin glasses.
I'd like now to present some other works I did during the almost four years of my PhD. Indeed, the issues that I had to solve concerning the extra heating due to the magnetic field gave me some time to use my experimental skills on other's researchers samples and provide them results quite difficult to get on their setup.
I will show you three different experiments entirely decorrelated (not with the same meaning than for the UCFs!) one with another.

6.1 Bolometers for millimetre wave absorption

At the end of my first PhD year, we've been contacted by a team working at the "Commissariat à l'énergie atomique et aux énergies alternatives-Laboratoire d'électronique et de technologie de l'information" (also called CEA-Leti). This team asked us if we could measure some devices at very low temperatures because their usual partners in their project had weird results.
This project is dedicated to developing new millimetre-wavelength light sensors for spatial purposes also known as bolometers[4].
So first, what is a bolometer? Well, the principle is quite simple.
It is a device designed to be a thermal detector of radiations i.e. it converts the energy of an incident electromagnetic wave into heat and thus, a temperature elevation can be measured.
It is divided in two main parts[31]:
-The absorber: As its name suggests, it is designed to absorb the incoming wave energy and convert it into heat. Its heat capacity has to be really low such that even if it receives a small amount of energy, the temperature elevation will be high. In the devices I measured, this absorber consists in a superconducting metal, whose critical temperature T_c is adjusted such that the elevation of temperature turns it normal.
-The thermometer: It allows to measure the elevation of temperature resulting from the energy absorbed by the absorber. In our case, the thermometer is a doped semiconductor. The good thing with such compounds is that the resistivity varies a lot around zero temperature even for a small ΔT.
One of the issue in creating such a device is then to precisely calibrate T_c as well as the resistivity profile of the thermometer.

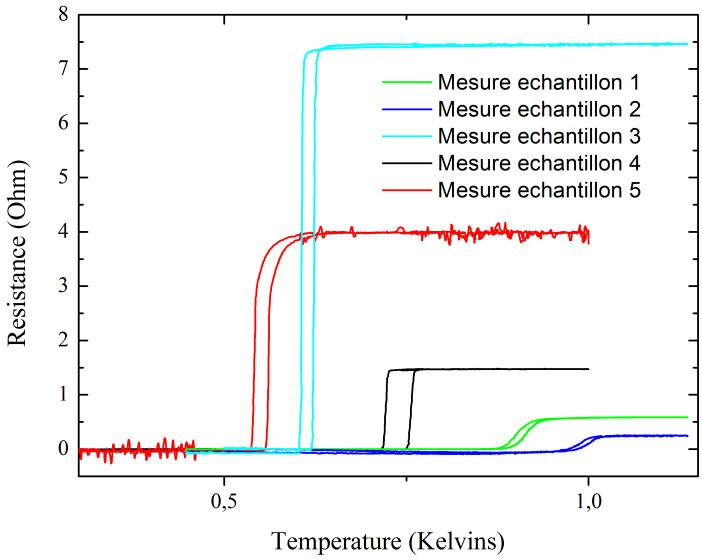

Figure 6.1: Resistance of different superconducting samples as a function of the temperature while cooling down and warming up. As can be seen, the different samples have a constant resistance before going down to zero while being cooled down, proving their superconductivity. The hysteresis that can be seen when we warm up is typical of superconductors.

That's why I measured the T_c for different superconducting layers to choose the best one for their purpose as well as the $R(T)$ of different semiconducting compounds.
The results for the superconducting absorbers are displayed in Fig.6.1
Those measurements were not difficult as long as it is done in a four-points configuration.

The tricky part came when measuring the thermometer part. For the less resistive ones (around 1kΩ), nothing in particular is to report. But, concerning the one whose resistance value was already of about 1 MΩ at 200mK, it is a totally different story!

At first we found something weird: the resistivity would decrease at very low temperature! After closer inspection, we realized that the phase of our signal was highly shifting as we decreased the temperature, making us realize that something unusual was going on.
In my previous first chapters I mentioned the fact that capacitive effects wouldn't play any role in my measurements as the samples we measure are little resistive. However, here, it has to be taken into account.
Indeed, the capacitance of our lines is of a few nano Farad[1]. Thus, if the resistance of our

1 Such a high capacitance on the measurement lines is pretty unusual. But here, it was designed on purpose for the lines to act as a low-pass filter.

system is too high, the cutoff frequency $f_c = \frac{1}{RC}$ becomes very low... to the point where it matches our measurement frequency!

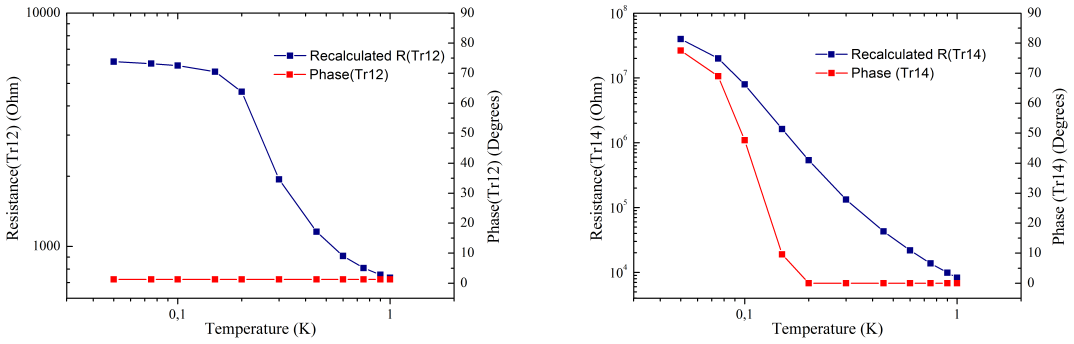

Figure 6.2: Resistance of two semi-conducting samples as a function of the temperature. On panel (a), we can see that the resistance is quite low and no phase shift appears. Unfortunately, the resistance saturates below 200mK, making it a bad sensor. On panel (b), however, the sample has a huge resistance and a phase shift due to RC circuit appears. The resistance thus have to be recalculated taking the phase into account. Since the resistance does not saturate, it is a good sensor but its high resistivity makes it really difficult to measure properly.

Fortunately, since we're also measuring the phase θ of our signal, we are able to retrieve the real resistance value. After considering the problem of impedance matching, we get that the measured modulus of the signal R_m is directly related to the real resistance value R by $R_m = R \times \cos(\theta)$.
Thus, we get the real values as displayed in Fig.6.2.
As we can see, the sample called Tr12 would be a really bad thermometer as it saturates below 200mK and exhibits a variation of only one order of magnitude between 1K and 50mK.
On the opposite, Tr14 is perfect! It has no saturation down to 50mK and varies of four order of magnitude on the same range of temperature, meaning that any ΔT will lead to a huge ΔR. But (and it's a big one), it is so resistive that a *straight forward* measure is quite impossible.
Indeed, as we've just seen, you cannot use an AC current because of the phase shift it will induce (and that you have to compensate by calculations). And even if you use DC current, another problem will arise: the impedance of your measurements setup! Here we've considered that all the current we're sending in the system goes to the sample. But your amplification system, or even your measurement devices, don't have an infinite impedance. We measured the resistance of our amplifiers to be around 1 GΩ, making measurements on over 100 MΩ resistors highly unprecise. When your measurement devices impedance is comparable to the one of your sample, some current will flow into them and you will underestimate the real resistance of the sample. And we're not done yet!

To explain why, I now have to present the usual way of measuring resistances. The

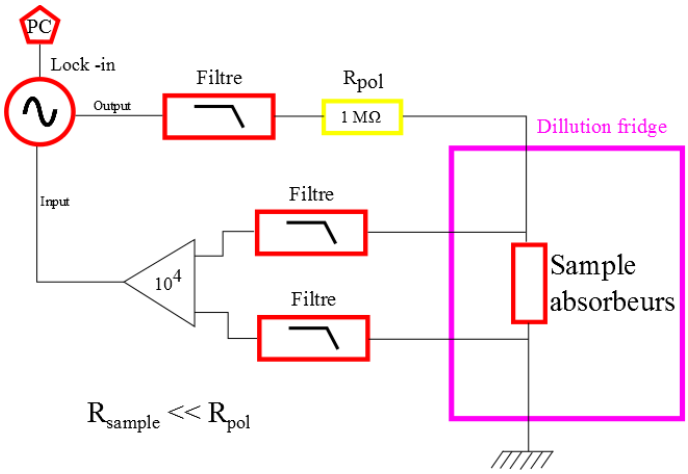

Figure 6.3: Representation of the setup we used to measure the samples. Filters are set to eliminate the incoming and outcoming noise. Since our samples are way less resistive than our polarization resistor R_{pol}, the current is simply $I = \frac{V_{pol}}{R_{pol}}$, with V_{pol} set by the lock-in. By measuring the voltage V_{sample} we thus simply have that $R_{sample} = \frac{V_{sample}}{I} = \frac{V_{sample} \times V_{pol}}{R_{pol}}$.

usual measurement devices work as a source of current and recover the voltage across the thermometer. To do so, a resistor R_{pol} is set in series with the measurement setup as shown in Fig.6.3. In that case the total current flowing in the circuit is given by $I = \frac{V_{pol}}{R_{sample} + R_{pol}}$. And if R_{pol} is way bigger than R_{sample}, the current flowing is driven only by the value of R_{pol}. Thus we know $I = \frac{V}{R_{pol}}$, we measure V_{sample} and, finally, we can easily get $R_{sample} = \frac{V_{sample}}{I}$. Unfortunately, the resistance we're looking at gets very large and the current cannot be precisely known anymore. The calculus of R_{sample} thus become unprecise and values are again underestimated.

In the end those measurements were useful to characterize the fabrication processes and check the effect of doping on their samples.

6.2 Conduction properties of boron-doped diamond at low temperatures

Another experiment I did during my PhD was concerning boron-doped diamond, that was studied by J.Bousquet for her PhD and her advisor T. Klein.
If one dopes enough almost any insulating material, it will become conductive. The transition between this insulating phase and the conductive one can take two forms.
Either we have a insulator-metal(-superconductor) transition or, sometimes, a direct insulator-superconductor one. Those kind of transitions attracted the interest of many theoreticians as well as many experimentalists because the status of those transitions (due

to disorder or not) is still heavily debated.
It is thus interesting to decorrelate the different factors involved.
The results previously obtained on boron-doped diamond seemed to plead for an insulator-superconductor transition, making it a possible system to study such transitions. But why is this particular compound so interesting? Actually, the interest of diamond is that it has a really nice crystalline structure that allows to boron-dope it by substitution, and thus to not increase too much the structural disorder compared to amorphous systems. Moreover, diamond can be grown with good control on its size and thickness, reducing the uncertainty about its dimensionality in terms of transport.
It is thus a good system to study the influence of doping content on the transport properties considering that it has never been studied thoroughly before.
To do so, J.Bousquet developed a high quality fabrication process that allowed them to have a very good control of the homogeneity of the doping and of the growth process. That way, they could get unmatched quality samples!
The final goal of that study is then to determine the phase diagram of the boron-doped diamond as a function of the temperature and the dopant concentration.
To do so, different samples are prepared with different thickness and different concentration.
Now comes the difficult part: how do you determine if the sample is a metal, a superconductor or an insulator? The answer lies in another question: what is a metal, a superconductor or an insulator?
The definition in terms of electronic transport is the following: *at zero temperature*, a metal has a finite resistance, a superconductor has zero resistance and an insulator has an infinite resistance.
Measuring the resistance of the boron-doped diamond as a function of temperature is thus a good way to determine the phase diagram. However, it has to be noticed that we cannot experimentally go to 0K and thus we can't distinguish between a metal and a superconductor if its T_c is inferior to 40 mK...
The first results obtained by J.Bousquet showed weird behaviours on some of her samples. Indeed, few samples displayed a saturation below 1K: either the metal-superconductor transition was incomplete (sudden drop of resistance but stopping at a finite value) or the resistance goes down as a classical metal but saturates...

Since saturation at low temperatures is something unusual in terms of transport, they decided to ask us for a measurement to confirm this.
The results are displayed on Fig.6.4

And, as can be seen, we do not see any saturation for any samples!
Moreover, the "metallic" samples behave exactly as expected theoretically for a 2D metal or a 3D metal according to their respective dimensionality, and the incomplete transition appears to be not-incomplete at all.
The reason for that is probably that the setup they used at first was not shielded enough from external radiations and thus, that their samples were not really cooled down below 1K!
To summarize, our measurements allowed us to confirm the existence of a never-observed-

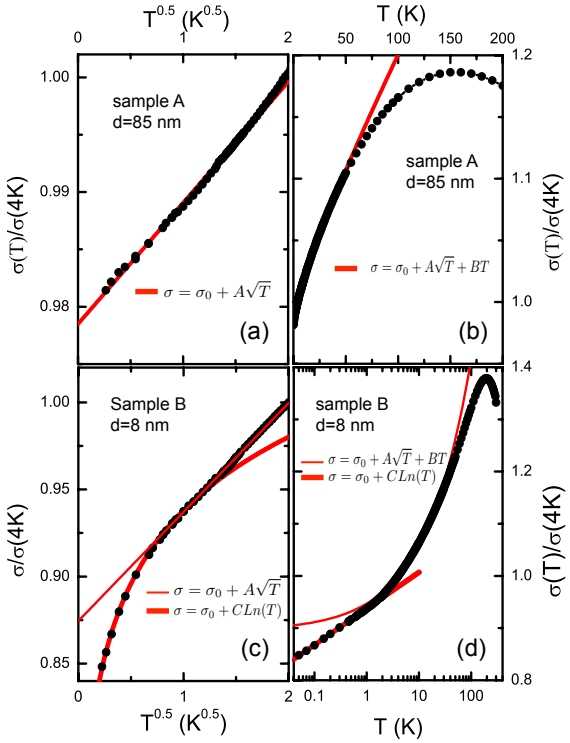

Figure 6.4: Normalized resistance of boron-doped diamond in a metallic regime. On panels (a) and (b) the results for a 3D sample is displayed. Both behaviours at high (panel(b)) and low (panel(a)) temperatures can be perfectly fitted the formulas expected for a 3D metal. The 2D sample can equally easily be fitted as can be seen on panels (c) and (d). High (panel(d)) and low (panel(c)) temperatures curves are perfectly consistent with a 2D metal behaviour.

before metallic phase between the superconducting and the insulating ones[16].

6.3 Phase coherence length in NiPtSi

My dear co-advisor François Lefloch had, beside my work, another subject going on with another PhD student, Anaïs Francheteau.
One of the aspect of her PhD was the study of transistors with Silicon On Insulator (SOI) technology.
And when one talks about transistors, one of the issue resides in its resistance. Indeed, if the resistance is too high, you have to apply quite a high voltage to it, leading to a high power consumption and a high thermal dissipation...
Actually the resistance of such a device is mainly due to the contact between the wires used to apply the voltage and the transistor itself (drain and source). To reduce this contact resistance, the idea they imagined was to make a superconducting contact that would turn the drain and source superconducting too by proximity effect.
The proximity effect is the fact, for a superconducting metal, to “propagate" its superconducting properties to a non-superconducting metal over a small distance. Basically, it means that the electrons coming from the superconducting metal continue to propagate as Cooper pairs in the normal metal as long as they are still in phase.
Unfortunately this approach was not very successful as they didn't observe any big proximity effect... Thus, what was wrong?
To answer that question we have to consider the definition of proximity effect. And actually we can see that the reason is quite simple: dephasing!
Indeed, if one of the electron of the Cooper pair is dephased, the Cooper pair is destroyed and so the superconductivity. Here, we can see two reasons for which the phase could be destroyed: the interface and the phase coherence inside the metal itself.
Indeed, if the interface between the superconductor and the metal is bad, the electrons will be dephased right away, before even entering into the metal... And the other possibility is that if L_ϕ is really small in the metallic part, proximity effect will be killed very fast since the electrons are dephased on a scale of L_ϕ.

To verify which of those assumptions is the good one, F. Lefloch asked me to measure L_ϕ for the metal they were using for transistors, namely NiPtSi.
And how do you measure L_ϕ in a metal? Weak (anti-)localization!
I explained and used weak localization measurements earlier in my PhD to determine L_ϕ in my samples and the principle here is exactly the same. A weak anti-localization peak can be measured in the resistivity at zero field. Its width and amplitude are directly related to the value of L_ϕ (see Chapt.2 for more details). Thus, by fitting the curves we measure, and knowing the geometry of the sample, we can extract L_ϕ with no adjustable parameters.
The results are displayed in Fig.6.5
We can see here that L_ϕ is of the order of a few microns whereas no proximity effect could be seen on that scale. It thus means that L_ϕ is not the limiting factor for their device to work and that the problem comes most probably from the fabrication process of the superconducting-metal contact!

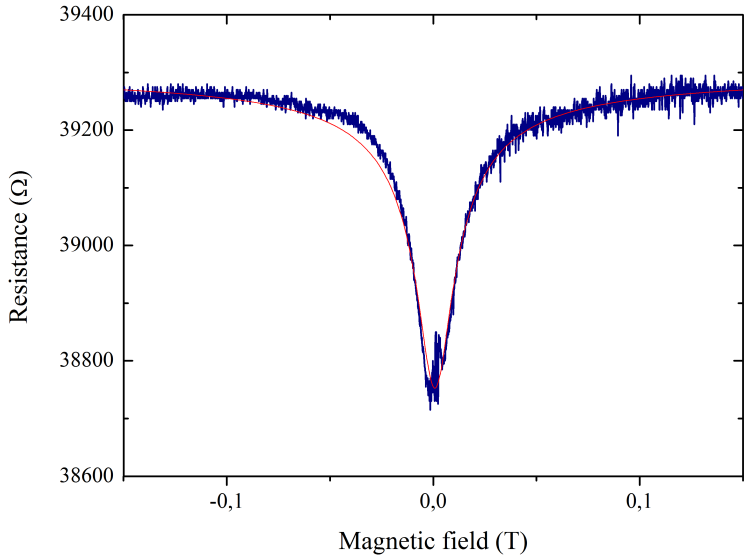

Figure 6.5: In blue, resistance of a NiPtSi sample as a function of the magnetic field. We clearly see a weak anti-localization peak at zero field. In red is a fit of the weak anti-localization peak. There is no other adjustable parameter than L_ϕ. Typically, L_ϕ is of the order of a few microns.

CHAPTER 7

General conclusion

For the last ten years, mesoscopic physics have been pointing towards quantum technologies such as qubits and is even sometimes reduced to single-electron physics. However, the concepts developed by Landauer on coherent electronic transport still haven't been used to their maximum extent. Even if some features were experimentally tested few years later with a great success such as Aharonov-Bohm effect in metallic rings or UCF on Si doped GaAs wires, its use has been mainly limited to experimental proofs of the theory.
Separately, but around the same years, the physics of spin glasses rised as one of the main domain in condensed matter physics. Both experimental and theoretical interests lasted for long and many amazing features were discovered, renewing the interest over the years. But, unfortunately, the lack of conclusive experiments to address the question of its ground state led to an impasse.
Surprisingly, those two fields were almost never considered together except for 1/f noise experiments. Recently, a theoretical work tried to recombine those two subjects in order to finally solve the remaining question of the spin glass ground state.
In this thesis, we based our work on this proposal to use coherent transport to quantitatively differentiate between the different ground states of the system and compare them.
I focused my PhD on two main different tasks.

The first one was to improve the experimental setup to be able to measure Universal Conductance Fluctuations without being destructive on Ag and AgMn mesoscopic samples. This has been achieved by creating a tin-free measuring setup that allowed to keep a constant temperature while measuring. Moreover, the setup had to be precisely calibrated to enhance the signal/noise ratio without loosing physical information. This process has been improved by optimizing the magnetic field sweep speed with time constant of the measuring instruments.
This allowed us to get raw resistance curves but to extract exploitable UCF traces I had to extract correctly the data. This process has been discussed and proved its reproducibility over time.

The second one was devoted to the interpretation of those data.
Calculating the correlations between two traces taken on the same sample before and after a heating gave us clues about changes in the disorder configurations. We thus showed that, unfortunately we were not sensitive to the magnetic disorder that would have enabled us to conclude about spin glasses.

However we showed some new and intriguing features.
A progressive decrease of the correlation values for heating temperature between 4 and 80K were proven. This is undoubtedly the sign of changes in the internal and static disorder of our samples. The results showing the wide energy distribution of the moving systems and the fact that, for a given temperature, the exact same set of those systems moves, would be coherent with Two-Level Systems (TLS) oscillating between positions.
Moreover, we demonstrated the limitations of such measurements by showing its strong dependence on several parameters depending on the samples, such as its length L or phase coherence length L_ϕ. This study gave evidences of the high sensitivity of correlations to the absolute number of changing defaults and showed the importance of the averaging to qualitatively discuss the results.

This whole study now leads us to new questions.
Is this behaviour reproducible on different materials such as gold or iron? How to be sensitive to the magnetic disorder in our systems?
First clues in AuFe systems obtained at the end of my PhD seems to point to a universality of this behaviour but also to the difficulty to measure the magnetic part of the UCF. The solution would be to have a more doped sample to increase the magnetic contribution in our measurements.

Bibliography

1. Aharonov, Y. and D. Bohm: 'Significance of Electromagnetic Potentials in the Quantum Theory'. *Phys. Rev.* (1959), vol. 115(3): 485â€“491 (cit. on p. 41).
2. Akkermans, Eric and Gilles Montambaux: *Mesoscopic Physics of Electron and photons*. Cambridge University Press, 2007 (cit. on pp. 40, 77).
3. Aleiner, I. and Ya. Blanter: 'Inelastic scattering time for conductance fluctuations'. *Phys. Rev. B* (2002), vol. 65(11) (cit. on p. 80).
4. Aliane, A. et al.: 'Superconducting Ti/TiN Thin Films for mm-Wave Absorption'. *Journal of Low Temperature Physics* (2018), vol. (cit. on p. 105).
5. Almeida, J R L de and D J Thouless: 'Stability of the Sherrington-Kirkpatrick solution of a spin glass model'. *Journal of Physics A: Mathematical and General* (1978), vol. 11(5): p. 983 (cit. on pp. 15, 16).
6. Al'Tshuler, B. L.: 'Fluctuations in the extrinsic conductivity of disordered conductors'. *JETP Letters* (1985), vol. 41: p. 530 (cit. on p. 44).
7. Al'Tshuler, B. L. and A. G. Aronov: *Electron-Electron Interactions in Disordered Systems*. Ed. by Efros, A. L. and North-Holland M. Pollak. 1985 (cit. on p. 77).
8. Al'tshuler B. L., Aronov A. G.: 'Magnetoresistance of thin films and of wires in a longitudinal magnetic field'. *JETP Letters* (1982), vol. 33(10): p. 499 (cit. on p. 81).
9. Al'tshuler B. L., Spivak B. Z.: 'Variation of the random potential and the conductivity of samples of small dimensions'. *JETP Letters* (1985), vol. 42(9): p. 447 (cit. on pp. 42, 55).
10. Al'tshuler B. L. Aronov A. G., Spivak B. Z.: 'The Aaronov-Bohm effect in disordered conductors'. *JETP Letters* (1981), vol. 33(2): p. 94 (cit. on pp. 40, 46).
11. Ashcroft, N.W. and N.D. Mermin: *Solide State Physics*. Saunders College Publishing, 1976 (cit. on pp. 33, 82).
12. Béal-Monod, M.-T. and R. Weiner: 'Negative Magnetoresistivity in Dilute Alloys'. *Phys. Rev.* (1968), vol. 170(2): pp. 552–559 (cit. on p. 82).
13. Benoit, A., S. Washburn, C. Umbach, R. Laibowitz, and R. Webb: 'Asymmetry in the Magnetoconductance of Metal Wires and Loops'. *Physical Review Letters* (1986), vol. 57(14): pp. 1765–1768 (cit. on p. 51).
14. Bergmann, Gerd: 'Weak localization in thin films'. *Physics Reports* (1984), vol. 107(1): pp. 1–58 (cit. on p. 79).

15. Blandin, A.: 'THEORIES VERSUS EXPERIMENTS IN THE SPIN GLASS SYSTEMS'. Anglais. *Journal de Physique Colloques* (1978), vol. 39(C6): pp. C6–1499–C6–1516 (cit. on p. 9).

16. Bousquet, J., T. Klein, M. Solana, L. Saminadayar, C. Marcenat, and E. Bustarret: 'Phase diagram of boron-doped diamond revisited by thickness-dependent transport studies'. *Physical Review B* (2017), vol. 95(16) (cit. on p. 110).

17. Büttiker, M.: 'Four-Terminal Phase-Coherent Conductance'. *Physical Review Letters* (1986), vol. 57(14): pp. 1761–1764 (cit. on p. 50).

18. Büttiker, M., Y. Imry, R. Landauer, and S. Pinhas: 'Generalized many-channel conductance formula with application to small rings'. *Phys. Rev. B* (1985), vol. 31(10): pp. 6207–6215 (cit. on p. 39).

19. Cannella, V. and J. A. Mydosh: 'Magnetic Ordering in Gold-Iron Alloys'. *Phys. Rev. B* (11 1972), vol. 6: pp. 4220–4237 (cit. on pp. 9, 10).

20. Capron, T., A. Perrat-Mabilon, C. Peaucelle, T. Meunier, D. Carpentier, L. P. Lévy, C. Bäuerle, and L. Saminadayar: 'Remanence effects in the electrical resistivity of spin glasses'. *EPL (Europhysics Letters)* (2011), vol. 93(2): p. 27001 (cit. on p. 57).

21. Carpentier, David and Edmond Orignac: 'Measuring Overlaps in Mesoscopic Spin Glasses via Conductance Fluctuations'. *Physical Review Letters* (2008), vol. 100(5) (cit. on pp. 58, 59, 84).

22. Casimir, H.: 'On Onsager's Principle of Microscopic Reversibility'. *Rev. Mod. Phys.* (1945), vol. 17(2-3): pp. 343–350 (cit. on p. 50).

23. Dominique Mailly and Marc Sanquer: 'Sensitivity of quantum conductance fluctuations and of $1/f$ noise to time reversal symmetry'. *J. Phys. I France* (1992), vol. 2(4): pp. 357–364 (cit. on pp. 44, 45).

24. Einstein, A.: 'Üœber die von der molekularkinetischen Theorie der Wärme geforderte Bewegung von in ruhenden Flüssigkeiten suspendierten Teilchen [AdP 17, 549 (1905)]'. *Annalen der Physik* (2005), vol. 14(S1): pp. 182–193 (cit. on p. 34).

25. Feynman, R.P. and A.R. Hibbs: *Quantum Mechanics and Path Integrals*. Ed. by McGraw-Hill. 1965 (cit. on p. 39).

26. Fisher, Daniel S. and David A. Huse: 'Equilibrium behavior of the spin-glass ordered phase'. *Phys. Rev. B* (1 1988), vol. 38: pp. 386–411 (cit. on pp. 4, 22).

27. Fisher, Daniel S. and David A. Huse: 'Ordered Phase of Short-Range Ising Spin-Glasses'. *Phys. Rev. Lett.* (15 1986), vol. 56: pp. 1601–1604 (cit. on pp. 4, 22).

28. Flouquet, J.: 'Influence of Kondo Effect and Relaxation Times on Nuclear Orientation Measurements in Dilute Mn-Ag Alloys'. *Physical Review Letters* (1970), vol. 25(5): pp. 288–289 (cit. on p. 79).

29. G. Forestier M. Solana, L. Saminadayar: 'Signature of the spin-glass phase transition in mesoscopic systems via resistivity measurements'. *To be published* (2018), vol. (cit. on pp. 58, 82).

30. Glattli, D. C., P. Jacques, A. Kumar, P. Pari, and L. Saminadayar: 'A noise detection scheme with 10 mK noise temperature resolution for semiconductor single electron tunneling devices'. *Journal of Applied Physics* (1997), vol. 81(11): p. 7350 (cit. on p. 65).

31. Goudon, V., A. Aliane, W. Rabaud, C. Vialle, S. Pocas, E. Baghe, L. Dussopt, P. Agnese, N. Lio Soon Shun, S. Becker, V. Reveret, J.-L. Sauvageot, L. Rodriguez, M. Solana, and L. Saminadayar: 'Design and fabrication of cooled silicon bolometers for mm wave detection'. *Nuclear Instruments and Methods in Physics Research Section A: Accelerators, Spectrometers, Detectors and Associated Equipment* (2017), vol. (cit. on p. 105).

32. Guerra, F.: 'Broken Replica Symmetry Bounds in the Mean Field Spin Glass Model'. *Communications in Mathematical Physics* (2003), vol. 233: pp. 1–12 (cit. on p. 16).

33. Herrmannsdörfer, T., S. Rehmann, and F. Pobell: 'Magnetic properties of highly dilutedPdFex andPtFex-alloys. Part II. Susceptibility at micro- and milli-kelvin temperatures'. English. *Journal of Low Temperature Physics* (1996), vol. 104(1-2): pp. 67–94 (cit. on p. 23).

34. Hewson, A. C.: *The Kondo Problem to Heavy Fermions*. Apr. 1997 (cit. on p. 55).

35. Imry, Yoseph: 'Random-Field Instability of the Ordered State of Continuous Symmetry'. *Physical Review Letters* (1975), vol. 35(21): 1399â€“1401 (cit. on p. 25).

36. J.Kondo: 'Resistance Minimum in Dilute Magnetic allloys'. *Prog. Theor. Phys* (1964), vol. 32: p. 37 (cit. on p. 53).

37. Jönsson, Claus: 'Elektroneninterferenzen an mehreren könstlich hergestellten Feinspalten'. *Zeitschrift für Physik* (1961), vol. 161(4): pp. 454–474 (cit. on p. 40).

38. Johnson, J.: 'Thermal Agitation of Electricity in Conductors'. *Phys. Rev.* (1928), vol. 32(1): pp. 97–109 (cit. on p. 65).

39. Jonason, K., E. Vincent, J. Hammann, J. P. Bouchaud, and P. Nordblad: 'Memory and Chaos Effects in Spin Glasses'. *Phys. Rev. Lett.* (15 1998), vol. 81: pp. 3243–3246 (cit. on p. 29).

40. Kasuya, Tadao: 'A Theory of Metallic Ferro- and Antiferromagnetism on Zenerâ€™s Model'. *Progress of Theoretical Physics* (1956), vol. 16(1): pp. 45–57 (cit. on p. 9).

41. Landauer, R. *Philosophical Magazine* (1970), vol. 21: p. 863 (cit. on p. 37).

42. Landauer, R.: 'Spatial Variation of Currents and Fields Due to Localized Scatterers in Metallic Conduction'. *IBM J. Res. & Dev.* (1957), vol. 1(3): pp. 223–231 (cit. on p. 37).

43. Lee, P. A. and A. Douglas Stone: 'Universal Conductance Fluctuations in Metals'. *Phys. Rev. Lett.* (15 1985), vol. 55: pp. 1622–1625 (cit. on pp. 42, 44).

44. Licini, J., G. Dolan, and D. Bishop: 'Weakly Localized Behavior in Quasi-One-Dimensional Li Films'. *Physical Review Letters* (1985), vol. 54(14): pp. 1585–1588 (cit. on p. 49).

45. London, H., G. Clarke, and Eric Mendoza: 'Osmotic Pressure of He3 in Liquid He4, with Proposals for a Refrigerator to Work below 1Â°K'. *Phys. Rev.* (1962), vol. 128(5): pp. 1992–2005 (cit. on p. 63).

46. Lundgren, L., P. Svedlindh, P. Nordblad, and O. Beckman: 'Dynamics of the Relaxation-Time Spectrum in a CuMn Spin-Glass'. *Phys. Rev. Lett.* (10 1983), vol. 51: pp. 911–914 (cit. on p. 25).

47. Mallet, F., J. Ericsson, D. Mailly, S. Ünlübayir, D. Reuter, A. Melnikov, A. D. Wieck, T. Micklitz, A. Rosch, T. A. Costi, L. Saminadayar, and C. Bäuerle: 'Scaling of the Low-Temperature Dephasing Rate in Kondo Systems'. *Phys. Rev. Lett.* (22 2006), vol. 97: p. 226804 (cit. on p. 54).

48. Mezard, M., G. Parisi, and M.A. Virasoro: *Spin Glass Theory and Beyond*. Lecture Notes in Physics Series. World Scientific, 1987 (cit. on p. 19).

49. Mulder, C. A. M., A. J. van Duyneveldt, and J. A. Mydosh: 'Susceptibility of the CuMn spin-glass: Frequency and field dependences'. *Phys. Rev. B* (3 1981), vol. 23: pp. 1384–1396 (cit. on pp. 26, 27).

50. Mydosh, J. A.: *Spin glasses : an experimental introduction*. Ed. by Taylor and London Francis. 1993 (cit. on pp. 7, 20).

51. Mézard, M. and Virasoro, M. A.: 'The microstructure of ultrametricity'. *J. Phys. France* (1985), vol. 46(8): pp. 1293–1307 (cit. on p. 21).

52. Nagata, Shoichi, P. H. Keesom, and H. R. Harrison: 'Low-dc-field susceptibility of CuMn spin glass'. *Phys. Rev. B* (3 1979), vol. 19: pp. 1633–1638 (cit. on pp. 26, 27).

53. Nigam, A. K. and A. K. Majumdar: 'Magnetoresistance in canonical spin-glasses'. *Phys. Rev. B* (1 1983), vol. 27: pp. 495–511 (cit. on p. 82).

54. Nozières, P.: 'A "fermi-liquid" description of the Kondo problem at low temperatures'. *Journal of Low Temperature Physics* (1974), vol. Volume 17, Issue 1-2: pp 31–42 (cit. on p. 54).

55. Nyquist, H.: 'Thermal Agitation of Electric Charge in Conductors'. *Phys. Rev.* (1928), vol. 32(1): pp. 110–113 (cit. on p. 65).

56. Onsager, Lars: 'Reciprocal Relations in Irreversible Processes. I.' *Phys. Rev.* (1931), vol. 37(4): pp. 405–426 (cit. on p. 50).

57. Parisi, G: 'A sequence of approximated solutions to the S-K model for spin glasses'. *Journal of Physics A: Mathematical and General* (1980), vol. 13(4). Ed. by Publishing, IOP: pp. L115–L121 (cit. on p. 17).

58. Parisi, G: 'Magnetic properties of spin glasses in a new mean field theory'. *Journal of Physics A: Mathematical and General* (1980), vol. 13(5): p. 1887 (cit. on p. 18).

59. Parisi, G: 'The order parameter for spin glasses: a function on the interval 0-1'. *Journal of Physics A: Mathematical and General* (1980), vol. 13(3). Ed. by Publishing, IOP: pp. 1101–1112 (cit. on p. 18).

60. Parisi, G.: 'Toward a mean field theory for spin glasses'. *Physics Letters A* (1979), vol. 73(3): pp. 203 –205 (cit. on pp. 4, 16).

61. Pierre, F., A. B. Gougam, A. Anthore, H. Pothier, D. Esteve, and Norman O. Birge: 'Dephasing of electrons in mesoscopic metal wires'. *Phys. Rev. B* (8 2003), vol. 68: p. 085413 (cit. on p. 70).

62. Rizzuto, C: 'Formation of localized moments in metals: experimental bulk properties'. *Reports on Progress in Physics* (1974), vol. 37(2): pp. 147–229 (cit. on p. 79).

63. Ruderman, M. A. and C. Kittel: 'Indirect Exchange Coupling of Nuclear Magnetic Moments by Conduction Electrons'. *Phys. Rev.* (1954), vol. 96(1): pp. 99–102 (cit. on p. 9).

64. Saminadayar, Laurent, Pritiraj Mohanty, Richard A. Webb, Pascal Degiovanni, and Christopher BÃ¤uerle: 'Electron coherence at low temperatures: The role of magnetic impurities'. *Physica E: Low-dimensional Systems and Nanostructures* (2007), vol. 40(1): 12â€“24 (cit. on p. 35).

65. Schopfer, Félicien, Fran çois Mallet, Dominique Mailly, Christophe Texier, Gilles Montambaux, Christopher Bäuerle, and Laurent Saminadayar: 'Dimensional Crossover in Quantum Networks: From Macroscopic to Mesoscopic Physics'. *Phys. Rev. Lett.* (2 2007), vol. 98: p. 026807 (cit. on p. 5).

66. S.F.Edwards and Anderson: 'Theory of spin glasses'. *Journal of Physics F : Metal Physics* (1975), vol. 5: pp. 965–974 (cit. on p. 10).

67. Sherrington, D and W Southernl: 'Spin glass versus ferromagnet'. *Journal of Physics F: Metal Physics (1971-1988)* (1975), vol. 5(5). Ed. by Publishing, IOP: pp. L49–L53 (cit. on p. 4).

68. Sherrington, David and Scott Kirkpatrick: 'Solvable Model of a Spin-Glass'. *Phys. Rev. Lett.* (26 1975), vol. 35: pp. 1792–1796 (cit. on pp. 4, 12, 15).

69. Springer, ed.: *Slow dynamics and aging in spin glasses*. Vol. 476. 1997 (cit. on pp. 4, 24, 25, 28).

70. Talagrand, Michel: 'The Parisi formula.' English. *Ann. Math. (2)* (2006), vol. 163(1): pp. 221–263 (cit. on p. 16).

71. Thouless, D.: 'Maximum Metallic Resistance in Thin Wires'. *Physical Review Letters* (1977), vol. 39(18): pp. 1167–1169 (cit. on p. 35).

72. Tielbürger, D., R. Merz, R. Ehrenfels, and S. Hunklinger: 'Thermally activated relaxation processes in vitreous silica: An investigation by Brillouin scattering at high pressures'. *Physical Review B* (1992), vol. 45(6): pp. 2750–2760 (cit. on p. 100).

73. Umbach, C., C. Van Haesendonck, R. Laibowitz, S. Washburn, and R. Webb: 'Direct observation of ensemble averaging of the Aharonov-Bohm effect in normal-metal loops'. *Physical Review Letters* (1986), vol. 56(4): pp. 386–389 (cit. on pp. 45, 46).

74. Vavilov, M. G. and L. I. Glazman: 'Conductance of mesoscopic systems with magnetic impurities'. *Phys. Rev. B* (11 2003), vol. 67: p. 115310 (cit. on p. 78).

75. Vegvar, P. de, L. Lévy, and T. Fulton: 'Conductance fluctuations of mesoscopic spin glasses'. *Physical Review Letters* (1991), vol. 66(18): pp. 2380–2383 (cit. on pp. 55, 56).

76. Webb, R., S. Washburn, C. Umbach, and R. Laibowitz: 'Observation of h/e Aharonov-Bohm Oscillations in Normal-Metal Rings'. *Physical Review Letters* (1985), vol. 54(25): pp. 2696–2699 (cit. on pp. 41, 42).

77. Weissman, M.: 'Comment on "Conductance fluctuations of mesoscopic spin glasses"'. *Physical Review Letters* (1992), vol. 68(23): pp. 3484–3484 (cit. on p. 56).

78. Y.Imry: *Introduction to mesoscopic physics*. Oxford University Press, 2002 (cit. on p. 34).

79. Yosida, Kei: 'Magnetic Properties of Cu-Mn Alloys'. *Phys. Rev.* (1957), vol. 106(5): pp. 893–898 (cit. on p. 9).

80. Ziman, J. M.: *Electrons and phonons The Theory of transport phenomena in Solids*. Oxford University Press, 1979 (cit. on p. 82).

81. Zorin, A. B.: 'The thermocoax cable as the microwave frequency filter for single electron circuits'. *Review of Scientific Instruments* (1995), vol. 66(8): p. 4296 (cit. on p. 65).